

UNIVERSITÀ DEGLI STUDI DI NAPOLI
“Federico II”



**FACULTY OF MATHEMATICS, PHYSICS AND
NATURAL SCIENCES**

PH.D. IN CHEMICAL SCIENCES - XXV CYCLE

***‘Fundamental investigation and screening of iminato
based titanium catalysts’.***

Applicant: Raffaele Bernardo.

Examiner: Ch.mo Prof. Giovanni Talarico.

Advisors: Ch.mo Prof. Vincenzo Busico.

Ch.ma Prof.ssa Roberta Cipullo.

Coordinator: Ch.mo Prof. Lucio Previtera.

Index of the Thesis

Chapter 1. Introduction.

1.1. EPDM, a special copolymer.	1
1.2. New catalysts for EPDM production.	4
1.3. High Throughput Screening and Fast Database Generation.	7
1.4. Scope and objectives of the thesis.	10

Chapter 2. Ziegler Natta Catalysis, a brief account.

2.1. Introduction.	14
2.2. Historical development of heterogeneous Ziegler Natta catalysis.	15
2.3. Historical development of homogeneous Ziegler Natta catalysis, group IV metallocenes.	17
2.4. Mechanism of ZN polymerization catalysis, a brief account.	20
2.5. Polymer microstructure and characterization.	26
2.6. Origin of the stereocontrol in metallocene ZN catalysis, the active centre symmetry/ polymer tacticity relationship.	28
2.7 . Activation of metallocene precursors, a brief account.	31
2.8 . Chain transfer processes.	33

Chapter 3. Mechanistic studies on amidinato catalysts.

3.1. Introduction.	37
3.2. Processes that control polymer molecular weight with the amidinato complexes	38
3.3. Catalyst dormancy study on amidinato catalyst C0 .	47
3.4. Experimental section.	50
3.4.1. HTS Freeslate PPR48 [®] ethene and propene polymerization protocol.	50
3.4.2. Low pressure propene polymerizations.	51
3.4.3. Ethene/propene co-polymerizations.	52
3.4.4. Polymer characterization via GPC and NMR.	52

Chapter 4. HTE tools and methods, protocol(s) benchmarking.

4.1. Introduction.	56
4.2. High Throughput Screening: the Freeslate PPR48 [®] Platform and the Self-Scavenging Protocol.	57
4.3. The relationship between catalyst productivity and copolymer composition.	64
4.4. A proper protocol for iminato catalyst screening with HTE technologies.	69
4.5. Validation of the copolymerization protocol, from mini-reactors to large scale batch reactors.	75
4.6. Experimental Section.	76
4.6.1. HTS Freeslate PPR48 [®] homopolymerization self scavenging protocol.	76
4.6.2. HTS Freeslate PPR48 [®] ethene/1-hexene co-polymerization protocol.	77
4.6.3. Large Scale Batch Reactor copolymerization protocol.	78
4.6.4. Polymer characterization via GPC and NMR.	78

Chapter 5. HTE Copolymerization Screening

5.1. Introduction.	82
5.2. HTS, the general experimental design matrix.	83
5.3. Kinetic data simulation and the deactivation constant, k_d .	86
5.4. Polymer characterization, copolymer composition and reactivity ratios.	89
5.5. Catalyst Screening Results, the experimental database.	93
5.6. Fast Database generation, the <i>in-situ</i> complexation approach.	97
5.7. Experimental section.	101
5.7.1. HTS Freeslate PPR48 [®] ethene/1-hexene co-polymerization protocol.	101
5.7.2. Kinetic Profile simulation.	102
5.7.3. EXtended Core Module TM Complexation protocol.	102
5.7.4. Polymer characterization via HT-GPC and NMR.	102
5.7.5. Complexation kinetics, ¹ H NMR kinetic assessment.	103
Appendix 5.1	107

Chapter 6. Molecular Modelling of iminato catalysts.

6.1. Introduction.	108
6.2. Computational methods.	109
6.3. Molecular modelling and QSAR approach, principles and applications.	115
6.4. QSAR modelling, molecular descriptors.	116
6.5. QSAR modelling, application and results.	119
6.6. Computational section.	122
6.6.1 . Molecular modelling	122
6.6.2 . QSAR modelling	122

<u>Chapter 7. Conclusions</u>	126
-------------------------------	-----

1.1 – EPDM, a ‘special’ copolymer.

In the huge world of synthetic rubbers, one of the most widespread product is EPDM, namely the ethylene-propylene diene monomer rubber. The employment of this plastic is ubiquitous, since the polymer properties enable both specialty and general-purpose applications¹ (table 1). Since their commercial introduction in the early ‘60s, sales have grown up to 870 metric tons in 2000; and nowadays the rubber is produced by several companies all over the world (Table1.1)².

Table 1.1. Major EPDM rubber production capacities (courtesy from reference 2).

Manufacturer	Country	Capacity, 10 ³ t/yr
Bayer/Polystar	U.S. and Germany	110
DSM Elastomers (LANXESS Elastomers B.V. from May 1 st , 2011) ^{3a}	U.S., The Netherland, Brazil, China [*]	216
Du Pont Dow	U.S.	90
EniChem Elastomeri	Italy	85
ExxonMobil Chemical	U.S., France	174
Herdilia	India	10
Japan Synthetic Rubber	Japan	65
Korea Polychem	South Korea	40
Mitsui Petrochemical	Japan	60
Sumitomo Chemical	Japan	35
Union Carbide	U.S.	90
Uniroyal Chemical, Co.	U.S.	93

^{*} From 2013^{3b}

As said before, EPDM belongs to the class of rubbers. A general formula is as depicted in figure 1.1, where the values are in the order of $m \approx 1500$ (60% mol), $n \approx 975$ (39% mol) and $o \approx 25$ (1% mol), and the monomers are (preferably) statistically distributed along the chain².

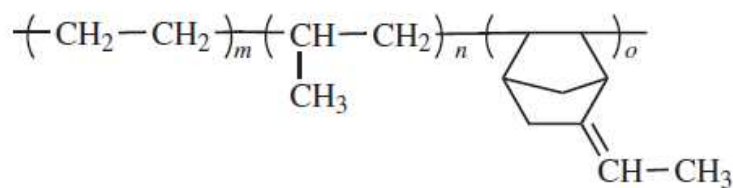


Figure 1.1. Basic chemical structure of a EPDM polymer, in this case the *ter*-monomer involved is the 5-ethylidene-2-norbornene (courtesy from reference 2).

The non-polar structure of the polymer ensures excellent resistance and ozone inertness, especially when compared to the most common natural rubber (*cis*-1,4-polyisoprene), the SBR (styrene-butadiene rubber), IR (isoprene rubber) and BR (butadiene rubber); moreover the extreme compatibility of EPDM towards fillers and plasticizers is of utmost importance, thus making the rubber very appealing to several customer applications². The market is growing strong and, even though this rubber has been available for more than 40 years, nowadays it is still possible to regard the technology of production as newborn.

The main applications of EPDM are both in the automotive and in the building industries; the EPDM is involved in the fabrication of seals, car radiator hoses, weather-strip profiles, roof sealing and cable insulation¹. Different applications for EPDM are in blending, and it is commonly used to divide the applications in two, namely the blending with rubbers and with thermoplastics. The former combination enables the production of a blended rubber with increased ozone resistance; the latter, on the other hand, is used nowadays to enhance the impact behaviour of the host polymer(s): particularly the blend with polypropylene works as a thermoplastic elastomer, enabling the usage for the automotive exterior application, such as bumpers and body panels².

As a matter of fact, polymer properties are strictly dependent on the molecular structure⁴; also with EPDM, it is possible to use molecular parameters to correlate directly the polymer properties with respect the structure, i.e. content of monomers in the chain, distribution of the monomers (random, blocky, alternate), the molecular weight, nature of the *ter*-monomer and the nature of the unsaturated moieties that the *ter*-monomer provides. The molecular parameters can be varied, after the proper design both of the catalyst system⁵ and the process involved, thus producing the different EPDM grades².

Even though a very high number of parameters are changeable and several compositions are affordable, the commercial unities stem (disregarding temporarily the *ter*-monomer) a ethylene/propylene composition from 55:45 to 80:20. In the limit of high propylene content the ozone resistance is lost, due to the lower oxidative stability of the propylene units compared to the ethylene units⁶; on the other hand, high ethylene content is responsible of the loss of rubber

character due to the higher tendency of the material to crystallize, especially (and this is largely dependent on the catalyst system involved) if the ethylene units are found in relatively long sequences⁷.

As it is clear from the molecular structure, the backbone of an EPDM chain is made of saturated carbons, any unsaturation in the main chain usually decreases the resistance towards light, radicals and heat, since double bonds, if incorporated in the main chain, are eligible to break and shorten the main chain length⁶. The presence of a non-conjugated diene as a third monomer is beneficial for the applications of the rubber. Even at very low molar amount, the diene is included in the main chain, providing a ‘dangling’ double bond at the side of the chain and enabling the conventional sulphur vulcanization and/or peroxide curing chemistry⁶. As a brief summary, in table 1.2, the most common properties of commercial EPDM are reported.

Table 1.2. General properties for the EPDM elastomers; the properties refer to the material before optional vulcanization/curing processes (courtesy from reference 2).

Property	Range / Value
Specific gravity	0.86-0.88
Appearance	Glassy-white
E/P ratio (wt)	
Amorphous types	45/55
Crystalline or sequential types	80/20
Onset of crystallinity	
Amorphous types, °C ^a	Below -50
Crystalline types	Below ~30
Glass transition temperature, °C ^a	-45 to -60
Heat capacity, kJ kg ⁻¹ K ⁻¹	2.18
Thermal conductivity, W m ⁻¹ K ⁻¹	0.335
Thermal diffusivity, m s ⁻¹	1.9×10^{-5}
Thermal coefficient of linear expansion per °C	1.8×10^{-4}
Mooney viscosity, ML (1 ++4) 125°C ^b	10-90

^a Dependent on third monomer content

^b Oil extended grades, when viscosity >100 for the raw polymer.

The production of EPDM is carried out in continuous processes and any of them is practically covered by the proprietary service; nevertheless it is possible to devise some general features of the production processes, which are divided in solution, slurry and gas-phase processes.

For the purpose of this thesis, we will describe only the distinguishing features of the solution production processes.

In these processes, all the components are kept dissolved in an inert solvent, most commonly an hydrocarbon, the catalyst choice is mainly dictated by the specifications of the polymer to be produced; it generally comprises two main components: a transition metal halide, such as TiCl₄, VCl₄, VOCl₃ - of which VOCl₃ is the most widely used - and a metal alkyl component such as AlEt₂Cl, AlEtCl₂ or a mixture of the two, i.e. ethylaluminum sesquichloride, Et₃Al₂Cl₃².

In the case of V based catalysts, the active centre of the transition metal halide is progressively reduced from V^{3+} to V^{2+} , being the latter able to polymerize only ethene⁸. In order to increase the ratio $[V^{3+}]/[V^{2+}]$, several molecules are coupled with the catalyst system as promoters, which task is to oxidise the V from the inactive form to the correct performing specie. Examples of promoters (which are known by various patents) are CCl_4 , Cl_3COOMe ⁸.

In the solution processes for the EPDM production via ZN catalysis, all the chemicals are fed in the reactor vessels continuously and proportionally; the chain growth is extremely fast and the polymerization is highly exothermic. Heat has to be completely removed, especially in the V based processes, in which the temperature is in the order of $40-50^{\circ}C$ ^{9a}; any increase of the temperature is highly detrimental to the average molecular weight of the product^{2,11}. The processes can be grouped in two categories, those which the reactor is completely full of liquid phase (in this case the heat has to be removed by cooling with water) and those in which is present a gas cap²(in this case the stripping of the gaseous monomers provides the dispersion of the heat). Most commonly, hydrogen is fed in the stream to control the molecular weight of the product^{2,10}.

As a matter of fact, in a liquid process the polymer is dissolved in the liquid phase after the detachment from the active site, thus determining an increase of viscosity. The practical limit of the viscosity is given by a 5-10% solid rubber concentration; heat transfer issues and insufficient liquid flow rate prevent the possibility of obtaining an higher concentration of the polymer, therefore the monomer conversion must be low in the reactor. At this polymer concentration, the reaction is stopped stirring the liquid phase with water and another step must be included for the recycling of the monomers. The activity of V based catalysts is usually low (*vide infra*), hence a purification step is often required, in order to remove the catalyst residues from the polymer, until an acceptable extent of ppm.

1.2 – New catalysts for EPDM production.

The first EPDM production technology almost entirely relied on V based catalysis, always in combination with an Al-alkyl compound as co-catalyst, due to the specific properties of this system regarding the copolymerization statistics^{9b}.

Even though the V-based technology is still well wide-spread, two drawbacks are present in the current processes: low temperature of polymerization ($\approx 40-50^{\circ}C$) and low catalyst activity ($50-100$ gpolymer/mmolV)^{9a}.

The relatively low temperature of polymerization for a solution process with V-based catalyst is meant to ensure adequate molecular mass of the produced materials¹¹, unfortunately, the viscosity

of the liquid phase is a severe issue and monomer conversion has to be kept as low as possible. Recycling of the monomer has to be taken in account, therefore adding one more step in the production plant.

The low activity of the catalysts, on addition, requires additional steps in the process to remove the catalyst residues from the product, before the processing of the material for the desired application.

Among the companies of table 1.1, the research is nowadays aimed to obtain catalysts for the production of EPDM with an increased resistance toward temperature (both with respect activity and molecular weight or the polymers) and an inherently higher activity (so to avoid costly steps of polymer purification).

The advent of the metallocene catalysts^{12a}, and, more importantly, of the ‘post-metallocenes’^{12b}, allowed for the search of different processes for the production of EPDM featuring higher temperature (so to enhance the monomer conversion due to the lower viscosity of the liquid phase) and more productive catalysts (in order to eliminate the tedious and expensive process of product cleaning); nevertheless the post-metallocene based technology for the industrial EPDM production is still, nowadays, at its early beginning.

The aftermath of the ‘post-metallocene’ catalysts for the production of new polymers was in the '90 with the discovery/design of the hemi-metallocene complexes of the column IV, i.e. the so called ‘Constrained Geometry Catalysts’ (CGC Catalysts)^{12b,13}, inspired by the Sc complexes discovered by Bercaw and coworkers. Being the complexes with the group IV metal patented by Dow chemical's and Exxon¹⁴, the ligand framework is mainly constituted by a cyclopentadienyl ring linked with a Si bridge to an amino ligand, and the metal is usually Ti (figure 1.2). In consequence of an increased steric accessibility for an hindered monomer to the metal coordination sphere, these catalysts feature high activity in ethene/1-alkene copolymerizations (being the 1-alkene usually 1-hexene and/or 1-octene), thus leading the way to the industrial production of *Linear-Low Density PolyEthylene* (LLDPE)¹⁵.

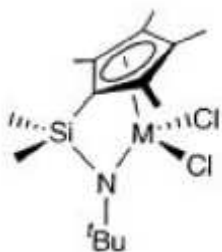


Figure 1.2. General structure of a CGC catalyst, the metal employed is Ti.

The possibility to copolymerize ethene effectively with other comonomers, brought to the synthesis of several complexes, in which one of the Cp fragment was substituted with a donor ligand, such as an iminato ligand (figure 1.3)¹⁶.

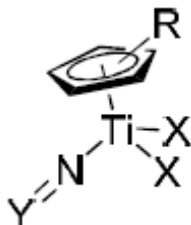


Figure 1.3. Prototype of the iminato hemi-metallocene class studied in this work.

For these complexes, the fragment iminato is similar, both electronically and sterically to a Cp moiety¹⁷; moreover the possibility of changing the substituent Y enables the structural amplification of the ligand framework and, subsequently, the variation of the complex behavior in polymerization (figure 1.4).

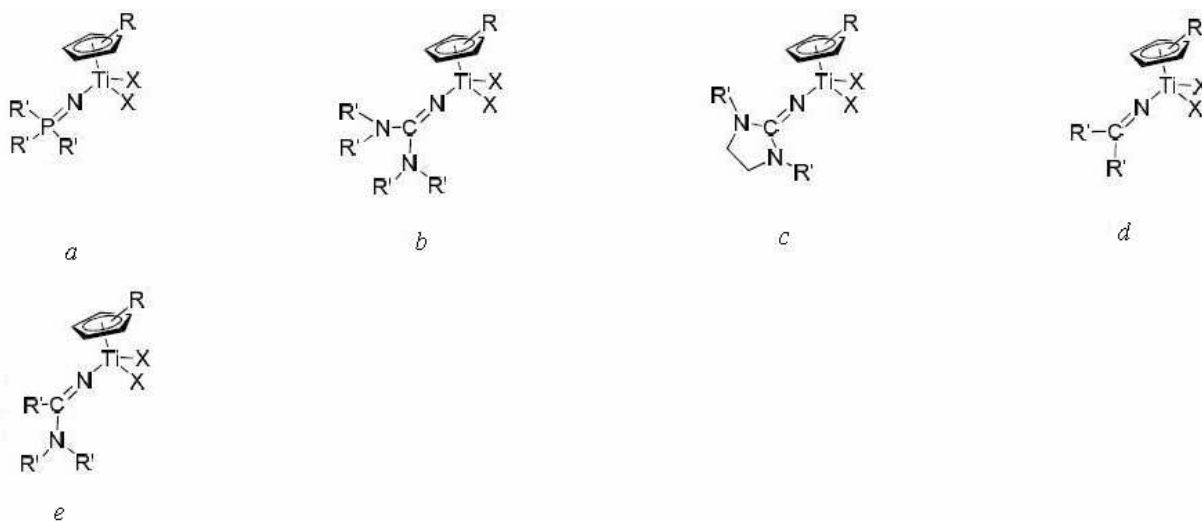


Figure 1.4. Structural amplification of the iminato complex for the production of elastomers:

- Phosphinininato complex, developed at Nova Chemicals and by Stephan, featuring high productivity^{16,18};
- Guanidinato complex, developed at Nova Chemicals and subsequently studied by Kretschmer in 2002, featuring low productivity^{16,19};
- Iminoimidazoliminato complex, further studied by Kretschmer¹⁹, featuring high productivity;
- Ketiminato complex, developed at Nova Chemicals and studied by Stephan^{16,18}, featuring low productivity and non-single centre behavior.
- Amidinato complex, developed by DSM Elastomers (now LANXESS Elastomers^{3a,20,21,3b}).

0 1 0 0

1. $\frac{1}{2}$ 2. $\frac{1}{2}$ 3. $\frac{1}{2}$ 4. $\frac{1}{2}$ 5. $\frac{1}{2}$ 6. $\frac{1}{2}$ 7. $\frac{1}{2}$ 8. $\frac{1}{2}$ 9. $\frac{1}{2}$ 10. $\frac{1}{2}$

[illegible]

combinatorial to parallel; needless to say that all the HTS methods feature a high level of automation and, correspondingly, an high grade of miniaturization²².

Very recently (2000) the HTS methods have been applied to the discovery of new olefin polymerization catalyst²³, and the first attempt proved indeed to be a remarkable success: the joint venture in 2003 between Dow Chemicals Co. and Symyx Technologies Inc. (a leader company in HTS, Freeslate[®], Inc. nowadays), brought to the discovery and patent of the pyridilamide Hf(IV) complexes for the industrial production of LLDPE (figure 1.7)²⁴.

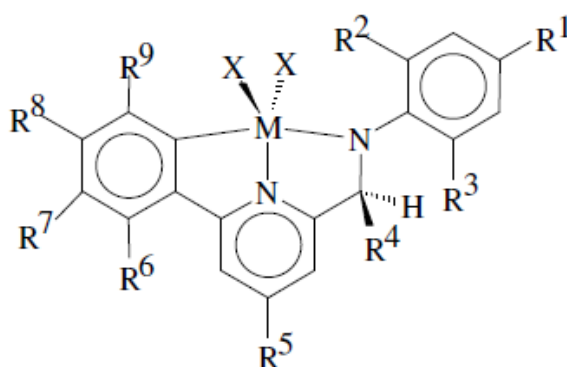


Figure 1.7. Pyridilamide systems discovered by the joint venture between Dow Chemicals Co. and Symyx Technologies Inc.; M = Zr, Hf X = Cl, R, NR₂.

The general workflow for the catalyst development passes through different levels of screening²². The first one is the so-called *primary screening*, in which the catalyst evaluation is performed in micro reactors (≤ 1 mL) and the number of experiment is in the order of 10^3 *per die*. To such a high number of experiments, only a rough evaluation of the catalysts corresponds to; nevertheless the low accuracy in the evaluation and assessment of the catalysts performance is completely compensated by the huge amount of the structures that can be screened and evaluated towards certain requested properties (catalyst productivity, comonomer incorporation, M_w capability). The most interesting structures arising from the ‘quick-and-dirty’ *primary screening* (*hits*) are tested at the *secondary screening* stage. In this section of the workflow, the number of experiment substantially decreases ($10 \div 10^2$ *per die*), but both the operative volume and the evaluation accuracy increase (~ 10 mL – RSD among identical experiments $\leq 20\%$). All the system that pass successful through the *secondary screening* (*leads*) are subjected to structural amplification and evaluation in larger reactors and conventional methods (figure 1.8).

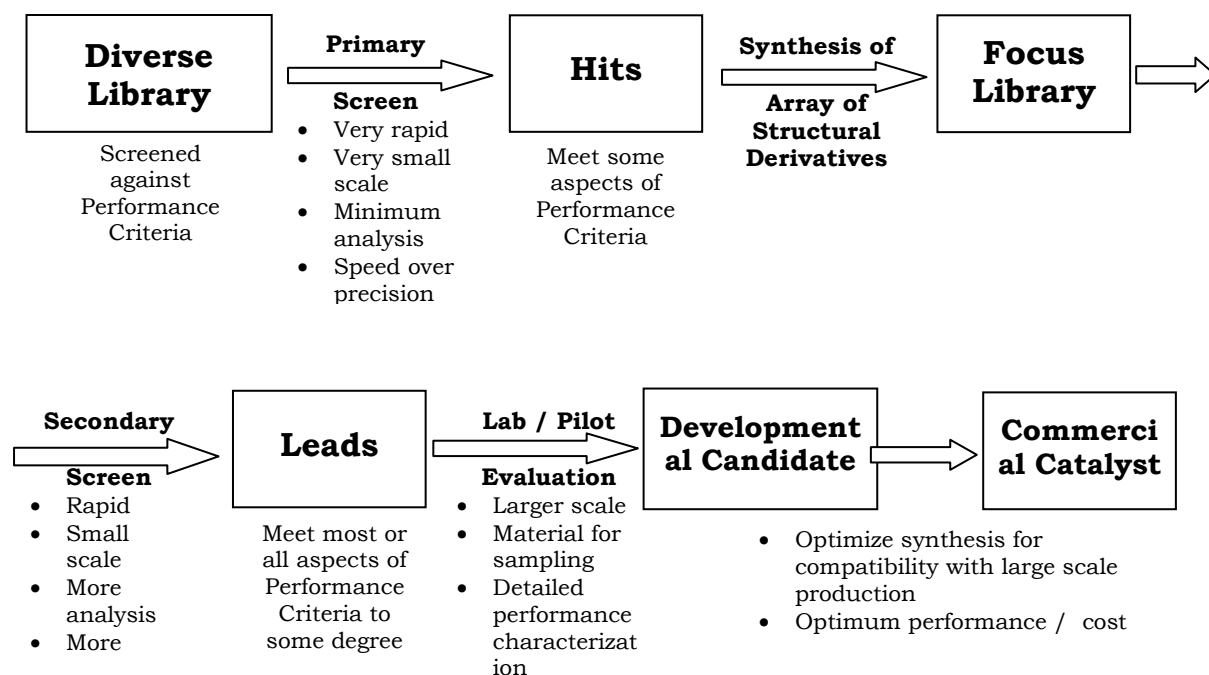


Figure 1.8. Typical HTS workflow for the industrial research and discovery of new catalysts (courtesy of John Stevens, Dow Chemicals).

Along with the usage of the HTS techniques for the rapid evaluation parallel-wise of an high number of *hits*, a new way of employment of the secondary screening apparatus was developed by Busico and co-workers²⁵, i.e. the detailed kinetic assessment of well known catalysts with respect the high number of physical and chemicals variables (pressure, temperature, catalyst/co-catalyst ratio). The rapidity of the approach and the high accuracy have already been demonstrated, thus revealing that HTS techniques of *secondary screening* can be used in academia to assess new mechanistic features of both homogeneous and heterogeneous catalysts.

As a matter of fact, the two ways of using the HTS techniques are complementary; moreover the exclusive usage of one of the two is detrimental to the correct workflow for catalysts screening.

This thesis aims at studying the fundamental behavior of amidinato complexes in polymerization and at rationalizing their structure/property relationships. The possibilities provided by the High Throughput Experimentation (HTE) tools are not only the maximization of experiments (which maximizes the probability of a serendipitous discovery), but also the possibility of fast building of reliable databases of structure/activity relationships, thus opening the way to the statistical modeling of structures (Quantitative Structure/Activity Relationships – QSAR, *vide infra*)²⁶.

Besides being powerful ‘discovery tools’, HTS platforms unfortunately prove to be useless without the precise knowledge of the molecular kinetics of the catalysts, as we will demonstrate throughout this work, the employment of the said techniques for a successful and meaningful screening are

bound to the kinetic assessment of the behavior in polymerization of the catalysts of interest, in order to achieve the development of the correct screening protocol²⁵.

1.4 – Scope and Objectives of the Thesis.

Research on olefin polymerization catalyst, had been, since the discovery in the '50s, extremely wide and attracted many scientists all over the world. Nevertheless, discoveries and improvements in this catalysis (and other fields of chemical research) have always been characterized by a certain percentage of serendipity; HTS techniques, in the early philosophy of HTE, were meant to increase the probability of having 'lucky-shot', just increasing the amount of, basically, shots.

In our opinion, HTS techniques are much more. The chance of fast database generation certainly opens the way to use and develop more precise statistical modelling of the huge amount of experimental results (QSAR), thus leading the way to a more-rational developing of catalyst and processes.

The work of this thesis is an additional step along this path.

The main scope is to develop proper HTE methods to screen amidinato catalysts; the extremely versatile synthetic route to these complexes makes them suitable for the HTS techniques, nevertheless, as it will shown in chapter 4, HTS techniques are powerful only in combination with the precise knowledge of the catalyst behaviour, which will be attained in the mechanistic evaluation of chapter 3.

After the developing of the protocols and the benchmarking of chapter 4, in chapter 5 the full potentialities of HTS techniques for the fast database generation will be shown on this class of catalysts. After that a proper, and statistically meaningful, database has been built, a QSAR approach will be applied in chapter 6, in order to build the instruments to generate new amidinato family toward specific product properties (polymer molecular weight, composition, etc.) (figure 1.9).

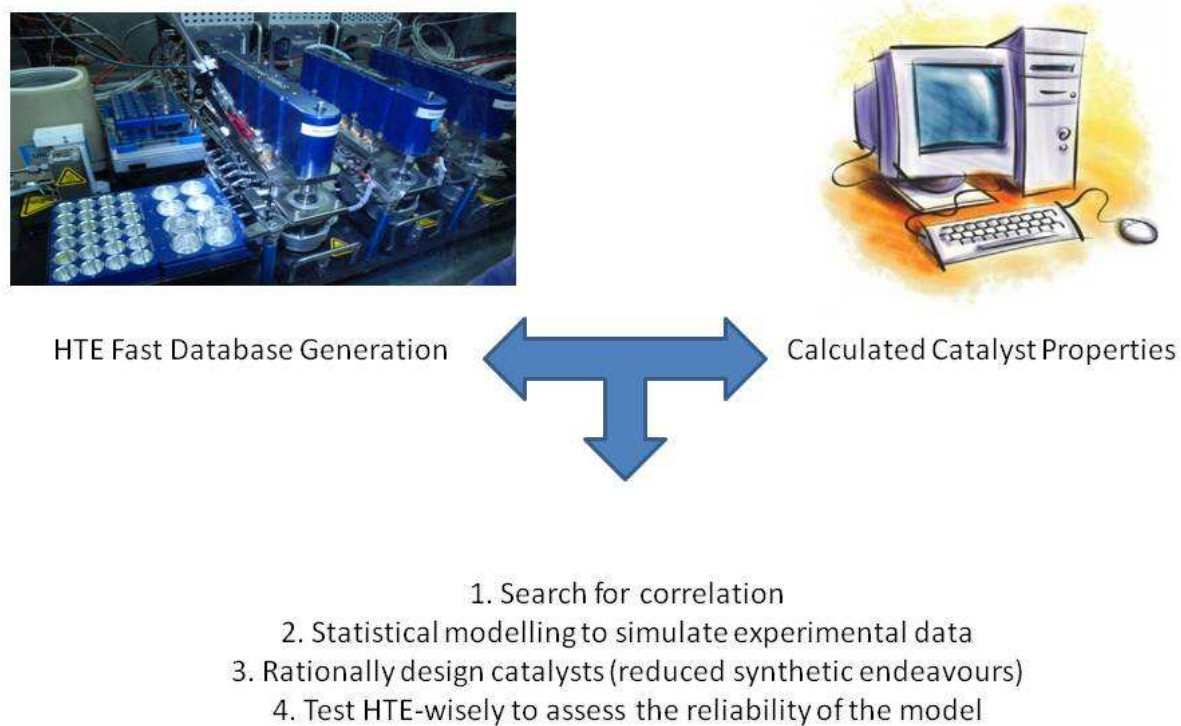


Figure 1.9. Ideal synergetic coupling of HTE tools and methods with QSAR modelling.

References

- [1]. <http://www.azom.com/article.aspx?ArticleID=1822>
- [2]. Noordermeer, Ethylene-propylene Polymers from Kirk-Othmer Encyclopedia of Chemical Technology, Vol. 10, 704-719, John Wiley and Sons; *World Rubber Statistics 2000*, International Institute of Synthetic Rubber Producers, Inc., Houston, Tex.
- [3]. (a) <http://lanxess.com/en/corporate/media/press-releases/detail/19048/>;
b) [http://keltan.com/en/keltan-news-events](http://keltan.com/en/keltan-news-events;);
- [4]. Sun, S.F., *Physical Chemistry of Macromolecules: Basic Principles and Issues, Second Edition*; **2004**, John Wiley & Sons, Inc.; Busico, V.; Cipullo, R.; *Prog. Pol. Science* **2001**, *26*, 443-533.
- [5]. Brintzinger, Hans H.; Fischer, David; Muelhaupt, Rolf; Rieger, Bernhard; Waymouth, Robert M., *Angew. Chem., Int. Ed. Eng.*, **1995**, *34*, 1143.
- [6]. (a) Ammala, A.; Bateman, S.; Dean, K.; Petinakis, E.; Sangwan, P.; Wong, S.; Yuan, Q.; Yu, L.; Patrick, C.; Leong, K.H.; *Prog. Pol. Science* **2011**, *36*, 1015-1049 and references therein.; (b) Orza, R.A.; Magusin, P.C.M.M. Litvinov, V.M.; van Duin, M.; Michels, M.A.J. *Macromolecules* **2009**, *42*, 8914-8924.
- [7]. Bruckner, S.; Allegra, G.; Pegoraro, M.; La Mantia, F.P., *Scienza e Tecnologia dei Materiali Polimerici*, Edises Seconda Edizione.
- [8]. (a) Christman, D.L.; *Journ. Pol. Sci. Part A-1: Polymer chemistry* **1972**, *10*, 471-487; (b) Adisson, E. *J. Polymer Sci. Part A* **1994**, *32*, 1033.
- [9]. (a) Christman, D.L.; Keim, G.I.; *Macromol.* **1968**, *1*, 358; (b) Doi, Y.; Suzuki, S.; Soga, K.; *Macromolecules* **1986**, *19*, 2896
- [10]. (a) Busico, V.; Cipullo, R. *Prog. Pol. Sci.* **2001**, *26*, 443; (b) Busico, V.; Cipullo, R.; Chadwick, J.C.; Modder, J.F.; Sudmeijer, O. *Macromolecules*, **1994**, *27*, 7538-7543.
- [11]. Kissin, Y.V. *Isospecific Polymerization of Olefins*; Springer-Verlag: New York, 1985.
- [12]. (a) Resconi, L.; Cavallo, L.; Fait, A.; Piemontesi, M. *Chem. Rev.*, **2000**, *100*, 1253-1345 ; (b) Mc Knight, A.L.; Masood, M.A.; Waymouth, R.M. *Organometallics* **1997**, *16*, 2879-2885; Britovsek, G.J.P., Gibson, V.C., Wass, D.F. *Angew. Chem. Int. Ed.* **1999**, *38*, 428-447.
- [13]. Shapiro, P.J.; Bunel, E.; Schaefer, W.P.; Bercaw, J.E. *Organometallics* **1990**, *9*, 867-9.
- [14]. (a) Canich, J.A.M. (Exxon) U.S. Patent 5,026,798, 1991; Stevens, J.C.; Timmen, F.J.; Wilson, D.R.; Schmidt, G.F.; Nicklas, P.N.; Rosen, R.K.; Knight, G.W.; Lai, S.Y. (Dow Chemical Company) Eur. Pat. Appl. 0416815A2, 1990; (b) Devore, D.D.; Timmens, F.J.; Hasha, D.L.; Rosen, R.K.; Marks, T.J.; Deck, P.A.; Stern, C.L. *Organometallics* **1995**, *14*, 3132-3134.
- [15]. Chum, P.S.; Swogger, K.W. *Progress in Polymer Science* **33** (**2008**) 797-819.
- [16]. Wang, Q.; Brown, S.J. U.S. Patent 6,486,276 B1, 2002.

- [17].(a) Mountford, P.; Bolton, P.D., *Adv. Synth. Catal.* **2005**, 347, 355-366; (b) Hoffmann, R. *Angew. Chem. Int. Ed. Eng.* **1982**, 21,711-800.
- [18].(a) Stephan,D.W.; Stewart, J.; Guerin, F.; Spence, R.E.v.H.; Xu, W.; Harrison, D.G. *Organometallics*, **1999**, 18, 1116; (b) Stephan, D.W.; Stewart, J.C.; Guerin, F.; Courtenay, S.; Kickham, J.; Hollink, E.; Beddie, C.; Hoskin, A.; Graham, T.; Wei, P.; Spence, R. E. v. H.; Xu, W., Koch, L., Gao, X., Harrison, D.G. *Organometallics* **2003**,22,1937; (c) Nomura, K.; Oya, K.; Imanishi, Y.; *Journ. Of Mol. Catalysis A: Chemical* **2001**, 174, 127-140; (d) Stelzig, S. H.; Tamm, M.; Waymouth, R.M. *Journ. Of Polymer Science: Part A: Polymer Chemistry*, **2008**, 46, 6064-6070.
- [19]. Kretschmer, W. P.; Dijkhuis, C.; Meetsma, A.; Hessen,B.; Teuben,J. H.; *Chem. Commun.*, **2002**, 608.
- [20].(a) E. G. Ijpeij, M. A. Zuideveld, H. J. Arts, F. van der Burgt and G.H. J. van Doremaele, WO, 2007031295, 2007; (b) E. G. Ijpeij, P. J. H.Windmuller, H. J. Arts, F. von der Burgt, G. H. J. van Doremaele andM. A. Zuideveld, WO, 2005090418, 2005.
- [21].Nomura,K.; Liu, J.; *Dalton Trans.* **2011**,40,7666-7682.
- [22].Hagemeyer,A.; Strasser,P.; Volpe,A.F., Jr. (Eds) *High Throughput Screening in Catalysis*; Wiley-VCH: Weinheim, **2004**.
- [23].Boussie,T.R.; Diamond,G.M.; Goh,C.; Hall,K.A.; LaPointe,A.M.; Leclerc,M.; Lund,C.; Murphy,V.; Shoemaker,J.A.W.; Tracht, U.; Turner,H.; Zhang, J.; Uno,T.; Rosen,R.K.; Stevens,J.C. *J.Am. Chem.Soc.* **2003**, 125, 4306-4317.
- [24].(a) Boussie, T.R.; Diamond, G.M.; Goh, C.; Hall, K.A.; Lapointe, A.M.; Leclerc, M.K.; Lund, C.; Murphy, V. (Symyx Technologies, Inc., USA) WO 0238628 A2, 2002.; (b) Stevens, J.C.; Vanderlende D. (Dow Chemical Co., USA) WO 03040201, 2003.
- [25]. (a) Busico,V.; Pellicchia,R.; Cutillo,F.; Cipullo,R. *Macromol. Rapid. Comm.* **2009**,30, 1697-1708; (b) Bernardo,R.; Busico,V.; Cipullo,R.; Pellicchia,R.; *Studying olefin polymerization kinetics in High-Throughput mini-reactors*, Poster at Blue Sky Conference 2010.
- [26].Muir,R.M., Hansch,C. *Nature* **1962**, 194, 178.

2.1 – Introduction.

At this point of the thesis, before entering in the details of the research work, it is needed to recall briefly some points of the Ziegler-Natta (ZN) catalysis, starting from an historical point of view and going to the, more exciting, scientific side.

The number of publication about the ZN catalysis is outstandingly high; any lists of references which would comprehend only the most important references would definitely be over 1000 quotes. Fortunately, the literature is plenty of excellent reviews and textbooks which periodically provide ‘snapshots’ of the state of the art. In the forthcoming paragraphs we will refer to these reviews/textbooks as most as possible, the quotation of an original work will be done only if strictly necessary.

Chapter 2 – Ziegler-Natta Catalysis, a brief account.

2.2 – Historical development of the heterogeneous Ziegler-Natta catalysis.

Since the first synthesis of the isotactic polypropylene by Natta in late '50s, the ZN catalysis went over a continuous development. The impact that this catalysis had on the society at that time was outstanding; new materials could be afforded via this technology and the dispose of 'wastes' from the cracking process (ethene, propene and 1-butene) was managed so efficiently, that they become a renewed product available on the market. From the scientific point of view, the ZN catalysis is the first example of a stereospecific and enantiospecific catalysis controlled by human technology rather than nature: 'Nature synthesizes many stereoregular polymers, for example cellulose and rubber. This ability has so far been thought to be a monopoly of Nature operating with biocatalysts known as enzymes. But now Professor Natta has broken this monopoly'¹.

In general, a ZN catalyst is made of the combination of an organometallic compound of column 1-3 of the periodic table (usually an Al-alkyl), with a transition metal compound of the column 4-10; of course not all the combinations are effective to explicate the catalysis and some of them are used only for particular applications².

From the discovery of Ziegler that a mixture of TiCl_4 and AlEt_3 was able to polymerize ethene and propene effectively, as we said briefly before, the first improvement was due to Natta, who introduced the pre-reduction of TiCl_4 to several crystalline forms of TiCl_3 (known to feature three polymorphic phases, α, γ, δ)³. This pre-reduced Ti species were able to polymerize propene with a higher degree of stereoregularity, which was evident from an higher boiling-heptane insoluble fraction of the polymer, the so-called Isotacticity Index (I.I.).

The addition of a third component (an ester, an amine or an ether) to the ZN systems brought to the generation of the first offspring of ZN catalysts, a real second generation, which afforded more productive catalysts and more stereoregular polymers.

From the knowledge that the active species of Ti are located only on the surface of the catalyst, the research was focused on improving the exposure of the active metal, hence raising the activity. The first attempts to support the active metal on traditional surfaces (SiO_2 and Al_2O_3) proved ineffective; the turning table was reached when anhydrous MgCl_2 was employed. The usage of MgCl_2 as a support resulted beneficial mainly for two reasons; first of all the structure of MgCl_2 is practically identical to the surfaces exposed by TiCl_3 ; a more subtle reason lies on electronic aspects of the TiCl_3 - MgCl_2 interaction: several results seemed to claim that the support enhances the Lewis acidity of Ti, with a beneficial effect to the catalyst activity. This development on the technology afforded the third generation of ZN catalysts, the so called 'high yield catalysts'⁴.

Chapter 2 – Ziegler-Natta Catalysis, a brief account.

The catalyst system $\text{MgCl}_2/\text{TiCl}_4\text{-AlEt}_3$ showed good activity but only moderate stereoselectivity, which is detrimental considering the polymer properties. This notwithstanding the stereoselectivity of the catalyst can be dramatically improved using some Lewis bases added both to the support (Internal Donors- ID) and to the co-catalyst (External Donors- ED); the activity of the catalyst is not dramatically affected, but the stereoregularity expressed by the adduct is greatly enhanced. In the last decade, some special ID were developed (namely diethers) to afford what are known as ‘ED-free’ systems, thus obtaining the fourth generation of ZN catalysts, which are nowadays the state of the art ZN catalysts for the isotactic polypropylene production².

An heterogeneous catalyst is, by definition, the collection of different active sites, due to the different positions that an active site can occupy on the support matrix (e.g. edges, different surfaces and cuts of a crystal unit). For this reason, researches have always kept alive the research on the homogeneous counterparts of the ZN catalysts², in order to both obtain more uniform products and have ‘easier’ systems to study. The advantage of the homogeneous ZN catalysis, which again took off from a laboratory curiosity to an industrial technology by serendipity, is to provide an easier subject to study the mechanism of the ZN catalysis thanks to the uniformity of the active centres involved in the catalysis; it is necessary to stress, however, that the ‘single-centre feature’ is not always granted⁶.

Chapter 2 – Ziegler-Natta Catalysis, a brief account.

2.3 -Historical development of the homogeneous Ziegler-Natta catalysis, group IV metallocenes.

The homogeneous ZN catalysts were studied since the development of this technology, as proper and more comprehensive species for mechanistic studies^{2b}. The first species were metallocene of the group IV of the periodic system, i.e. complexes of the type $\text{Cp}_2\text{TiCl}_2/\text{AlR}_n\text{Cl}_{3-n}$, which afforded a modest activity system in ethene homopolymerization; with propene, on the other hand, the yields were constituted only by traces of atactic polymer⁷. Similar results were obtained by Breslow with the analogous compound with the Zr⁸. In 1973, however, Reichert and Meyer found that traces of water⁹ slightly enhance the activity of the catalysts and the same result was confirmed by Breslow with the homologous Zr compounds. The turning table occurred only in the end of the '70s, when Sinn and Kaminsky found, by serendipity, that the controlled hydrolysis of AlMe_3 brings the synthesis of the methyl-alumoxane (MAO)¹⁰, an oligomeric organometallic compound which is an excellent co-catalyst for the system Cp_2ZrCl_2 .

Beside the complex structure of MAO, it was certain from the results of Sinn and Kaminsky that, at high $[\text{Al}]/[\text{Zr}]$ ratio, the activity of the homogeneous catalysts was greatly enhanced toward the ethene polymerization, less satisfactory were the results for propene and higher 1-alkene polymerizations.

Even though very interesting, these results could not be of immediate application, but the possibility to change the ligand framework to obtain catalysts with different properties made the development possible.

The general structure of a metallocene is as figure 2.1, two cyclopentadienyl rings are interacting h^5 with a metal ion of the group IV, the electron count is of $16e^-$ and the electroneutrality is granted from the h^1 ligand L (usually a chlorine or a methyl ligand).

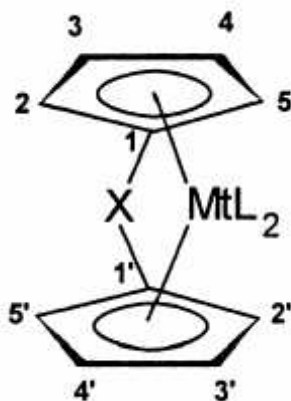


Figure 2.1. General structure of a metallocene. The numbers refer to the position which are eligible of substitution.

The substitution of a metallocene can be wide and a great number of complexes have been synthesized during the last decades. What is worthy to note is that the symmetry of the ligand framework is responsible of the polymer structure (provided that a definite kinetic regime control the polymerization, *vide infra*); the structures are fluxional unless a bridge between the aromatic moieties is included (atom X in figure 2). During the '80s several complexes have been produced, stemming various structural amplifications and complexes' symmetries (figure 1.3)^{2b}; before going on the structure/properties relationships, it is necessary to clarify the mechanism of Ziegler-Natta polymerization both for heterogeneous and homogeneous catalysts; once the mechanism is clarified, it will be possible to correlate the structure of an active polymerization center to the polymer produced.

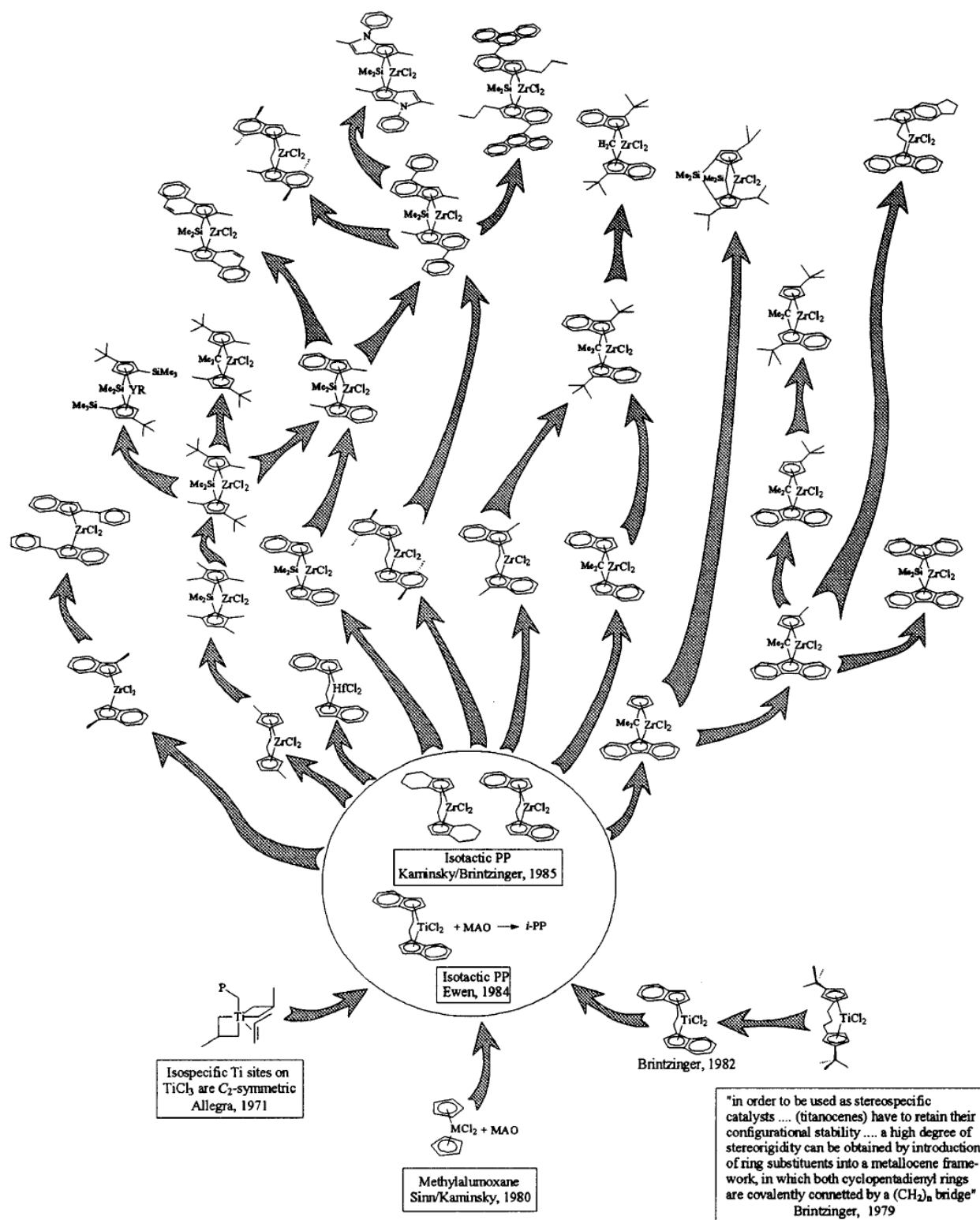


Figure 2.2. Evolution 'tree-diagram' of the metallocene catalysts (courtesy from reference 2b).

Chapter 2 – Ziegler-Natta Catalysis, a brief account.

2.4 – Mechanism of ZN polymerization catalysis, a brief account.

Despite the huge amount of empirical approach and serendipity in the ZN catalysis, the main aspects of polymer growth are well known, probably better than any other catalysis involved in industrial processes.

Since the school of Natta, it was clear that the link between the polymer tacticity and the catalyst stereoselectivity lied in the structure of the active sites during the polymerization. For this reason, a great effort was done in the elucidation of the structure of the various modifications of TiCl_3 . Going into deep with details, the studies brought to light that any modifications of the violet TiCl_3 crystalline forms are made of packing along a common axe of identical structural layers, any of which is made of a double plane of Cl atoms in closed packing and Ti atoms lie in the octahedral holes. The stoichiometry of the compound (Cl/Ti 3 to 1) implies that Ti has to occupy only 1/3 of the octahedral holes in the whole crystal; in order to adapt to a layer structure, Ti occupies 2/3 of the octahedral holes in each plane, leaving a void between Cl planes. This structure has a direct impact on the material: the mechanical properties of the TiCl_3 modification are similar to micaceous stones, i.e. fractures on the solid go along planes, due to the low energy connection of the planes themselves (only Van der Waals interactions are involved).

The polymorphic behavior of TiCl_3 rises only on the way that the planes are packed; in particular the α form is characterized by an hexagonal packing, whereas the γ form is obtained after a cubic stacking of the planes. Disordered succession of plane stacking are known to belong to the δ form¹¹. The description of a mechanism from the crystal structure is due to Cossee, who presented his studies in the end of the '60s¹². The first hypothesis, which was granted of experimental confirmations¹³, was that the active sites lied on lateral edges rather than of planes; moreover the coordinative unsaturation of the sites granted the reactivity. It is possible to list, even thought briefly, the hypotheses of Cossee as below:

- 1) The Ti atoms in TiCl_3 planes are chiral, any of them is linked to three Ti atoms via bridged Cl atoms (which can be regarded as a chelating ligand, see figure 2.3). The screw-like structure is chiral but, since no net chirality must occur due to the lackness of chiral unbalancement, these structures are in racemic pairs (Δ and Λ).
- 2) Typical side 'cuts' of the crystal planes are obtained with a symmetrical cut of the three double bridge (e.g. on the 110 Miller's direction); in this case Ti 'enantiomorphic strings' are obtained with the double Cl bridge pointing toward the crystal, a terminal Cl atom to maintain the electroneutrality and a coordination vacancy.

- 3) The active species are constituted by a σ Ti-C bond, which is generated after the alkylation with the Al-alkyl; the monomer can coordinate to the coordination vacancy and thereafter inserts in the preformed Ti-C bond.
- 4) In case of prochiral monomer (i.e. propene and higher 1-alkenes), the insertion occurs preferentially with an enantioface, the chirality of different active sites can discriminate the proper monomer enantiofaces (figure 2.3 – steps 1 to 4).

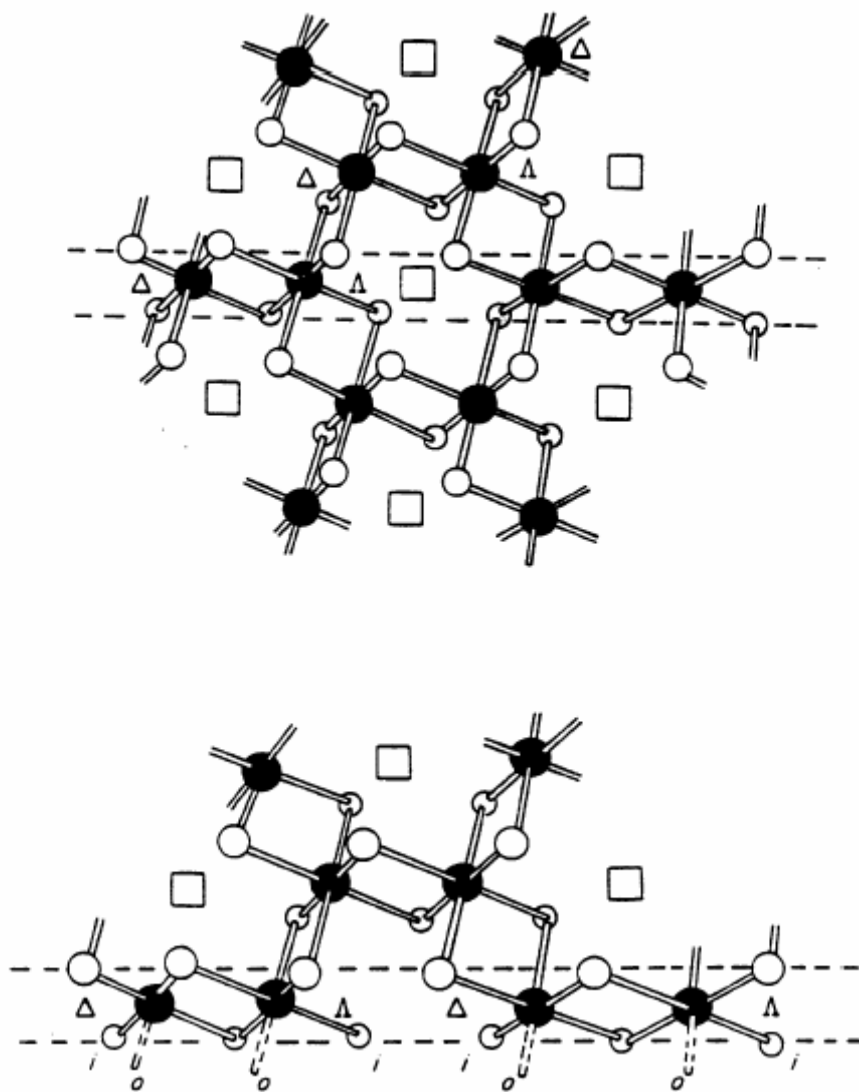


Figure 2.3. Representation of a violet TiCl_3 edge (top) with the schematic (110) cut of the crystal (bottom). A Cl-Cl bridge can be regarded as a chelating ligand, therefore the chirality of the complexes can be easily recognized.

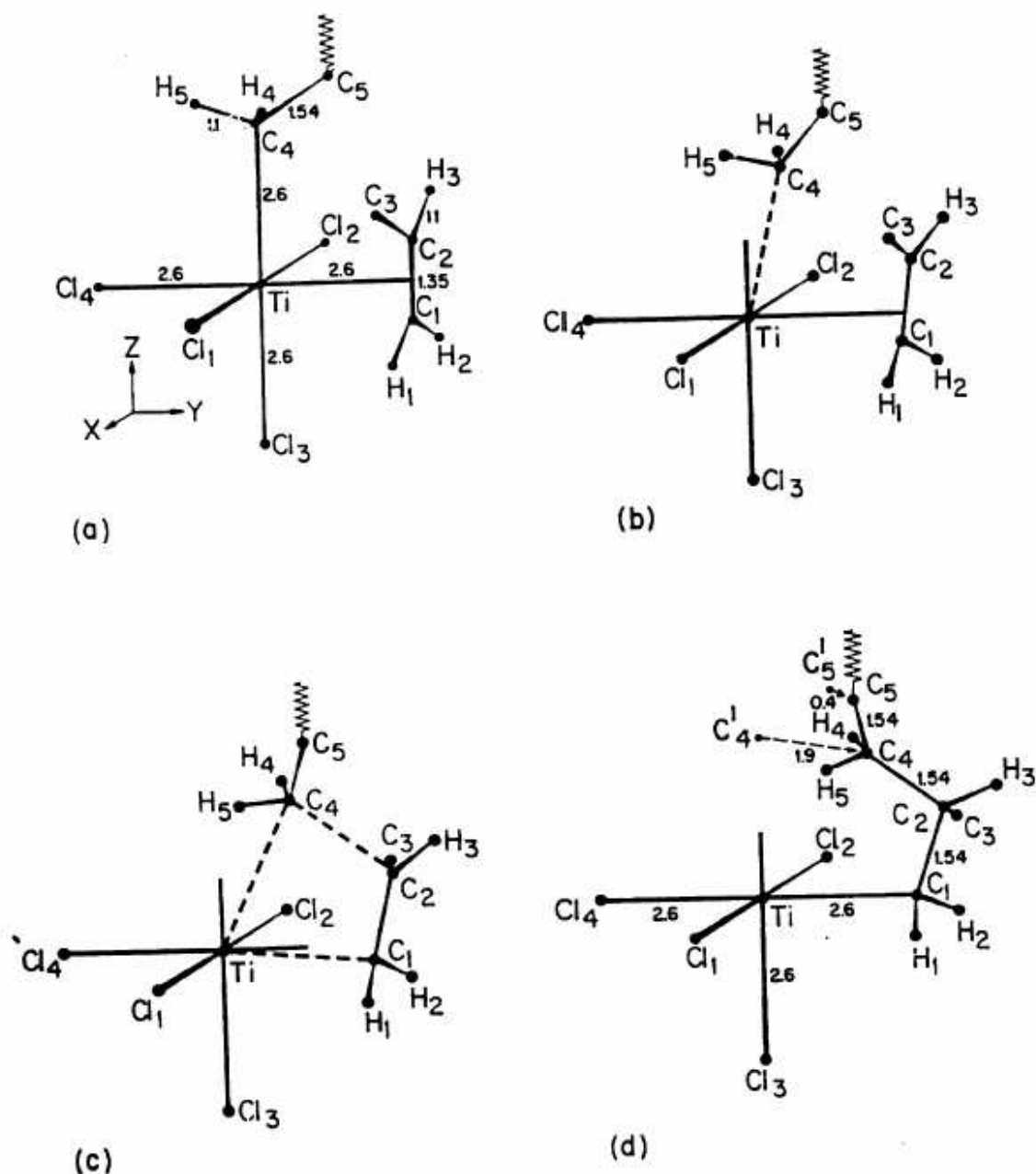


Figure 2.4. Representation of the olefin insertion in an active site (a-d sequence of events), after the hypotheses of Cossee on the heterogeneous ZN catalysts.

The mechanism of Cossee can, in general, be well represented and simplified by a two states process: monomer coordination to the metal and *cis*¹⁴ insertion of the olefin in the M-C σ bond (figure 2.4). The driving force is given by the strong polarization of the reactive fragment rather than a π back-donation from the metal to the olefin, thus meaning without bond order decreasing effect (figure 2.5).

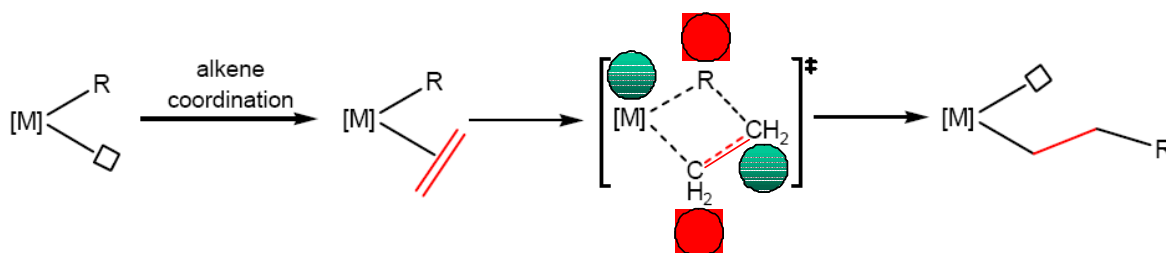


Figure 2.5. Insertion mechanism according to Cossee.

In this insertion mechanism, it is hard to identify the rate limiting step; quantum mechanical studies, however, revealed that, as far as the olefin is from propene to higher 1-alkene, the rate limiting step is the insertion; for ethene the situation is less clear until now. It is worthy to note that for some systems (especially if the metal involved is of group IV and/or V), the olefin coordination step does not represent a ‘net’ energy minimum.

Concerning the stereochemistry of insertion of the olefin in to the M-C bond, several studies with deuterated monomers¹⁴ have proved that the stereochemistry of insertion is *cis*; i.e. from the polymerization of the *cis*-1*d*-propene the resulting polymer is poly(propylene-1*d*) *eritro*-diisotactic, from the polymerization of the *trans*-1*d*-propene the resulting polymer is poly(propylene-1*d*) *theo*-diisotactic (figure 2.6)¹⁵.

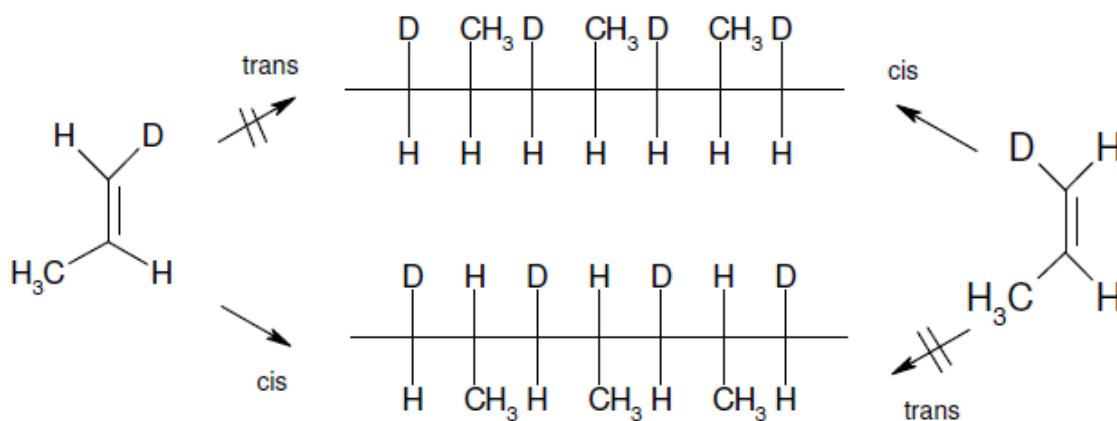


Figure 2.6. *Cis* insertion of a monomer molecule in a M-C bond in the ZN catalysis.

Once clarified that the insertion of the monomer is always *cis* in the M-C bond, it is easy to recognize that a prochiral olefin, e.g. propene, can insert following four different options (figure 2.7)¹⁶. The preference is driven either by electronic or steric factors.

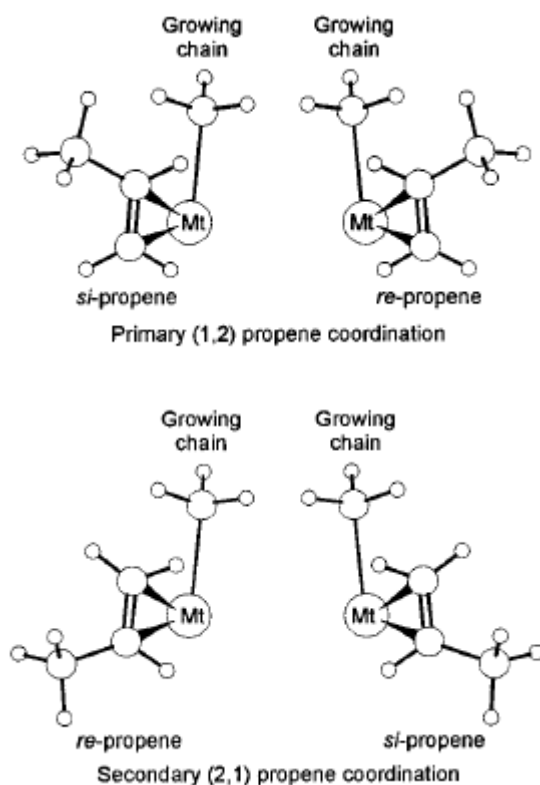


Figure 2.7. Four insertion modes for a prochiral olefin (e.g. propene) in a σ M-C bond.

Depending on the carbon atom which is bound to the metal after the monomer insertion, the enchainment is referred either to a 1,2 insertion (also primary since the C1 is bound to the metal) or a 2,1 insertion (also secondary since the C2 is bound to the metal); in general the insertion mode is not random during the propagation, one of the two insertion mode is largely preferred, in case of a constant repetition of a kind of insertion (ideal case), the produced macromolecule is said to be *regioregular*.

In the four modes of insertion, it is clear that the two kinds of insertion bring two couples of structures which are in an enantiomeric relationships with each other; whether the sequence of insertion lead to all the tertiary carbons to have the same configuration, the polymer is said to be 'isotactic'¹⁶; whether the sequence is alternated, the polymer is known as 'syndiotactic'¹⁷; whether the sequence is random, the polymer is said 'atactic'¹⁶ (figure 2.8).

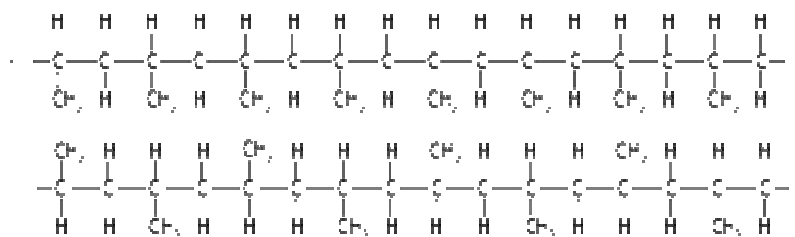


Figure 2.8. Different tacticity of a poly-1-alkene, in this case isotactic polypropylene (iPP on top) and syndiotactic polypropylene (sPP on the bottom); the atactic polymer lacks any repetitive regularity, therefore is omitted for clarity.

The tacticity of a polymer *per se* has influences, almost exclusively after certain thresholds of molecular average mass, on the crystal like packing of the chain and so on the main mechanical properties of the polymer, i.e. the quality and the applications of the material are direct function of the degree of tacticity (figure 2.9).

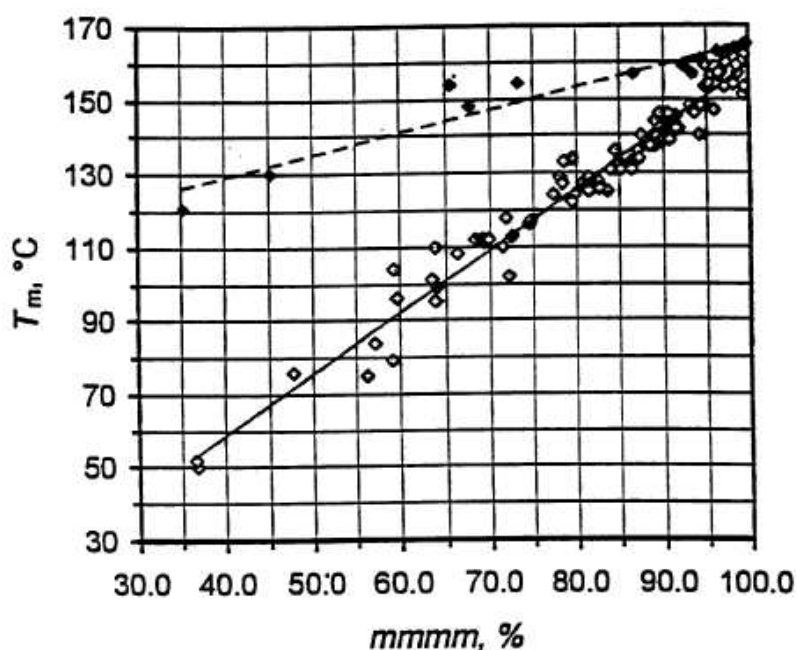


Figure 2.9. DSC melting temperature (T_m , second heating scan) of (predominantly isotactic) PP samples as a function of polymer tacticity (expressed as *mmmm*, mol% *vide infra*). The interpolating lines are only orientative (courtesy from reference 19).

2.5. Polymer microstructure and characterization.

The description of a polymer chain – among the polyolefin polymers, we will refer in general to a polypropylene chain but the same holds for all the higher 1-alkene polymer – is necessary done using statistics since no two macromolecules are equal. Concerning the molecular weight convenient averages have already been found (M_n , M_w , M_z), for the structure, instead, it was found convenient to describe a polymer making use of the *sequence of the monomeric units distribution*; unfortunately the methods employed (even the powerful ^{13}C NMR, vide infra) enable the elucidation only of (relatively) short sequences; this local information is what is called polymer *microstructure*¹⁸. For most vinyl polymers, the ^{13}C NMR is the election technique for the microstructural analysis, since it enables to look at very long segments of the polymer chain due to its highest sensitivity.

The microstructure of a polymer is a direct method for the evaluation of tacticity, which, as said before, is greatly responsible for the physical properties of the material; on addition it is worthy to stress that the microstructure and the polymerization kinetic are intimately correlated, a beautiful analogy is provided by Busico and Cipullo, i.e. *‘Each macromolecule is like a tape, where the story of the catalytic process that led to its generation is faithfully and sequentially recorded: in order to know what the story, one must be able to read the tape’*¹⁹.

In the previous paragraph the main features of a polyolefin born from a pro-chiral monomer have been already listed, this notwithstanding the description of a ‘real’ polymer chain (polypropylene will be taken as a convenient model) is still to be provided. The regular enchainment of monomeric units provides a regioregular polymer (ideal case), of course in a polymer chain one regio-enchainment is ‘only’ largely predominant over the other, a perfectly regio-regular polymer is never obtained though; however, it is common practice to ignore the regio-defects if they are lower than 5%mol. In this case the concept of microstructure of a polymer is practically coincident with the *microtacticity*¹⁹.

In order to describe the tacticity of a polymer, it is useful to introduce some definitions; since the mere list of the chirality of each single carbon atom does not lead to unambiguous description (the so called cryptochirality phenomenon for poly-1-alkenes): the best choice is to take, as the minimum descriptor, the relative configuration of a pair of chiral tertiary C atoms: we will refer to *diads*, which can be *meso diad* (m)^{18,20} or *racemo diads* (r)²¹, whether the configuration of the two C atoms is the same or not (figure 2.10).



Figure 2.10. Convenient Fischer projection of two propylene units (for clarity H are omitted), meso diad (left) and racemo diad (right).

If we extend this nomenclature to longer sequences, we will obtain *triads*, *tetrads*, *pentads* and so on. It is needless to say that a perfectly isotactic polymer can be described by an infinite repetition of meso diads (...mmmmmmmm...), a syndiotactic polymer by an infinite repetition of racemo diads (...rrrrrrrr...) and, in the end, an atactic polymer is described by a random sequence of meso and racemo diads (e.g. ...mmrmrmrrrrmr...). From the ideal description of the tacticity of a polymer using the diad nomenclature, it takes only one step further toward the description of a real polymer, i.e. the inclusion of *stereodefects* (*vide infra*).

As it is clear from § 2.4, any monomer insertion can be regarded as a single enantioselective reaction; in general, for a reaction to be enantioselective, the chiral induction is provided by the cross-coupling of two chiral elements, the asymmetric induction is thus made by the energy difference between diastomeric situations (intermediates or transition states). In the case of ZN 1-alkene polymerization, there are three main chirality elements, as listed below:

1. Different monomer coordination at the metal centre (*re/si* coordination, figure 2.11)²²;
2. Different chirality of a tertiary chain C (most commonly the tertiary C on the last inserted monomer unit has effects);
3. Strict chirality of the active site.

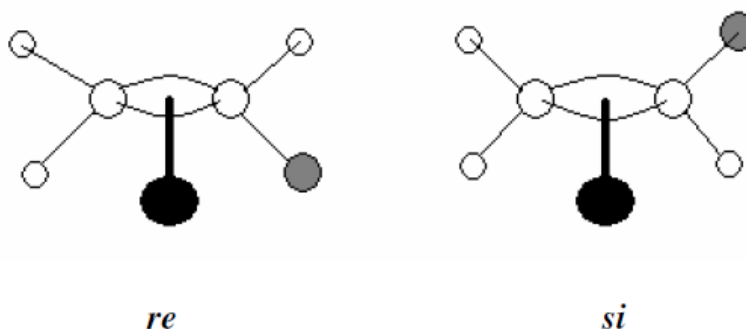


Figure 2.11. Different coordination modes of a propene molecule (*rectus* or *sinister*) on the metal atom (in black is the metal atom, in grey the methyl of the propene).

In general, the asymmetric induction is driven by the coupling either of the factors 1-3 (site control mechanism) or of the factors 2-3 (chain end control).

It has been long debated about the sources of information concerning the mechanism of steric control that the ZN catalysts can exert; from the microstructural studies on macromolecules, the best source of information is constituted by *stereodefects*. The analysis of stereodefects can, for instance, discriminate between the two situations listed before, i.e. the site control mechanism or the chain end control mechanism. It is possible to start considering the kind of stereodefects generated by the chain end control in the synthesis of a predominantly isotactic polymer: over a long sequence of *m* diads, an error occurs and generates a racemo diad. The following insertion will lead to another sequence of *m* diads, but the mistake is perpetuated along the chain (polymer chain end control mechanism, figure 2.12 on the left). In case of a site control mechanism, a stereo-mistake is isolated, since the site will force the previous asymmetric induction ‘back on track’ (figure 1.14 on the right).



Figure 2.12. Different microstructural patterns for the two stereocontrol mechanism for the ZN polymerization of 1-alkene, chain end control on the left and site control mechanism on the right.

As we said before, ^{13}C NMR is the election technique for polyolefin microstructural characterization; a good proof is given by the ability of this technique to discriminate between these two stereocontrol mechanisms at *pentad* level. In the analysis of the methyl region of a predominantly isotactic PP obtained under chain end control, in addition to the *mmmm* pentad (from an ‘error free’ region of the chain), there will be the pentads *mmmr* and *mmrm* in a 1:1 ratio; on the other hand, if the polymer chain had been produced under site control, in addition to the *mmmm* pentad, the presence of the pentads *mmmr*, *mmrr* and *mrrm* would have been detected in a ratio 2:2:1¹⁹.

2.6 – Origin of the stereocontrol in metallocene ZN catalysis, the active-centre symmetry/polymer tacticity relationship.

As was said before in § 2.3, the invention of the metallocene catalysts provided the unique opportunity to have a well defined active centre, due to the proper synthesis of the ligand framework. As from figure 2.3 the number of complexes published until today is very high,

nevertheless it is possible to do a classification of all the complexes according to the symmetry around the metal, as was done by Farina (figure 2.13)²³.

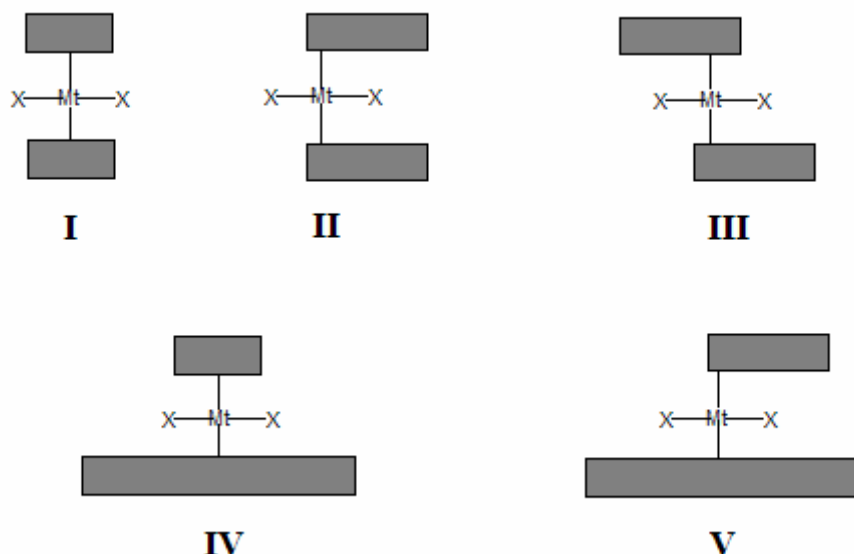


Figure 2.13. Schematic classification of the five metallocenes classes of symmetry, according to Farina.

The site of the reaction for the polymerization is the σ M-C bond and the olefin is coordinated to a coordination vacancy at the metal; after the activation of this complexes²⁴ (*vide infra*) the position of reaction are the ones where the X atoms lie on figure 2.13, leaving, in general, the remaining ligand framework untouched. It is easy to classify the five classes according to the symmetry of the complexes systematically²³:

1. Class I : the symmetry of the general complex belongs to the point group C_{2v} , the two X sites are equal to each other, the remaining ligand framework is not able to force the chain in a chiral orientation, the sites are not chirotopic;
2. Class II : the two X sites are different from each other, nevertheless unable to provide any asymmetric orientation to the polymer chain (*meso*- C_2 symmetry – non-chirotopic sites);
3. Class III : the two X sites provide an asymmetric orientation of the chain, the symmetry element providing the relationship between them is a binary axe (C_2 symmetry – homotopic sites);
4. Class IV : an asymmetric orientation of the chain is provided by both the X sites, the symmetry correlation between them being a mirror plane (C_s symmetry – enantiotopic sites);
5. Class V : the asymmetric orientation of the chain is provided only by one of the two X sites, no symmetry correlation exists between them (C_1 symmetry – diastereotopic sites).

The origin of stereocontrol had been elucidated by Corradini and co-workers²⁵, both for the heterogeneous catalysts and the homogeneous counterparts; this is one more example that polymer microstructure and polymerization kinetic always go ‘hand in hand’. In figure 2.14 a model of an heterogeneous catalyst is reported along with the model of a metallocene one during an insertion of a propene molecule.

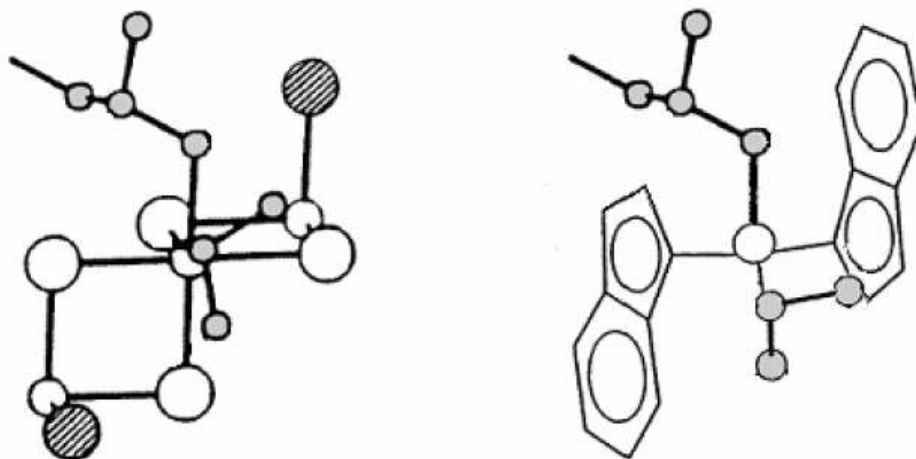


Figure 2.14. Model of isotactic-selective active species, the representation is made for the heterogeneous ZN catalysts and the bis-indenyl metallocenes of class III of figure 2.13.

As it is possible to see from figure 2.14, the indenyl ligand of the metallocene ‘forces’ the chain to bend in a chiral direction (the same holds for the Cl atom on a surface of a ZN catalysis in the case of an isotactic selective active center); therefore the monomer inserts to the M-C with the methyl moiety *anti* respect the C-C bond of the polymer chain, in order to minimize the non-bonded interaction during the transition state of the insertion (according to figure 2.14, the enantioface of the propene molecule is *re*). After the insertion, the minimum nucleus movement principle ensures that the chain is occupying the place of the monomer (migratory insertion); since the sites are homotopic by symmetry, the propene molecule will insert always with the *re* enantioface; the tacticity is, therefore, uniquely determined and the polymer is isotactic, as it is confirmed from the microstructural studies¹⁹. This stereocontrol mechanism is completely general for class III metallocene, whereas the extent of the isotacticity of the polymer, is strictly dependent on the precise structure of the ligand framework.

This being elucidated, it is straightforward to predict the polypropylene tacticity arising from a metallocene of class IV; from a quick glance of figure 2.15, the ligand framework is able to orient chirally the chain, the propene molecule coordinates at the metal pointing the methyl in *anti* position with respect the first C-C bond of the chain. The two active sites of the catalyst are

enantiotopic, meaning that the sequence of insertion, *as far as each insertion step is migratory in nature (i.e. kinetic regime)*^{25,19}, will choose specular images of the prochiral olefin: the resulting polymer is, therefore, syndiotactic.

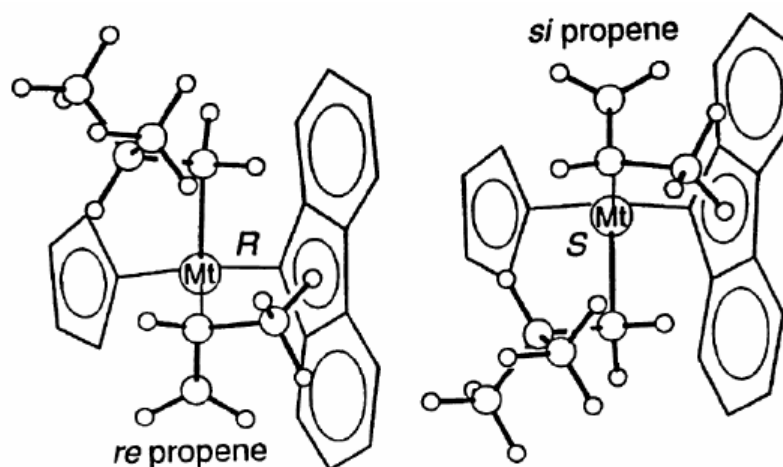


Figure 2.15. Models for the active species of a class IV metallocene; the polymer chain is chirally oriented and, as far as the chain always changes the position after each insertion, opposite coordinations of the propene occur; the polymer results, therefore, syndiotactic.

The case of the class V metallocene is more complicated, since only one site can provide the chiral orientation of the chain, the tacticity of the resultant polymer is not easy to understand *a priori*. Nevertheless, the experimental condition and the polymerization kinetic regime can provide, along with the microstructural analysis of the polymer, the right correlation between polymer tacticity and metallocene symmetry¹⁹.

2.7 – Activation of metallocene precursors, a brief account.

As was said before, the active site of the ZN catalysis, both in heterogeneous and in homogeneous phase, is a σ M-C in which a monomer molecule is able to insert. Concerning the metallocene catalysts, the propagating molecule is an alkylated cation with a coordination vacancy able to coordinate the monomer prior to the insertion; the general metallocene L_2MX_2 ($L = h^5$ ligand framework, $X = h^1$ Cl or R substituent) has to be activated to yield a cation and, whether the h^1 ligand is not an alkyl, a σ M-C bond needs to be provided: the treatment of the complex with a suitable co-catalyst is therefore necessary²⁴.

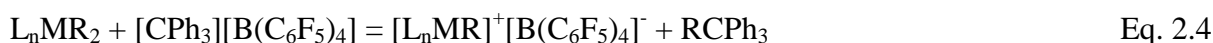
The first co-catalyst was discovered by serendipity, as was said in § 2.3: the ‘controlled’ hydrolysis of $AlMe_3$ brought to synthesis of methylalumoxane (MAO)²⁴; before that, the co-catalyst were adopted directly from the heterogeneous ZN catalysis, with poor results. The structure of MAO has not been elucidated yet, but still the evidences point to a polymeric structure of the repetitive unit

Chapter 2 – Ziegler-Natta Catalysis, a brief account.

$[\text{Al}(\text{CH}_3)\text{O}]_n$, being the Al based polymer a wide distribution of cage-like agglomerates, with different dimensions and always in equilibrium with remaining free AlMe_3 ²⁴. The activation reaction can be written as a Lewis acid-base reaction, like in equation 2.1:



The activation yields an ion couple and, since the cations are very susceptible of being attacked by any donor atom, the solvent must be as ‘innocent’ as possible (usually is an aromatic or an aliphatic hydrocarbon). The success of the MAO compared to the usual Al-alkyls relies in the fact that the cage structure enables the dispersion of the negative charge on the whole structure, rather than specific atoms: this ensures the ion couple to be loosely associated, thus leaving enough space to the monomer to coordinate to the metal coordination vacancy and engage the insertion in the M-C bond. From this results, and knowing that the anion must be poorly coordinative, several activators were designed, different with respect the MAO. This is the case of the boron based activators, i.e. the $\text{B}(\text{C}_6\text{F}_5)_3$, the protic activator $[\text{PhNMeH}][\text{B}(\text{C}_6\text{F}_5)_4]$ and the Lewis activator $[\text{CPh}_3][\text{B}(\text{C}_6\text{F}_5)_4]$ ²⁷. The activation of a metallocene brings to the active ion couples, as is described by equations 2.2 ÷ 2.4:



The use of the compound $\text{B}(\text{C}_6\text{F}_5)_3$, brings to a more coordinative anion with respect the other two boron based salts, since the alkyl moiety R can be polarized toward the coordinative unsaturation of the metal^{24,26}; the other two salts bring to exactly the same ion couple, however the mechanism of ligand abstraction is different: in equation 2.3 a Brønsted acid-base reaction occurs (the dimethyl aniline is usually harmless to the ion couple), while in equation 2.4 a Lewis acid-base reaction is described.

The use of a certain co-catalyst with respect the others is generally dependent on the particular application of interest for the catalysis; both systems have pros and cons. The MAO, as said in § 2.4, has the advantage to both alkylate the complex and perform the ligand abstraction in the activation, moreover the reactivity of the Al-CH₃ bonds toward O₂, H₂O and ubiquitous impurities, protects the active couple from the deactivation by impurities (it is used to refer to this protection as *Al-scavenging*). Unfortunately, for reasons still to be clarified yet, the effectiveness of MAO is only

guaranteed when it is used in large excess respect to the catalysts ($[Al]/[M] \approx 10^2\text{-}10^4$), thus enhancing the costs (and lowering the atom economy). The boron based salts are therefore cheaper, since the reaction is stoichiometric with the active metal and only a slight excess is, possibly, needed ($[B]/[M] \approx 1.0\text{-}2.0$); nevertheless the catalyst precursor must be pre-alkylated to afford the M-C bearing molecule for the catalysis. In order to pre-alkylate the complex, it is common practice to use Al^iBu_3 as a third component in the activation; if used in a 'fair' excess with respect the metallocene ($[Al]/[M] \approx 10\text{-}10^2$), the Al^iBu_3 provides both the alkylation of the complex and the scavenging of the reactor; unfortunately the Al^iBu_3 can be aggressive toward the ion couple reducing the active metal (mostly Ti based catalysts) or providing a chain transfer route in polymerization (*vide infra*).

2.8 – Chain transfer processes.

In conclusion to this quick overview of the ZN catalysis, it is necessary to provide a brief paragraph concerning the chain transfer phenomena and mechanism that have been documented in the ZN catalysis.

In general, the ZN catalysis is not living; this would imply a major technological drawback since the number of polymer chains produced should be equal to the number of moles of the catalyst employed. Even though very high molecular masses for the polymer chain can be afforded (M_n in the order of 10^6 Da), many chain transfer processes have already been documented (figure 2.16).

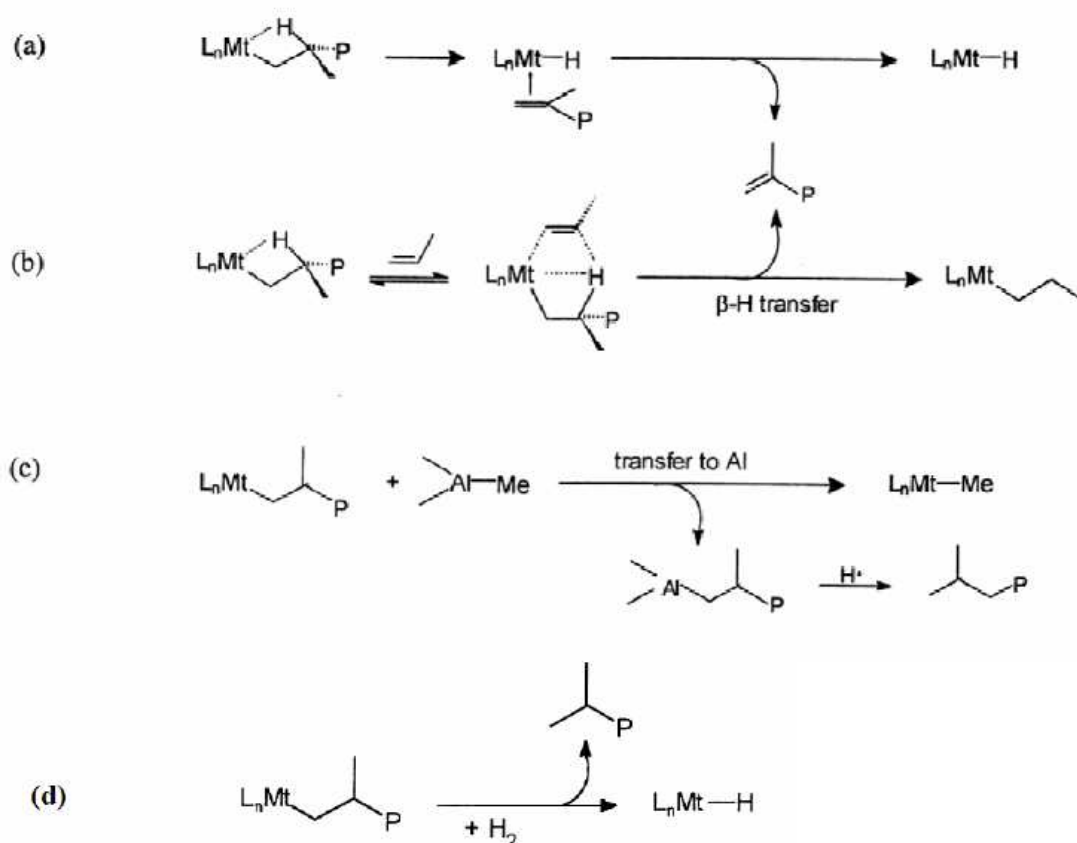


Figure 2.16. Chain transfer processes for the ZN catalysis.

In general, the most important processes are the a and b entries of figure 2.16, a β -H abstraction from the polymer chain, which can be either an intramolecular reaction (figure 2.16-a) or assisted by the monomer (figure 2.16-b). In general the monomer assisted β -H abstraction is the most wide spread, especially with the heterogeneous catalysts; this notwithstanding the intramolecular pathway is more favorable entropically and typically occurs when the monomer assistance is unavailable (low monomer concentration, close ligand framework)^{27,28}. The terminal group produced with both the monomer assisted and the intramolecular β -H elimination are identical, nevertheless it is possible to discriminate the mechanism within the polymerization kinetic²⁷ (chapter 3 and 6, *vide infra*).

A less common pathway is the chain transfer to the Al co-catalyst via trans-alkylation, practically absent with the heterogeneous ZN catalyst, but relevant with the homogeneous catalyst, especially when the activity is low¹⁹.

A most facile pathway is the chain transfer mechanism with hydrogen (σ bond metathesis); needless to say that in the industrial plants the molecular hydrogen is added on purpose in order to control the molecular weight of the polymer and, hence, the product processes²⁹.

References

- [1]. From the Presentation Speech by Professor A. Fredga, member of the Nobel Committee for Chemistry of [the Royal Academy of Sciences](#)); [Nobel Lectures](#), Chemistry 1963-1970, Elsevier Publishing Company, Amsterdam, 1972.
- [2]. a) Boor, J. *Ziegler Natta Catalysts and Polymerization*, Academia press, New York, 1979; b) Resconi, L.; Cavallo, L.; Fait, A.; Piemontesi, F.; *Chem. Rev.* **2000**, *100*, 1253-1345.
- [3]. Cotton, A.; Wilkinson, G. *Advanced Inorganic Chemistry*, John Wiley and Sons, Third edition 1972, page 815.
- [4]. German. Pat. Appl. 2663143 Montedison and Mitsui Petrochemical 1975.
- [5]. Albizzati, E.; Giannini, U.; Morini, G.; Galimberti, M.; Barino, L.; Scordamaglia, R. *Macromol. Symp.* **1995**, *89*, 73.
- [6]. Busico, V.; Cipullo, R.; Pellecchia, R.; Rongo, L.; Talarico, G.; Macchioni, A.; Zuccaccia, C.; Froese, R.D.J.; Hustad, P.D. *Macromolecules* **2009**, *42*(13), 4369-4373.
- [7]. Natta, G.; Pino, P.; Mazzanti, G.; Giannini, U. *J. Am. Chem. Soc.* **1975**, *79*, 5072.
- [8]. (a) Breslow, D.S. US Pat. Appl. 537 039 (1955); (b) Beslow, D.S.; Newburg, N.R. *J. Am. Chem. Soc.* **1957**, *79*, 2975.
- [9]. Reichert, K.H.; Meyer, K.R.; *Makromol. Chem.* **1973**, *169*, 163.
- [10]. Sinn, H.; Kaminsky, W.; Vollmer, H.J.; Woldt, R. *Angew. Chem.* **1980**, *92*, 396 and *Angew. Chem. Int. Ed. Engl.* **1980**, *19*, 396.
- [11]. Natta, G.; Corradini, P.; Bassi, I.W.; Porri, L. *Atti Accad. Naz. Lincei, Rend. Sc. Fis. Mat. E Nat.* **1958**, *24*, 121.
- [12]. Cossee, P.; *The mechanism of Ziegler-Natta polymerization. II. Quantum Chemical and crystal-chemical aspects*. In: The stereochemistry of macromolecules, Ketley AD editor, Marcel Dekker, New York, 1967, vol.1.
- [13]. Rodriguez, L.A.M.; Van Looy, H.M. *J. of Polym. Sci., Polym. Chem. Ed.* **1966**, *4*, 1951.
- [14]. Natta, G.; Farina, M.; Peraldo, M. *Chim. Ind. (Milan)* **1960**, *44*, 173
- [15]. Zambelli, A.; Giongo, M.G.; Natta, G. *Makromol Chem.* **1968**, *112*, 183; Miyazawa, T.; Ideguchi, *J. Polym. Sci., Part B*, **1963**, *1*, 389.
- [16]. a) Natta, G. *Atti Accad. Naz. Lincei, Mem., Cl. Sci. Fis. Mat. Nat., Sez. 2a* **1955**, *4*, 61. b) Natta, G.; Corradini, P. *Atti Accad. Naz. Lincei, Mem., Cl. Sci. Fis. Mat. Nat., Sez. 2a* **1955**, *4*, 73.
- [17]. a) Natta, G.; Corradini, P. *Rend. Accad. Naz. Lincei*, **1955**, *19*, 229. b) Natta, G.; Corradini, P. *J. Polym. Sci.*, **1955**, *20*, 251.
- [18]. Farina M. *Topics Stereochem* **1987**; *17*, 1.

- [19]. Busico, V.; Cipullo, R. *Progr. Polymer Sci.* **2001**, 26, 443-533, and references therein.
- [20]. Mislow, K.; Siegel, J. *J. Am. Chem. Soc.*, **1984**, 106, 3319.
- [21]. Bovey, F. A. *High Resolution NMR of Macromolecules*; Academic Press: New York, 1972.
- [22]. Corradini, P.; Paiaro, G.; Panunzi, A. *J. Polym. Sci., Part C*, **1967**, 16, 2905.
- [23]. Farina, M. *Makromol. Chem., Macromol. Symp.* **1995**, 89, 489.
- [24]. Chen, E.Y.Y.; Marks, T.J. *Chem. Rev.* **2000**, 100, 1391.
- [25]. Corradini, P.; Busico, V.; Cavallo, P.; Guerra, G.; Vacatello, M.; Venditto, V. *J. Mol. Catal* **1992**, 74, 433.
- [26]. Bochmann, M.; Lancaster, S.J.; Hurtshouse, M.B.; Malik, K.M.A.; *Organometallics* **1994**, 13, 2235-2243; Correa, A.; Cavallo, L., *J. Am. Chem. Soc.*, **2006**, 128, 10952-10959.
- [27]. Stehling, U.; Diebold, J.; Kirsten, R.; Röhl, W.; Brintzinger, H.H.; Jungling, S.; Mülhaupt, R.; Langhauser, F. *Organometallics* **1994**, 13, 964.
- [28]. Margl, P.; Deng, L.; Ziegler, T. *J. Am. Chem. Soc.* **1999**, 121, 154.
- [29]. Tsutsui, T.; Kashiwa, N.; Mizuno, A. *Makromol. Chem. Rapid Commun.* **1990**, 11, 565; Busico, V.; Cipullo, R.; Chadwick, J.C.; Modder, J.F.; Sudmeijer, O. *Macromolecules* **1994**, 27, 7538; Talarico, G.; Budzelaar, P.H.M., *Organometallics*, **2008**, 27, 4098-4107.

3.1- Introduction.

As stated in chapter 1, the amidinato catalysts are well suited for the HTS techniques since the complex synthesis is bound to follow general paths¹. This notwithstanding a proper screening cannot be afforded without the detailed knowledge of the catalyst behaviour during the polymerization process. In this chapter we will assess the general behaviour of a prototypical amidinato catalyst (referred to as **C0**) with specific emphasis on the study on the chain transfer mechanisms. Besides the molecular structure of the catalyst studied (of the type of figure 3.1), on which we cannot be explicit due to confidentiality, the mechanistic studies are aimed to define the general behaviour in copolymerization, in order to put the basis for the copolymerization kinetic rationalization and HTE protocol development.

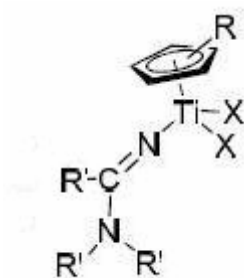


Figure 3.1. General structure of an amidinato complex (**C0** was studied in this work).

3.2 - Processes that control polymer molecular weight with the amidinato complexes.

The choice of increasing the temperature is never easy for an industrial processes, nevertheless, for olefin polymerization in solution, high temperatures are beneficial in order to decrease the viscosity of the liquid phase and enhance the monomer conversion in the plant reactor²; unfortunately at higher temperature, the molecular weights of the polymer have the tendency to shorten, due to the higher activation energy of a termination process compared to the growth of a polymer chain³.

The mechanistic study of copolymerization is known to be in general a tough task⁴: indeed it is hard to identify, both with experiments and *in silico*, the rate limiting step and model the results. As a starting point to study the catalyst behaviour, an easier process must be studied, i.e. the homopolymerization (both of ethene and propene) with the complex **C0**, eventually checking whether or not the information gained could be generalized to the whole copolymerization process.

The first choice was to look at the ‘simple’ ethene homopolymerization. Despite the fact that the rate limiting step is unknown for such a process, we tried to test the prototype catalyst in our high-throughput screening platform Freeslate PPR48^{®5} (*vide infra*, chapters 4 and 5), in order to assess the activity for the complex **C0**. The results we obtained from the very first preliminary test were unsatisfactory, the kinetic assessment proved to be impossible to be carried out, due to the extremely high activity of the catalyst; in a 5mL reactor only poorly controlled polymerizations were attained, injecting 0.5 nmol of catalyst, without a decent reproducibility (*vide* chapter 4, RSD $\geq 40\%$).

On the other hand, the system is very well behaved with propene (Figure 3.2) even at a relatively high temperature, thus enabling us to extract some pieces of information on the mechanistic behaviour these complexes feature.

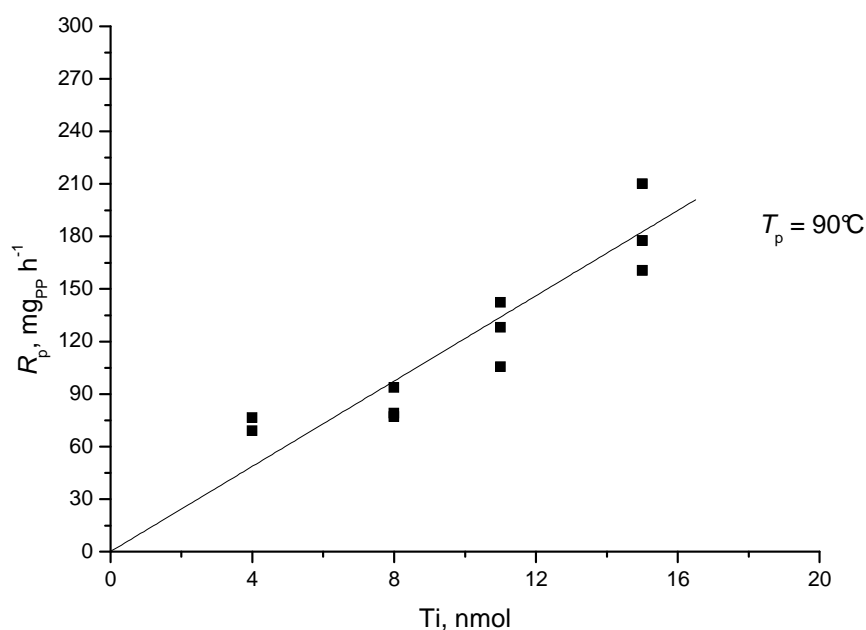


Figure 3.2. Propene homopolymerization control in the Freeslate PPR^{®5} platform with the **C0** catalyst.

A typical ¹³C NMR spectrum of polypropylene sample from the complex **C0** in the methyl region is shown in Figure 3.3. On inspection, it can be seen that the polymer is predominantly atactic, just moderately enriched in syndiotactic diads, similar to what occurs with CGC catalysts⁶ in propene homopolymerization. Quantitative analysis of the stereosequence distribution pointed out a mild chain-end stereocontrol, 2nd-order Markov statistic yielding the best-fit. The regioregularity is only moderate (1.5 ± 0.5 mol% of regiodefects); moreover the addition of ethene to the polymerization system changes dramatically the polymerization kinetic; i.e. the activity raises and the polymer microstructure changes, especially regarding the end-group analysis.

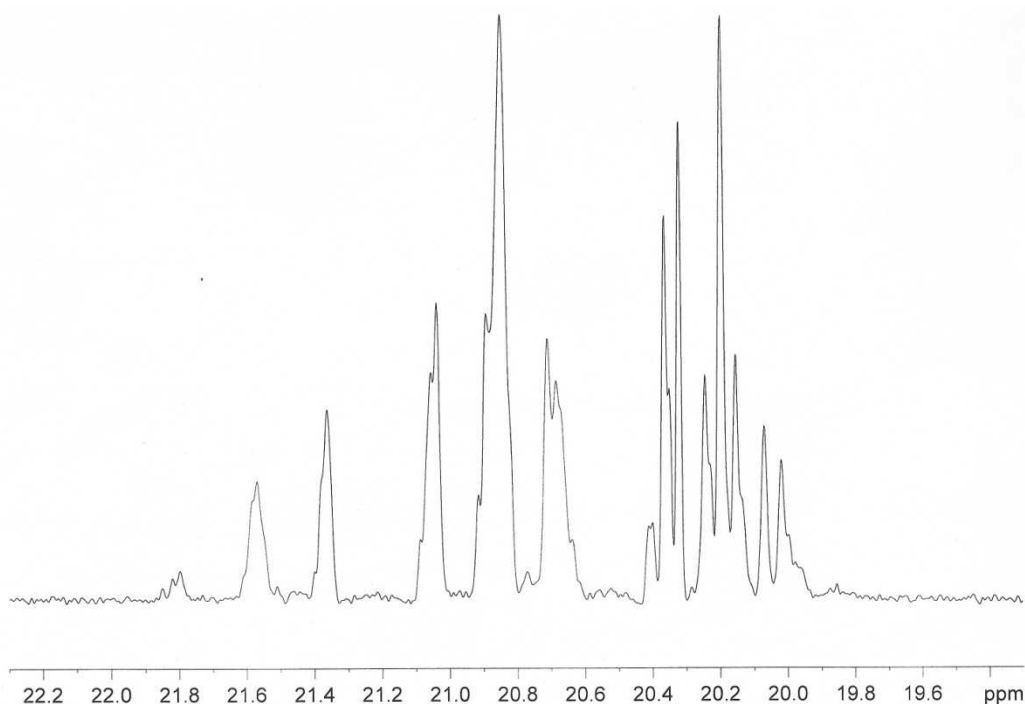


Figure 3.3. ^{13}C NMR spectrum, methyl region, of a PP sample obtained with catalyst **C0**.

A typical comparison of the olefinic pattern of the ^1H NMR spectra of a PP sample produced with catalyst **C0**, with respect two spectra of EPR-like copolymers is shown in Figure 3.4.

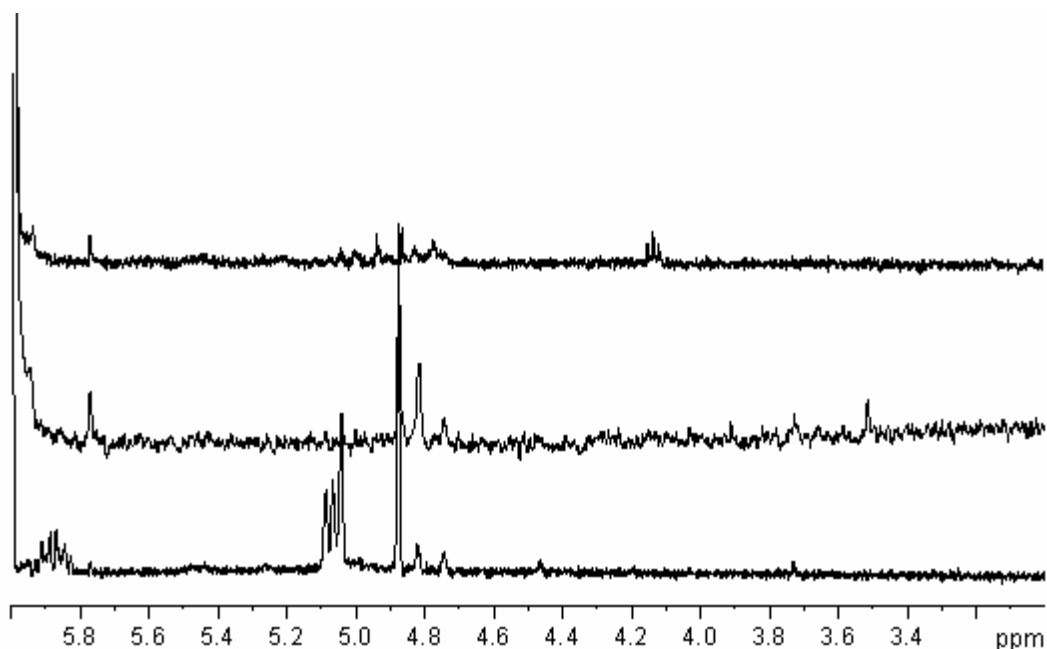


Figure 3.4. Olefinic region of the ^1H NMR spectra for PP sample (bottom) with respect EPR-like copolymers (top).

From the olefinic region is quiet clear that the chain termination mechanism changes from propene homopolymerization to ethene/propene copolymerization; this aspect, combined with the different catalyst activity, is a strong evidence of a peculiar catalyst behaviour with substituted 1-alkene; from the inspection of the PP sample, it is possible to detect that chain termination occurs also after secondary propylene units, being the pattern diagnostic of precise terminal structures⁷.

The absence of olefinic terminals arising from propene 2,1 last insertion in ethene/propene copolymers signals that ‘dormant chains’ exist during propene homopolymerization, thus the kinetic assessment of the catalyst in homopolymerization is not representative of the whole copolymerization process. Nevertheless, the higher number of olefinic chain terminations signals that propene homopolymerization may represent ‘the worst scenario’ for a chain to grow with this catalyst.

For this reason, we decided to study the PP microstructure and MWD obtained from catalyst **C0** at different propylene concentration in the liquid phase⁸, thus finding an unexpected behaviour of this complex. The polymerizations were carried out according to the procedure described in the experimental section and the results are summarized in table 3.1.

Table 3.1. Polymerization results for catalyst **C0** in homopolymerization of propene at different monomer concentration, co-catalyst = [HMe₂NPh][B(C₆F₅)₄], $T_p = 90^\circ\text{C}$, $t_p = 1\text{h}$.

Entry	$n_{\text{(Ti)}}$ (μmol)	$n_{\text{(B)}}$ (μmol)	$P_{\text{C}_3\text{H}_6}$ (bar)	$[\text{C}_3\text{H}_6]^{(1)}$ (M)	Yield (mg)	$Y_p^{(2)}$	$M_n^{(\text{GPC})}$ (KDa)
1	7.5	18.2	0.83	0.21	897	570	12.5
2	7.7	15.7	0.61	0.15	1900	1600	8.4
3	9.1	16.0	0.12	0.03	199	730	5.0

(1) Evaluated using the equation $[\text{C}_3\text{H}_6] = P_{\text{C}_3} \times 2.72 \times 10^{-3} \times \exp(3260/1.98T_p)^{9a}$.

(2) $\text{Kg}_{\text{PP}} \text{mol}_{\text{Ti}}^{-1} [\text{C}_3\text{H}_6]^{-1} \text{h}^{-1}^{9b}$.

The degree of polymerization can be written according to the equation below, adapted from the one derived by Natta and Pasquon¹⁰:

$$P_n = M_n/M_0 = k_p[\text{C}_3\text{H}_6]/(k_t[\text{C}_3\text{H}_6] + k'_t + k''_t[\text{Al}]^{0.5}). \quad \text{Eq.3.1}$$

In the equation (3.1) the term on the numerator refers to the chain propagation, whereas the three terms at the denominator refer respectively to the processes of chain transfer to the monomer, to the active metal and to the Al-alkyl. From the results of table 1, it is evident that the M_n of the produced PP (and hence the P_n) decreases with the lowering of the monomer concentration, and this signals that the only term significant in the chain transfer mechanism is k'_t ; the main process of chain transfer is therefore β -H transfer to Ti¹¹ (chapter 2, paragraph 2.8). From the ¹H NMR spectra of the

polymers of entries 1 and 3 of table 1 it is possible to detect the olefinic chain ends of the polymer after the β -H transfer to the Ti atom¹² (figure 3.5).

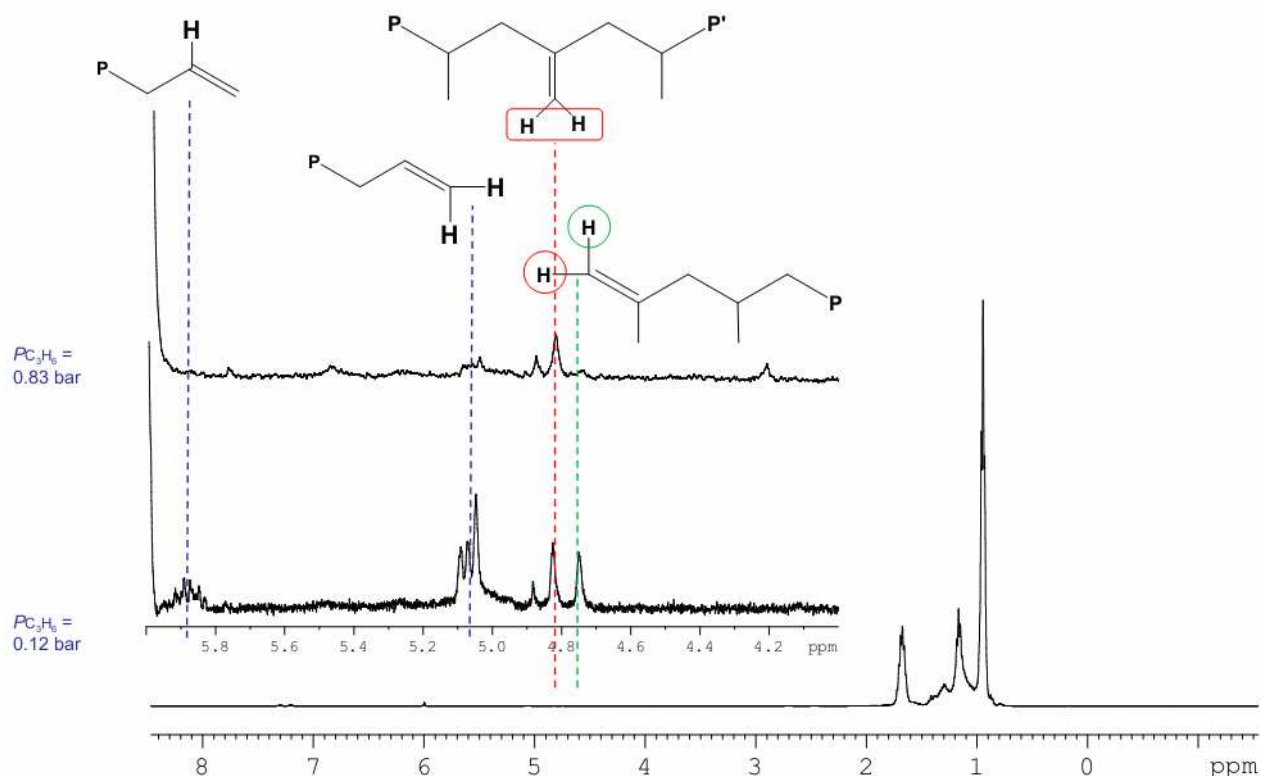


Figure 3.5. Olefinic region of ¹H NMR spectra of entries 1-3 of table 2.1.

From the chain end analysis, it is clear that the chain transfer occurs both after a 2,1 propylene last inserted unit (allyl termination - $\delta = 5.10$ -2H and $\delta = 5.90$ -1H) and/or after a 1,2 propylene last inserted unit (vinylidene termination $\delta = 4.75 - 4.82$). It is worthwhile to note that the intensity of all the termination signals fades out when increasing the monomer pressure, except the signal at $\delta = 4.82$ ppm; this is due another olefinic structure present in the polymer, whose signal overlaps with one of the vinylidene structure¹². This internal vinylidene is due to allylic activation of the polymer chain by the catalyst, with H₂ release¹² (figure 3.6).

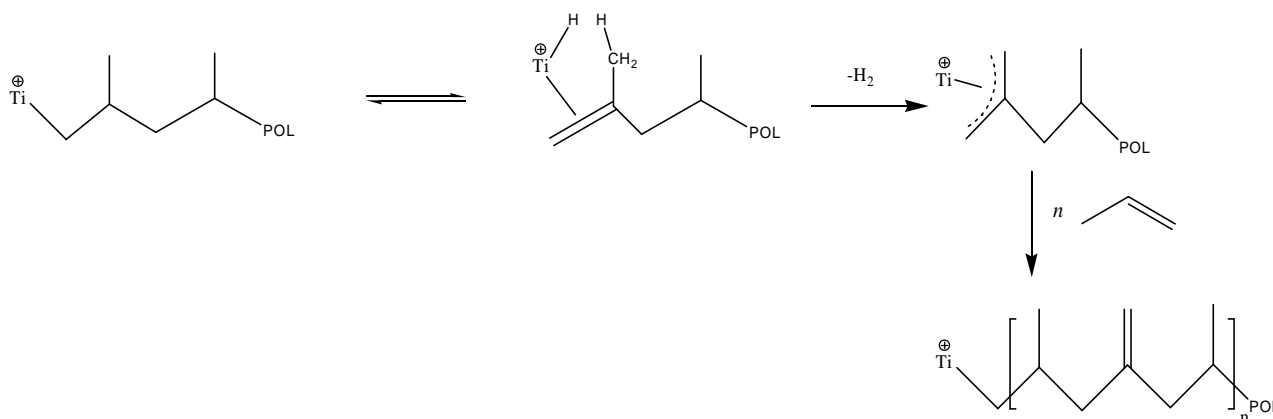


Figure 3.6. Proposed mechanism for the allylic activation of a 2,1 last inserted unit, the ligand framework is omitted¹³.

From the ¹H NMR characterization the olefinic pattern was resolved in order to establish the precise mechanism of chain transfer, moreover the comparison between the *P_n* obtained by ¹H NMR is a double check on the consistency of the mechanism. The results are consistent in the direct proportionality between the average degree of polymerization *P_n* and the monomer concentration; unfortunately the inconsistency relies on the slope of the two lines, being the one from the ¹H NMR evaluation far higher than the one from the GPC measurement (figure 3.7).

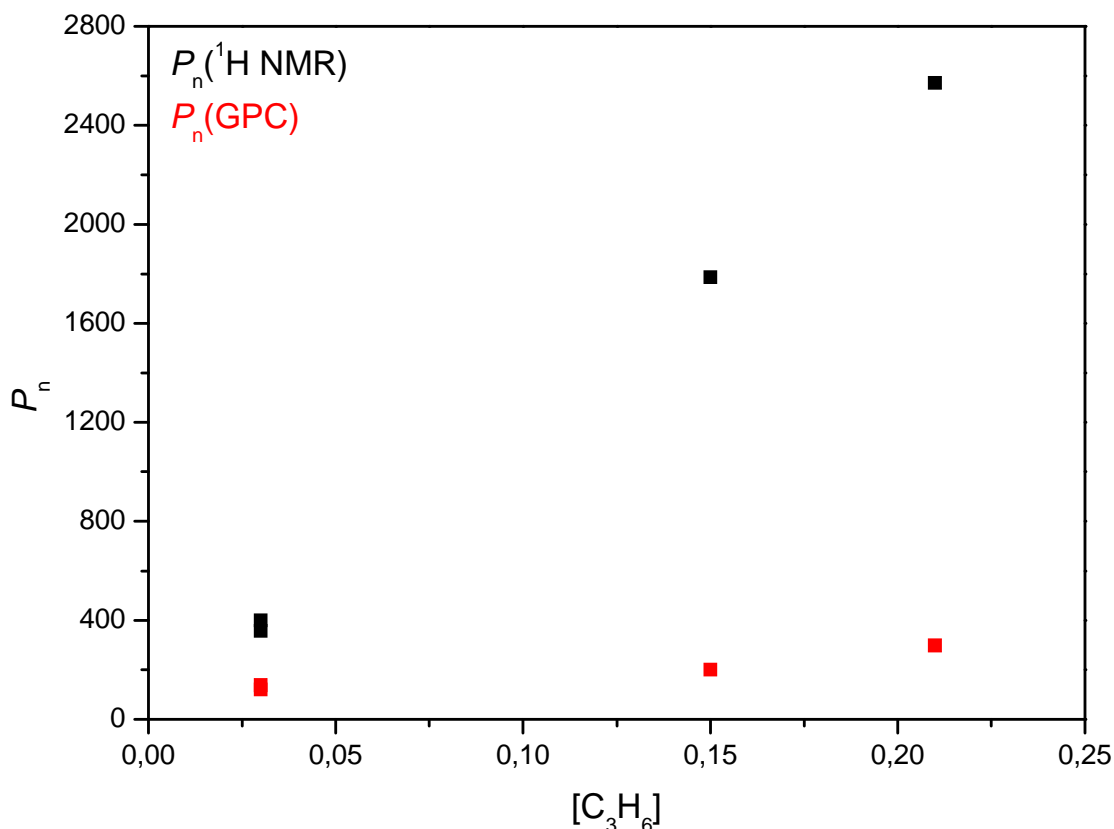


Figure 3.7. Direct proportionality between *P_n* and [C₃H₆] for the PP produced with the C0 catalyst (red- GPC measurement; black- ¹H NMR measurement).

This discrepancy signals that β -H transfer to the Ti is not the only chain transfer pathway occurring under the inspection conditions; the investigation of the saturated and additional chain-end structures with ^{13}C NMR revealed, therefore, to be mandatory. From the ^{13}C NMR spectra, the total amount of saturated chain ends in the spectra overwhelms the ones that are expected to arise after the insertion of a propene molecule in a Ti-H bond, i.e. in consequence of the process of β -H transfer to the Ti (figure 3.8).

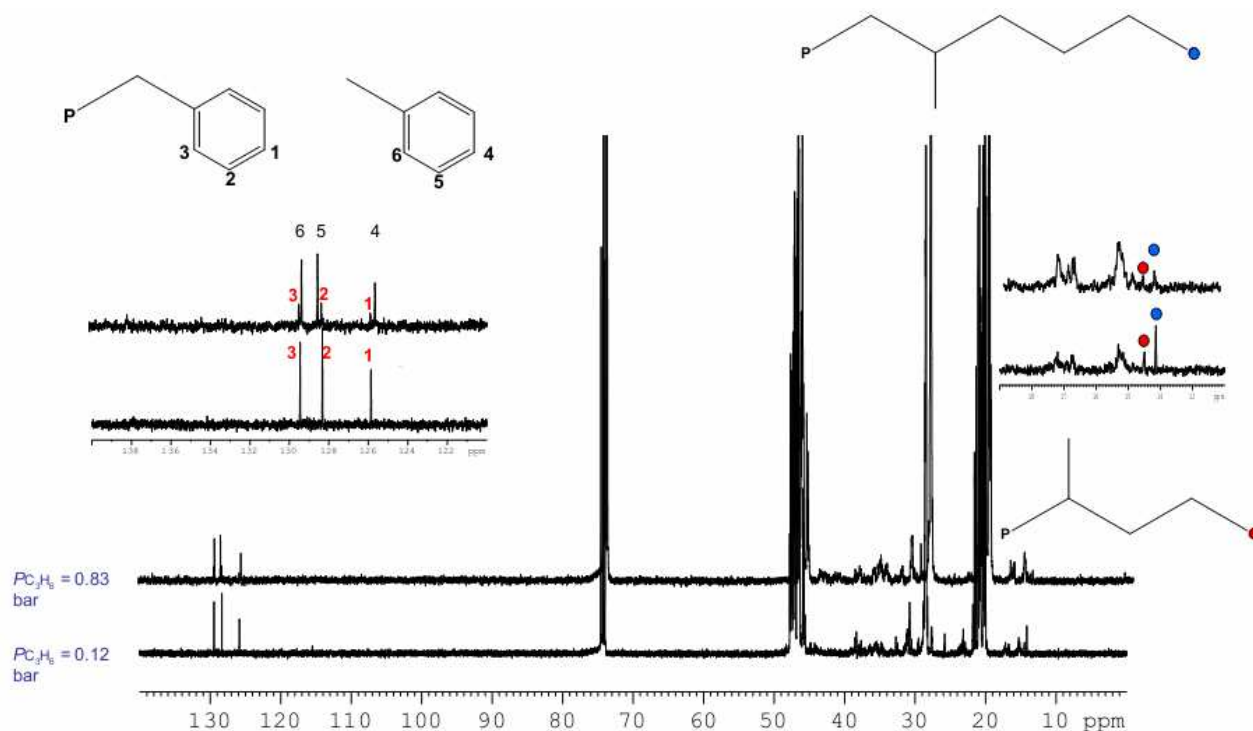


Figure 3.8. ^{13}C NMR spectra at different propene pressure; the benzyl and saturated ends regions are enlarged for sake of clarity.

From the identification of chain end signals in the ^{13}C NMR spectra of the polymers, it is possible to detect n propyl ends, n butyl ends and, most interestingly, benzyl ends.

From the integration of the spectra (both the ^1H and the ^{13}C), it was possible to balance the amount of the chain ends, thus obtaining the following relationships:

$$[n\text{butyl ends}] > [n\text{propyl ends}]$$

$$[n\text{propyl ends}] \sim [\text{total olefinic chain ends}]$$

$$[n\text{butyl ends}] \sim [\text{benzyl ends}].$$

From the relationships obtained from the ^{13}C NMR spectra of the polymers, it is possible to calculate the dependency of the molecular weight of the polymers from NMR, including all the

unsaturated/saturated chain ends arising from both the ^1H and ^{13}C NMR. The linear trend is retained, moreover the agreement with the GPC data becomes satisfactory (figure 2.7).

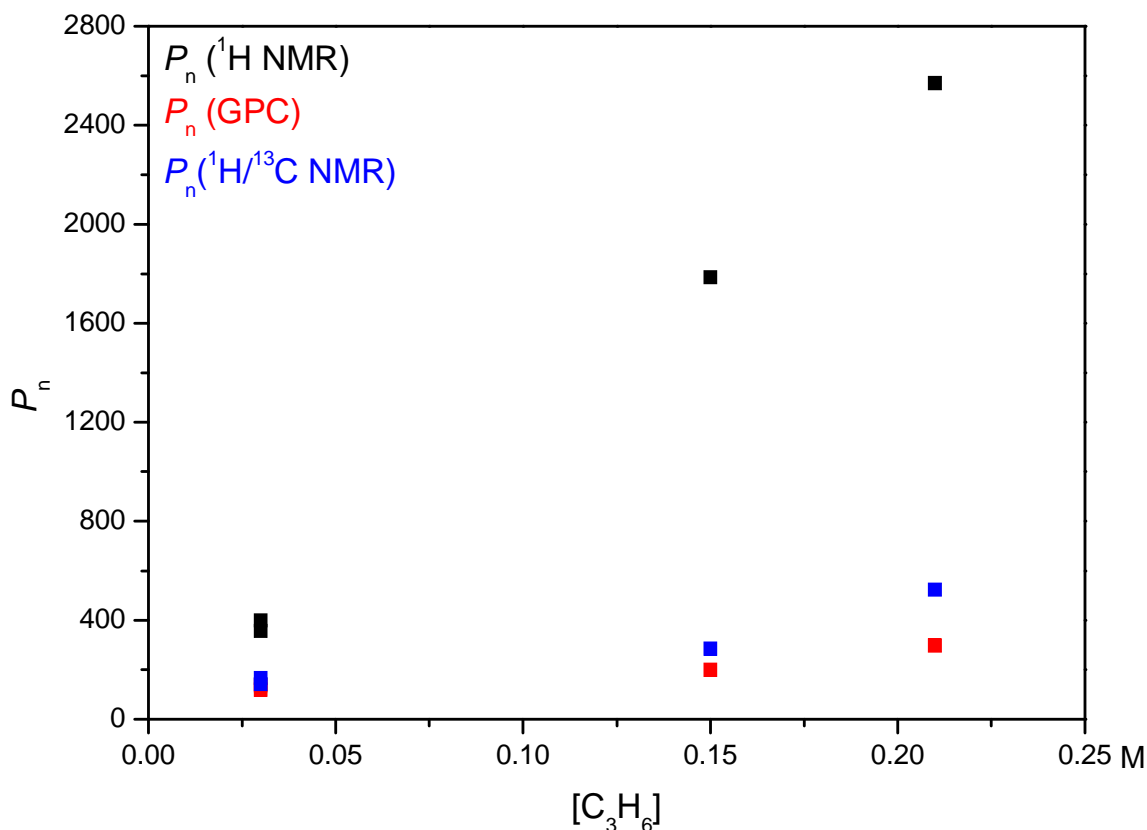


Figure 3.9. Direct proportionality between P_n and $[\text{C}_3\text{H}_6]$ for the PP produced with the **C0** catalyst (red - GPC measurement; black - ^1H NMR measurement; blue - combined $^1\text{H}/^{13}\text{C}$ NMR measurement).

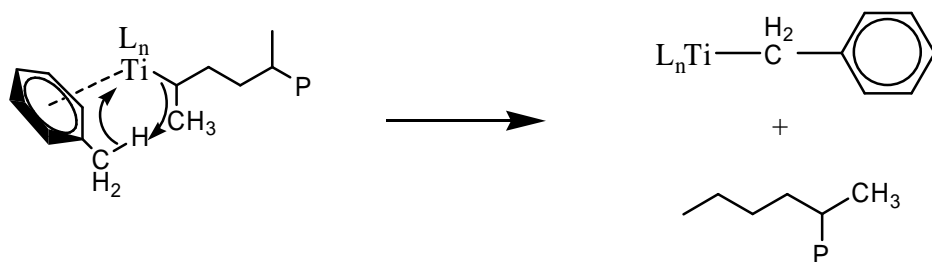
The phenomenon of termination of a chain involving a toluene molecule (which is the polymerization solvent, *vide* experimental section) has, to the best of our knowledge, never been recorded for a polymerization catalyst and a mechanism involving the C–H activation of the toluene methyl moiety could be plausible after a 2,1 propene insertion (scheme 3.1); this mechanism also takes in account the equal molar content of the benzyl and "butyl ends, 'head' and 'tail' of a polypropylene chain arising from this transfer mechanism. Unfortunately, due to the polymer tacticity^{13a}, it is hard to detect the CH_2 resonance for the link between the phenyl ring and the polymer chain.

One more possibility, along with the mechanism of scheme 3.1, is the reactivity of hydride species. It is well known that Ti–H bonds are able to activate C–H bonds of aromatic molecules both in the

ortho position and in activated positions (methyl of a toluene molecule)^{13b,c}; the natural counter-analysis in this specific case is that a Ti-H bond is also extremely reactive toward the insertion.

At the moment DFT calculations are running for the identification of the proper mechanism of toluene activation which, clearly from the experimental evidences, occurs during the propene homopolymerization.

Scheme 3.1. Proposed mechanism for the benzyl C-H activation at the **C0** catalyst after a 2,1 insertion ('dormant' site) at very low monomer concentration.



The subtle reactivity of the 2,1 last inserted propylene units chains toward unexpected reaction in competition with the chain propagation, signals that, as a matter of fact, the reactivity of a Ti bearing a misinserted propylene unit is different from the Ti bearing an usual 1,2 growing chain toward the monomer insertion. This aspect, conceptually linked to the fact that the PP obtained is poorly regioregular with the catalyst **C0**, signals that an accumulation of dormant chain ('catalyst dormancy')¹⁴ can occur during the propene homopolymerization. For this reason, any fundamental study on the amidinato-type catalysts without a proper analysis of catalyst dormancy is meaningless.

3.3 – Catalyst dormancy study on amidinato catalyst **C0**.

From the analysis of the chain ends via ^1H NMR for PP and EPR-like copolymers obtained with catalyst **C0**, it is evident that the polymerization kinetic changes passing from the propene homopolymerization to the EP copolymerization; moreover the process of chain termination involves an intramolecular process, but the last unit is different (a 2,1 propylene unit in the PP homopolymerization, whereas in the ethene/propene copolymer spectra no chain ends arising from 2,1 propylene enchainment are detected). From this starting point, it is evident that in propene homopolymerization a ‘dormant’ pool of active species is present and generated by the lower activity of active centres bearing a last 2,1 propylene insertion. In order to quantify the pool of ‘dormant chains’ the proper kinetic study on this topic was engaged¹⁵.

The fraction of dormant sites is given by equation 3.2:

$$C_s^* = (1 + k_{sp}/k_{ps})^{-1} \quad \text{Eq. 3.2}$$

such a value can be estimated with the ethene/propene copolymerization approach developed by Busico and co-workers¹⁴. The copolymerization results are summarized in table 3.2, in table 3.3 we report the microstructural analysis of the obtained copolymers.

Table 3.2. Ethene/propene copolymerization results for complex **C0**/MAO/BHT at 70°C, $[\text{Al}]/[\text{Ti}] = 500$.

Entry	$[\text{C}_2^-]$ (gas phase, mol%)	$[\text{C}_2^-]/[\text{C}_3^-]$ ⁽¹⁾	Ti (μmol)	Yield (g)	$Y_p \times 10^{-3}$ ⁽²⁾
1	33.0%	0.0910	1.4	2.57	11.0
3	5.0%	0.0096	1.4	1.82	7.8
2	2.5%	0.0047	1.4	2.38	10.2
4	1.5%	0.0028	1.4	2.05	8.8
5	0	0	5.1	3.20	3.7

(1) Estimated in the liquid phase.

(2) $\text{Kg}_{\text{POL}} \text{mol}_{\text{Ti}}^{-1} \text{h}^{-1}$.

Table 3.3. Microstructural analysis of the copolymers obtained with the complex **C0**/MAO/BHT at 70°C in ethene/propene copolymerization.

Entry	$[\text{C}_2^-]$ (gas phase, mol%)	$[\text{C}_2^-]$ (copolymer, mol%)	$Q_{\text{SE}}^{(1)}$ (mol%)	r_E^2	r_P^2	$r_E r_P$
1	33.0%	31.1	2.1	5.0	0.25	1.3
2	5.0%	5.8	1.9			
3	2.5%	3.3	1.5			
4	1.5%	2.3	1.2			

(1) Molar fraction of ethylene units after a 2,1 propylene enchainment.

(2) Estimated according to reference 16.

From the results of table 3.2, it is possible to estimate the ‘upper limit’ amount of 2,1 regiodefects formed in propene homopolymerization; the data points are well fitted by a standard saturation function, the fitting yields a value of 3.1₁ mol% of regiodefects (figure 3.8, from the $Q_E \rightarrow \infty$ limit of the fitting function) as the superior limit that the catalyst can produce in the homopolymerization of propene.

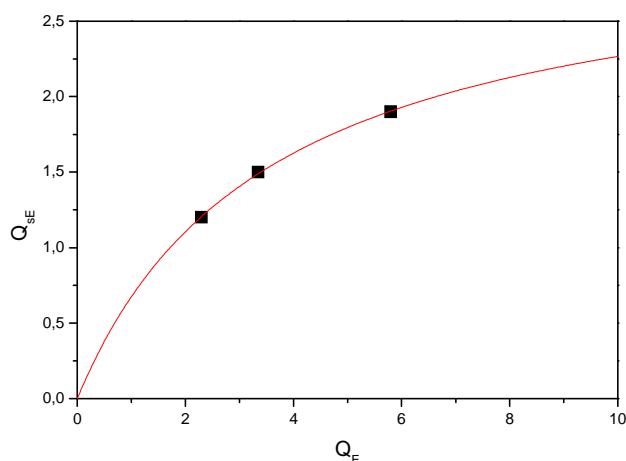


Figure 3.8. Estimation of the upper limit of regiodefects in PP samples produced with catalyst **C0**.

From the dormancy definition, though, the total amount is not informative on the fraction of dormant chains (the total amount of regiodefects gives an estimation of the k_{ps}/k_{pp} ratio); in order to assess this quantitative measurement, it is instead the ratio k_{sp}/k_{ps} that must be evaluated. From the steady-state kinetic analysis, the value of catalyst dormancy can be determined from a plot of the type of figure 3.9, which is the linear plot of the function in equation 3.3:

$$Q_{pE}/Q_{sE} \approx (k_{pE}/k_{sE})(k_{sp}/k_{ps}) + k_{pE}/k_{ps} [E]/[P]. \quad \text{Eq. 3.3}$$

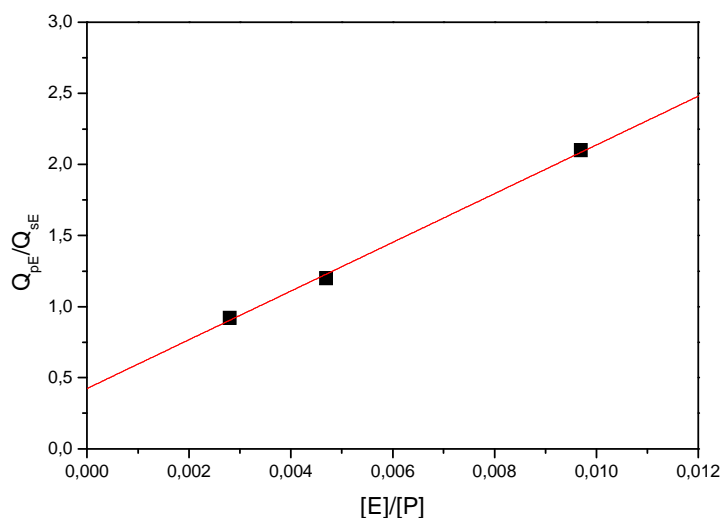


Figure 3.9. Evaluation of dormant chains for the propene homopolymerization with catalyst **C0**.

From the plot of figure 3.9, it is possible to calculate the ratio k_{sp}/k_{ps} , making the assumption that the ratio $k_{pE}/k_{sE} \approx 1$ (which is reasonable since ethene is able to insert ‘well enough’ after both a 1,2 and a 2,1 last inserted propylene unit). The number of the dormant chains is hence $C_s^* \approx 70\%$; even though this could be regarded as a ‘fair’ estimation, it is worthy to note that more than half of the active metal can be ‘dormant’ in propene homopolymerization, after a 2,1 propylene inserted unit. This percentage of dormant chains and the ability of the metal to escape from the dormancy are, of course, strictly dependent on the ancillary substitution framework of the catalyst involved, so the value measured for catalyst **C0** cannot be general for all the catalysts belonging to a certain family; nevertheless an educated guess is that similar dormancy (where ‘similar’ means in the same decade) is expected for similar catalysts within a certain ligand ‘leitmotiv’, i.e. with a donor ligand Y of the same class (amidinato, guanidinato, *et cetera*). This reason simply implies that the propene homopolymerization cannot be used as a representative process to screen the amidinato-type catalyst properly to obtain structure/activity relationships in polymerization.

3.4 – Experimental section.

All the catalyst/co-catalyst handling were performed under N₂ or Ar atmosphere, thus using either Schlenk techniques or glove-boxes MBRAUN Lab Master 130, able to keep the O₂ and H₂O value as low as 1ppm_v.

3.4.1 – HTS Freeslate PPR48[®] ethene and propene polymerization protocol.

HTS polymerization experiments were carried out with a high throughput parallel reactor setup (PPR48[®] available from Freeslate), with six reactor modules each containing eight reaction cells (5 mL working volume per cell). The whole system is housed in a triple MBraun LabMaster glovebox maintaining a pure nitrogen atmosphere (oxygen and water levels <1 ppm_v). The monomer gas and quench gas lines are plumbed directly into the reactors and controlled by automatic valves; ethene or propene is fed after purification by passing through columns containing a mixed bed of 4Å molecular sieves (3.2 mm pellets) and an activated copper catalyst (BASF R 3-11G). Liquid reagents are robotically added to individual cells by syringes. Solvents are previously purified in an MBraun SPS unit.

The cells are fitted with a pre-weighed glass vial insert and a disposable stirring paddle. The reactor is then closed, and 4.10 mL of solvent (HPLC grade from Romil, dried and deoxygenated by passing through MBraun SPS mixed bed columns) and 5.0 µmol of MAO/BHT scavenger (MAO from Chemtura, 10%wt toluene solution, 100 µL of a 50mM solution in toluene, [Al]/[BHT] = 1.0) are injected into each cell through a valve. The reactors are thermostated at 90°C, hence the cells are pressurized with ethene or propene (Rivoira, Polymerization Grade, further purified by passing through Grubbs-type columns) at the desired pressure.

The proper amounts of pre-catalyst and activator (MAO/BHT; [Al]/[BHT] = 1.0, [Al]/[Ti] = 500) are pre-contacted in toluene at RT for 2 min in a 1.2 mL glass vial and then injected in to the cells. The polymerization is run at constant temperature and monomer partial pressure for 20 minutes, then quenched with dry air at 50 psi (3.4 bar) overpressure. The reactors are vented and opened, and the glass inserts are unloaded from the cells, transferred to a centrifuge/vacuum drying unit (Genevac EZ-2 Plus), and dried to constant weight, after which the polymer samples are recovered and weighed on a Bohdan BA-100 Balance Automator unit until constant weight. The experiments of propene homopolymerization are summarized in table 3.4.

Table 3.4. PPR results for the homopolymerization of propene with catalyst **C0**/MAO/BHT. ([Al]/[Ti] = 500; [C₃H₆] = 0.86 M; t_p = 20', T_p = 90°C).

Library Id	Cell	Ti (nmol)	Yield (mg)	R_p (mg _{PP} h ⁻¹)
114460	4E	4.0	25.5	76.5
	4F	4.0	23.0	69.0
	3B	8.0	31.2	93.6
	3E	8.0	26.4	79.2
	3F	8.0	25.7	77.1
	3C	11.0	47.4	142.2
	4C	11.0	42.7	128.1
	4D	11.0	35.2	105.6
	3A	15.0	53.5	160.5
	3H	15.0	70.0	210.0
	4A	15.0	59.2	177.6

3.4.2 – Low pressure propene polymerizations.

All the reactions were carried out in a 500mL Pyrex reactor, equipped with a thermostatic jacket, a magnetic stirrer, a silicone rubber septum, and a gas inlet/outlet, with the following procedure. The reactor, charged under nitrogen with variable amount of dry toluene (130-140mL, Romil, purified by passing through an MBRAUN SPS unit) and 2.0 mmol of MAO/BHT mixture 1:1 ratio (1.3 mL of MAO solution 10%wt and 440mg of BHT), was thermostated at the chosen polymerization temperature (90°C). The reactor was then saturated with propene (accordingly to the final pressure the N₂ gas phase was evacuated or not) and the pressure was checked with GC-FID analysis of the gas phase.

The reaction was then started by injecting through the rubber septum the proper amount of catalyst, dissolved in ~ 2.0 mL toluene, and thereafter the proper amount of boron-based co-catalyst (5.0-8.0 mL of toluene).

The reaction was allowed to proceed for 1h and the pressure was checked by GC-FID analysis of the gas cap.

After 1h, the polymerization was stopped injecting 10mL of a HCl/MeOH solution (95/5 v/v) to quench the catalyst, the reactor was vented, cooled and the polymer coagulated with excess acetone, worked up and dried overnight.

A summarization of the experiment is listed in table 3.2 within the chapter.

3.4.3 – Ethene/propene co-polymerizations.

All the reactions were carried out in a 500mL Pyrex reactor, equipped with a thermostatic jacket, a magnetic stirrer, a silicone rubber septum, and a gas inlet/outlet, with the following procedure. The reactor, charged under nitrogen with 140 mL of dry toluene (purified by passing through an MBRAUN SPS unit) and 5 mL of a MAO/BHT mixture (1:1 molar ratio), was thermostated at the chosen polymerization temperature (70°C). A gaseous mixture of propene and ethene at the appropriate composition, prepared with vacuum line techniques and standardized by gas chromatography, was bubbled through the liquid phase at atmospheric pressure and a flow rate higher than 1.2 nL/min, until the gas/liquid equilibrium was attained. The reaction was then started by injecting through the rubber septum the proper amount of catalyst, previously dissolved in 2.0 mL of dry toluene and MAO/BHT mixture as a co-catalyst ($[Al]/[Ti] = 500$, $[Al]/[BHT] = 1.0$), and allowed to proceed for 20 min, during which the comonomer mixture was kept flowing through the liquid phase. Under the said conditions, total monomer conversion were lower than 10%, which ensured a nearly constant comonomer feeding ratio. After the reaction was quenched with 5mL of methanol/HCl (95/5 v/v), the copolymer was coagulated with excess acetone, filtered and vacuum dried overnight.

3.3.4 – Polymer characterization via GPC and NMR.

The GPC curves were recorded at 135°C with a Waters Alliance GPCV2000 system with dual detection (differential refractometric and differential viscometric), on polymer solutions in 1,2-dichlorobenzene (added with 0.25 mg mL⁻¹ of BHT as a stabilizer). A set of 4 mixed-bed Styragel columns (1 HT-2 and 3HT-6E) was used. Universal calibration was carried out with 12 samples of monodisperse polystyrene (M_n between 1.3 and 3700 KDa). In each carousel of 24 samples, 2 were of a known iPP produced with an *ansa*-zirconocene catalyst used as a standard, to check for consistency. In case the measured M_n and M_w values of the said iPP sample turned out to differ by more than $\pm 20\%$ and $\pm 10\%$ respectively from the “true” values, the calibration procedure was repeated and the whole set of samples re-measured.

Quantitative NMR spectra of all polypropylene samples were recorded at 120°C, on 35 mg mL⁻¹ solutions in tetrachloroethane-1,2-*d*₂, with a Bruker DRX 400 Avance spectrometer operating at 100.6 MHz (for ¹H) with a 5 mm probe, under the following conditions:

- For ¹H NMR: 90° pulse; acquisition time, 4.0 s; relaxation delay, 2.0 s; 32 transients.

Chapter 3 – Mechanistic studies on amidinato catalysts.

- For ^{13}C NMR: 80° pulse; acquisition time, 2.7 s; relaxation delay, 2.5 s; >10K transients. Broad-band proton decoupling was achieved with a modified WALTZ16 sequence (BI_WALTZ16_32 by Bruker). The spectra were fully simulated with the Shape2004 software package (by Prof. M. Vacatello, University of Naples Federico II; vacatello@chemistry.unina.it).

References.

- [1]. Hagemeyer,A.; Strasser,P.; Volpe,A.F., Jr. (Eds) *High Throughput Screening in Catalysis*; Wiley-VCH: Weinheim, **2004**.
- [2]. Noordermeer, Ethylene-propylene Polymers from Kirk-Othmer Encyclopedia of Chemical Technology, Vol. 10, 704-719, John Wiley and Sons.
- [3]. In general increasing the temperature will enhance the rate of both chain propagation and termination, nevertheless the polymer will have a tendency to shorten due to the competing effect of enhancement, strongly in favor of the chain termination; e.g. the activation enthalpies for both the chain propagation and termination is provided for a model catalyst in 1-hexene polymerization in Liu,Z.; Somsook,E.; White,C.B.; Rosaaen,K.A.; Landis,C.R.; *J. Am. Chem. Soc.* **2001**, *123*, 11193-11207.
- [4]. Friederichs,N. , Wang,B., Budzelaar, P.H.M., Coussens, B.B., *Journal of Molecular Catalysis A: Chemicals* **2005**, *242*, 91-104.
- [5]. Busico,V., Pellecchia,R., Cutillo,F., Cipullo,R. *Macromol. Rapid. Comm.* **2009**, *30*,1697-1708; the platform and the main protocols used in this thesis will be extensively described in chapter 4.
- [6]. Busico,V., Cipullo,R., Cutillo,F., Talarico,G., Razavi,A., *Macromol. Chem. Phys.* **2003**, *204*, 1269-1274.
- [7]. Carvill,A.; Zetta,L.; Zannoni,G.; Sacchi,M.C., *Macromolecules* **1998**, *31*, 3783-3789; Schaverien, J., Ernst,R.; Schut,P.; Dall’Occo,T., *Organometallics*, **2001**, *20*, 3436-3452.
- [8]. Stehling,U.; Diebold,J.; Kirsten,R.; Roll,W.; Brintzinger,H.H.; Jubgling,S.; Mulhaupt,R.; Langhauser,F.; *Organometallics*, **1994**, *13*, 964-970.
- [9]. a) Kissin, Y. V. *Isospecific Polymerization of Olefins*; Springer-Verlag: New York, NY, 1985; The estimation of the monomer concentration relied on a simple model, in which specific interactions between the chemical nature of both monomer and solvent are neglected. Nevertheless more sophisticated thermodynamical models are available for the monomer concentration evaluation, such as the Peng-Robinson model. (Peng,D.Y; Robinson *Ing. Eng. Chem., Fundam.*, vol.15,No.1, **1976**). Unfortunately that specific model was not available at the time of the experiment, therefore the absolute accuracy of the experimental value should suffer from this. This notwithstanding it is worthwhile to note that the interest is in the *trend* of P_n with respect the monomer concentration. (b) the low reproducibility in the Y_p values arises from the inherent difficulty of polymer work-up, i.e. low molecular weight atactic polypropylene.
- [10]. Natta,G., Pasquon,I., *Adv. Catal.* **11**, 1 (1959).
- [11]. Busico,V; Cipullo,R. *Prog.Pol.Science*, **2001**, *26*, 443-533;

- [12]. Schaverien, J., Ernst,R.; Schut,P.; Dall’Occo,T., *Organometallics*, **2001**, 20, 3436-3452; Kawahara,N.; Kojoh,S.; Toda,Y.; Mizuno,A.; Kashiwa,N.; *Polymer*, **2004**, 45, 355-357; Busico,V.; Cipullo,R.; Friederichs,N.; Lissen,H.; Segre,A.; Van Axel Castelli,V.; Van Der Velden,G.; *Macromolecules* **2005**, 38, 6988-6996.
- [13]. a) Busico,V.; Talarico,G.; Cipullo,R.; *Macromol. Symp.* **2005**, 226, 1-16; Busico,V.; Cipullo,R.; Friederichs,N.; Ronca,S.; Talarico,G.; Togrou,M.; Wang.,B.; *Macromolecules*, **2004**, 37, 8201-8203; b) Ma,K.; Piers,W.; Parvez,M. *J. Am. Chem. Soc.* **2006**, 128,3303-3312.
- [14]. Busico,V.; Cipullo,R.; Romanelli,V.; Ronca,S.; Togrou,M.; *J.Am.Chem.Soc.* **2005**, 127, 1608-1608.
- [15]. Busico,V.; Cipullo,R.; Talarico,G.; Caporaso,L.; *Macromolecules*, **1998**, 31, 2387-2390; Busico,V.; Cipullo,R.; Ronca,S.; *Macromolecules*, **2002**, 35,1537-1542.
- [16]. Randall,J.C.; *Macromol. Sci. Rev., Macromol. Chem. Phys.* **1989**, C29, 201.

4.1 – Introduction.

After the mechanistic behaviour of the prototypical amidinato-type catalyst is properly cleared, a kinetic evaluation of the catalyst is doable. The employment of HTE tools and methods will enable the fast kinetic database generation, therefore a new screening protocol must be developed; the proper illustration of HTE tools and method and, consequently, the screening protocol development/benchmark are the main objects of this chapter.

In the first part, the HTS platform employed will be described along with a new protocol in homopolymerization (i.e. the self-scavenging approach); thereafter, starting from the mechanistic knowledge of chapter 3, a new protocol for copolymerization will be developed.

The protocol will be subjected to a benchmarking process with two known amidinato catalysts (*vide infra*) and the reliability will be assessed through the comparison of the experimental results from the mini-reactors setup to large batch scale reactors.

4.2 – High Throughput Screening: the Freeslate PPR48[®] Platform and the Self-Scavenging Protocol.

The HTS platform employed for this study is the Freeslate PPR48[®] (Parallel Pressure Reactors), (figure 4.1 and table 4.1), already well described in the literature¹. A more in-depth description of the platform and polymerization protocols is provided in the experimental section of this chapter.



Figure 4.1. Freeslate PPR48[®] Secondary Screening Platform.

Table 4.1. Freeslate PPR48[®] description, courtesy of reference 1.

- 48 parallel, individually controlled olefin-polymerization mini-reactors (5 mL working volume, 35 bar maximum operating pressure, 200°C maximum operating temperature), with dual injector ports (for solutions and slurries), disposable glass insert, mechanical stirring with magnetically coupled heads and disposable paddles (800 rpm maximum stirring speed).
- Full containment in a triple glove-box (MBraun LabMaster).
- Dual-arm, integrated liquid-handling robot (with solution and slurry injection needles).
- Mbraun SPS-5 Solvent Purification System with solvent line termini inside the glove box.
- Mixed-bed catalyst columns for the purification of gaseous monomer (ethene and propene), with distribution lines plumbed into the mini-reactors.
- Genevac EZ-2 Plus Drying Station.
- Off-line-integrated Bodhan Robotic Weighing Station.
- Symyx Software (PPR Client[®], Library Studio[®], PolyView[®], Epoch[®], Impressionist[®] Packages).
- Symyx Renaissance Application Server.
- Oracle Database Server.

The Freeslate PPR48[®] is able to run in parallel 48 polymerization reactions, with individual control and monitoring concerning the operational temperature, pressure, gas uptake and gas uptake rate. The complete handling of the instrument (reactor management and robot handling) is performed via the software Symyx Impressionist PPR Client[®], in which the experiment is acquired on-line (Active Experiment) and any actions of the machine is properly managed through script procedures (figure 4.3).

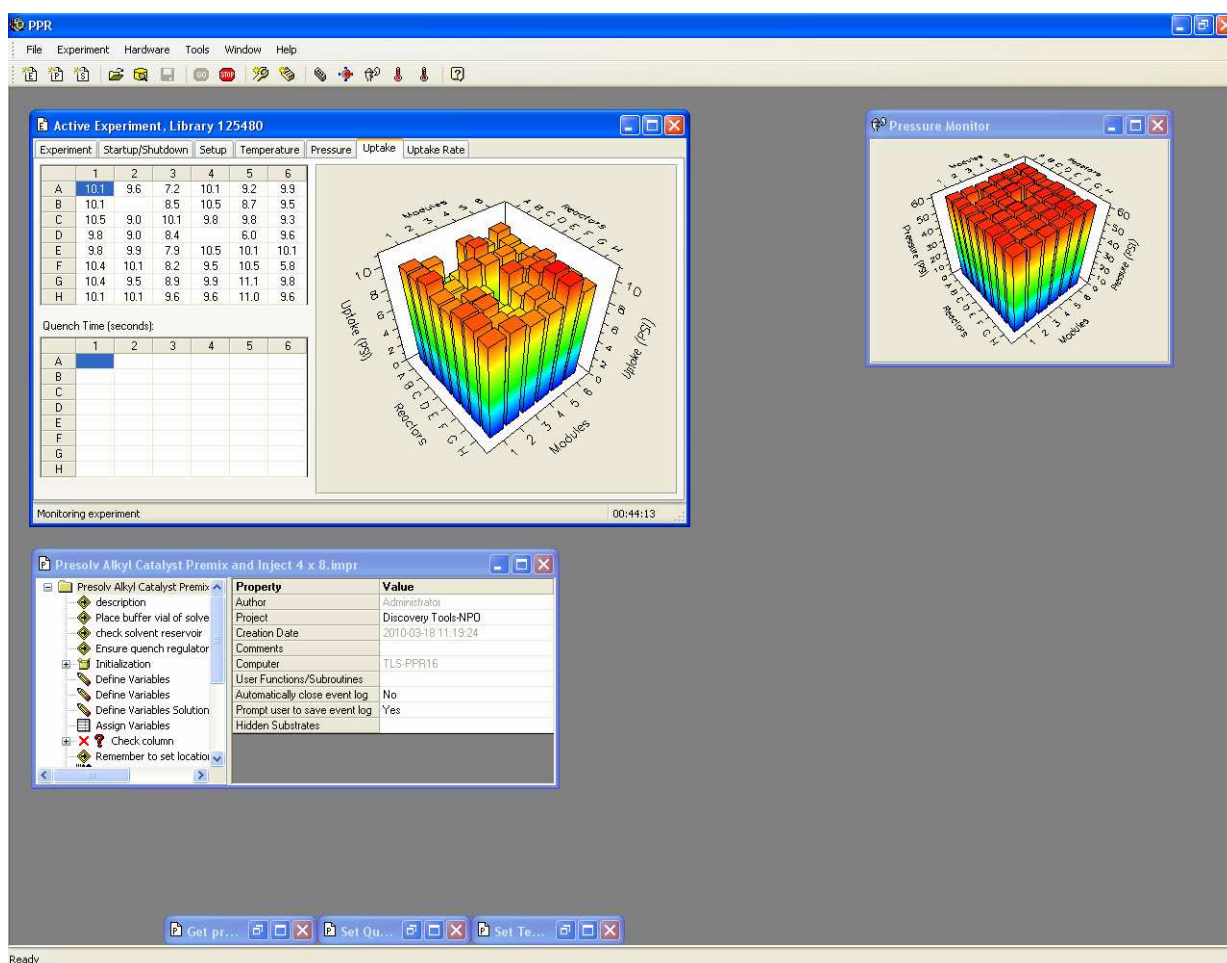


Figure 4.3. Screenshot of the Active Experiment and script procedures for the Freeslate PPR48[®] platform. In particular it is possible to see the Active Experiment with the Gas Uptake collection for the 48 reactors, the Pressure Monitor on the right and a Catalyst Injection procedure.

Along the machine management, the experiment design is computed and controlled via the software Symyx Library Studio[®], in which the single polymerizations are arranged as elements of matrix (in general a 6×8 matrix); moreover it is possible to relate the chemicals (which are matrix elements in the frame of the design program) between each others via mathematical functions (e.g. a formula can be devised to fix a molar ratio between element, or a gradient to change a definite parameter – e.g. a concentration – accordingly to a definite slope). For each reaction, the design provides all the quantities (in relative and in absolute) of the chemicals involved; moreover the design can be updated at will and *during* the experiment, due to the perfect communication between the two softwares (figure 4.4).

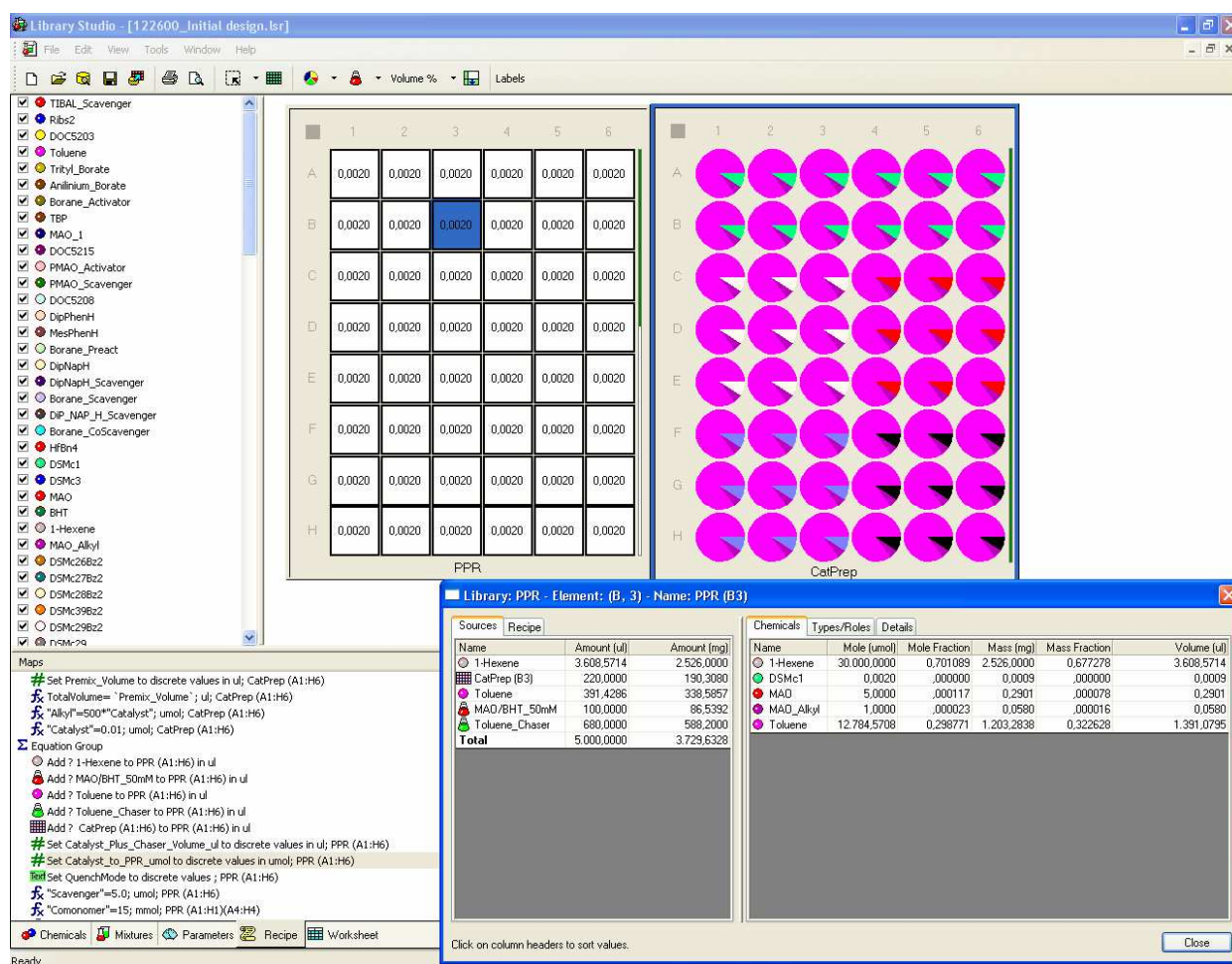


Figure 4.4. Screenshot of the Library Studio[®] experimental design with the matrix of elements. In particular it is possible to see the composition of the cell 3B in which each chemical is listed in volumetric, molar and mass amount.

The inherent features of the PPR48[®] platform enable an high degree of customization: the possibility of looking at the experimental protocols (and modify them via a reliable and ‘easy-to-handle’ program codification) enables the creation of several experimental protocols for precise and innovative experiments (figure 4.5).

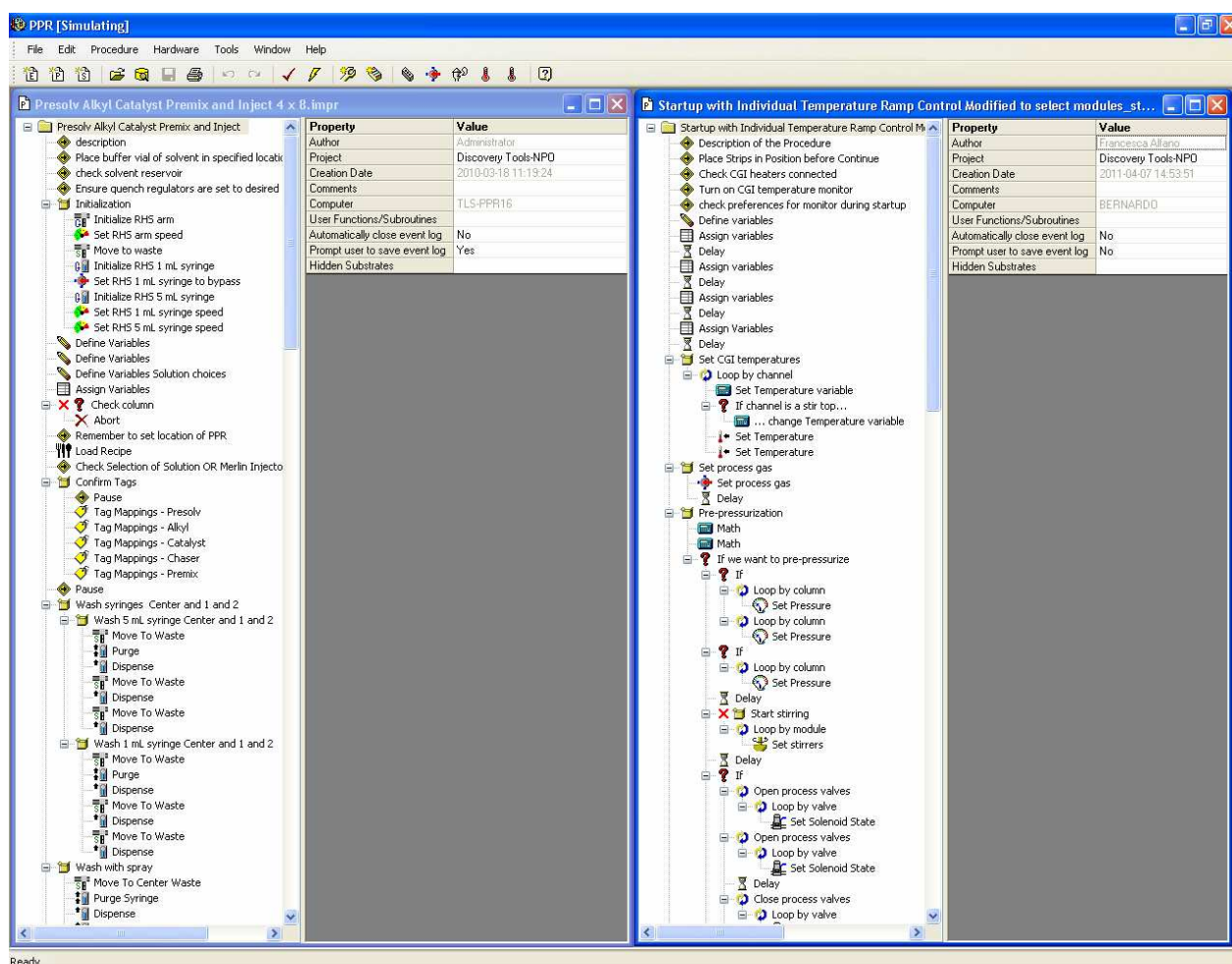


Figure 4.5. Experimental protocols for the PPR48[®] platform, an injection protocol (left) and a start-up/pressurization protocol (right). As it is possible to see, each protocol is the collection of several actions script-wise listed. It is possible to modify protocol via moving, adding or editing a single action. For decision blocks, the common Boolean algebra is applied.

The developing of experimental protocols on purpose enlarges enormously the potentiality of this secondary screening platform and, even a very *naive* modification is able to provide important pieces of information in a catalyst kinetic assessment: in the forthcoming pages of this section, the oxidation state of a Ti-based CGC and amidinato catalysts is assessed with a protocol modification of the PPR48^{®2}.

As it is possible to see from table 4.1, the working environment of this HTS platform is extremely pure, only traces of O₂ and H₂O can be detected. In general, good reproducibility of experiments is granted by the further cleaning of the reaction environment by a scavenger molecule, usually an Al-Alkyl. Unfortunately, even competent scavengers like bulky Al-Alkyls are not always innocent toward the catalysts, and can negatively affect one or more aspects of catalyst performance³. In fact, a variety of reversible and/or irreversible deactivations have been documented as a result of the interaction of active transition metal cations with main group metal-alkyl species. Moreover, the

occurrence of trans-alkylation can lower the average molecular weight of the polymerization products. A facile way to shut down the reactivity of Al-Alkyls is to react them with suitable Lewis bases, such as hindered phenols (e.g. 2,6-*t*Bu-4-R-C₆H₂OH; R = H, Me)^{3,4}; unfortunately this approach is not general.

In order to investigate important catalyst features, without the bias of any possible interactions with the scavenger, a protocol of self-scavenging polymerization(s) had been devised with the PPR[®] platform to investigate the catalyst behaviour *per se*.

The self-scavenging polymerization protocol had proved to work successfully in the PPR[®] platform, due to the highest purity of the environment (monomer, solvent and atmosphere); needless to say that the reaction medium is cleaned by the catalyst itself, with the sacrifice of M-C bonds². For the benchmarking of the protocol, we used an pyridilamide-Hf-based⁵ model catalyst (figure 4.6) in combination with B(C₆F₅)₃ at 40°C in ethene polymerization (toluene as solvent); this complex undergoes fast trans-alkylation with Al-alkyls and reacts even with highly hindered phenols (such as 2,6-ditertbutylphenol). The choice on the co-catalyst went on a B compound since MAO or other Al-based co-catalyst could have acted as a scavenger and bias the protocol results from the beginning.

In Figure 4.7 we report ethene polymerization results, moreover a comparison with other polymerizations using Al(*i*Bu)₃ as a scavenger, is provided.

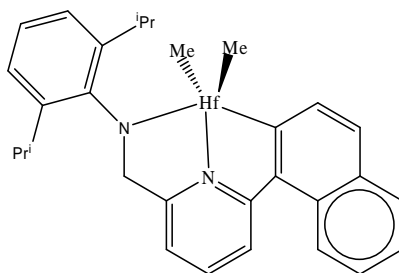


Figure 4.6. Pyridylamide Hf based catalyst employed for the self-scavenging protocol benchmark.

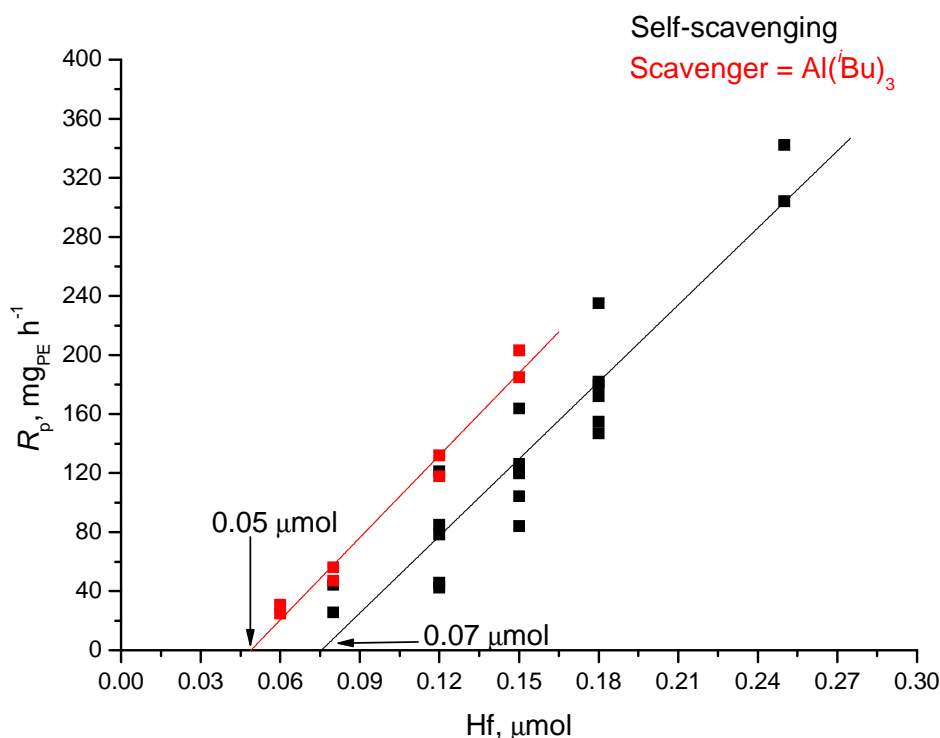


Figure 4.7. Absolute polymerization rate versus catalyst amount for the self-scavenging protocol benchmarking. As a matter of fact, the scavenging action with this catalyst does only influence the amount of complex which is lost in the polymerization due to ubiquitous impurities and the average productivity is unchanged.

As it is clear from figure 4.7, the self-scavenging protocol (*vide infra*) works reliably with pre-alkylated catalysts; moreover the average catalyst productivity (estimated through the derivative of regression lines for the data of figure 4.6) is the same ($Y_p = 6 \text{ Kg}_{PE} \text{ mmol}_{Hf}^{-1} \text{ h}^{-1} [\text{C}_2\text{H}_4]^{-1}$)⁶ irrespective of the presence of the scavenger (of course the cell yield is higher whenever the scavenger is employed and the amount of deactivated catalyst is accordingly lower).

From the first proof of principle with a model catalyst, the approach was moved towards the catalysts of interests, namely a model Ti-based CGC ($\text{Cp}^*\text{SiMe}_2\text{N}^t\text{Bu-TiMe}_2$) and the amidinato catalyst **C0**. The two catalysts were tested in industrially relevant conditions ($T_p = 90^\circ\text{C}$) in propene polymerization: besides the lowest reproducibility of the experiments ($\text{RSD} > 30\%$), it is possible to carry out polymerizations with the self-scavenging protocol for both of the two complexes (figure 4.8). The activation of the catalysts had been performed with $\text{B}(\text{C}_6\text{F}_5)_3$ in both cases; what is worthwhile to note for these two systems is that, since no Al is involved in polymerization, no reduction of the Ti occurs during polymerization, even though catalyst deactivation is severe (figure 4.9)⁷. The oxidation state of the amidinato catalyst is cleared without any ambiguities: it is

indeed possible to state without any doubt that, for these systems, the oxidation state of Ti in polymerization is IV².

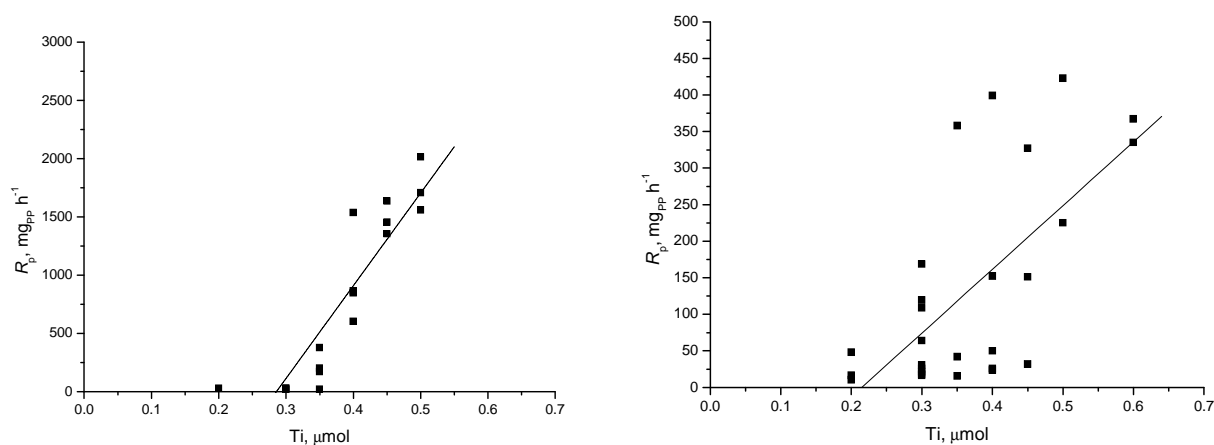


Figure 4.8. Absolute polymerization rate versus catalyst amount for **CGC** catalyst (left) and **C0** catalyst (right); as a matter of fact the reproducibility is poor, but the polymerization data clearly reveal that the oxidation state of the catalyst is unchanged with respect the molecular precursor.

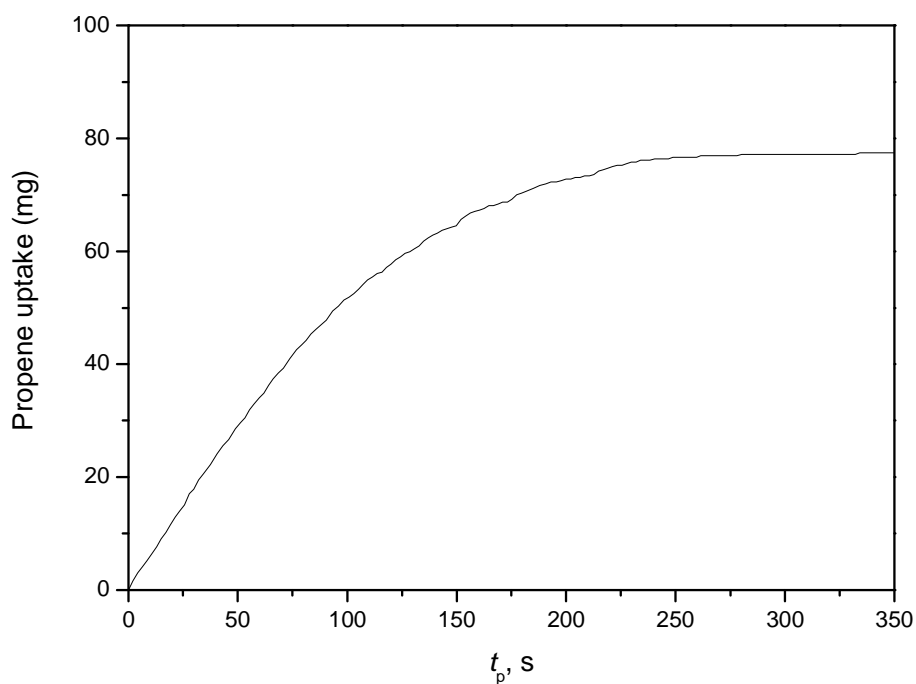


Figure 4.9. Monomer Uptake curve (i.e. polymerization kinetic profile) for the **C0** propene polymerization. As it is possible to see from the profile, the catalyst deactivation is severe under the quoted conditions.

4.3 – The relationship between catalyst productivity and copolymer composition.

From the previous chapter, it was understood that the amidinato catalyst features an extremely high activity in ethene homopolymerization. This is detrimental to any kinetic investigations, since, in order to control the reactions and devise the proper kinetic effects that a specific catalyst imprints to the polymerizations, the absolute amount of complex to be dosed in the laboratory scale reactors are less than homeopathic ($[\text{Catalyst}] < 0.2 \mu\text{M}$)⁸. Besides the obvious (and not trivial *per se*) issues related to the proper handling of such a low amount of complex, the high oxophilicity of early transition metals organometallic complexes adds complications in an already tough scenario⁸: the absolute quantity of ubiquitous ‘pollutant’ (O_2 , H_2O and S-based compounds, which may come along with the monomer, solvent, *etc.*), even if brought down to ppm values, is still comparable with the amount of catalyst, thus leading to an inherent low reproducibility of experiments and resulting in an unreliable kinetic assessment⁸(figure 4.10).

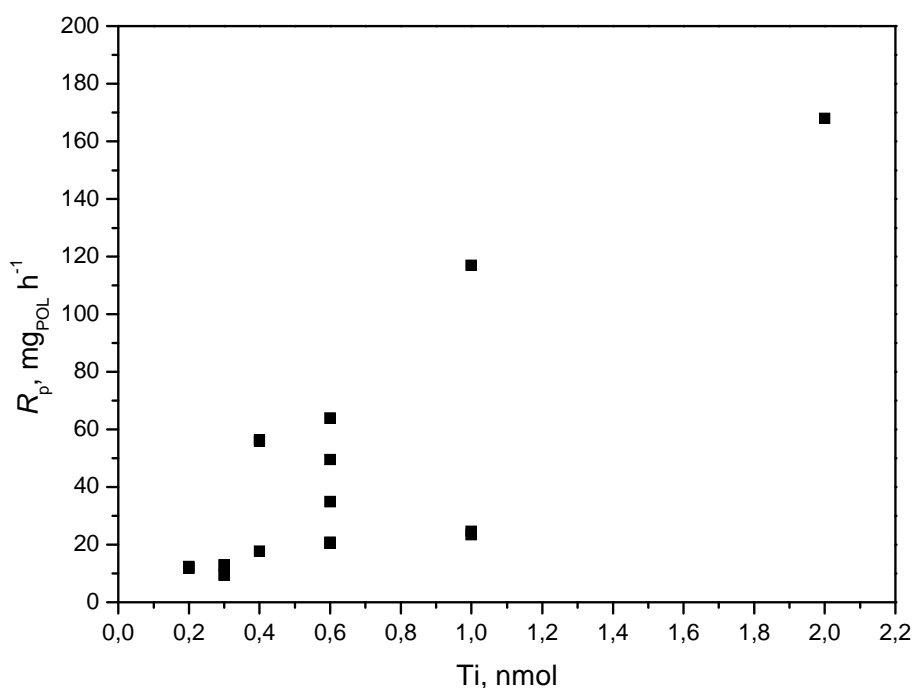


Figure 4.10. Low reproducibility of ethene polymerization with catalyst **C0** due to extremely low amount of catalyst loading ($< 1\text{-}2 \text{ nmol}$).

Needless to say, it is necessary to slow down the catalyst productivity, in order to handle higher catalyst amounts and make the deactivation by impurities negligible during the experiments. Moreover, the lowering of the activity must be pursued *non-specifically*, meaning that all the processes through which the catalyst undergoes must be slowed down of the same entity, not to

favour one process over the others and bias the kinetic evaluation of the complexes in polymerization.

In general, the kinetic equation of a copolymerization can be written according to the ‘simple’ form of equation 4.1⁹:

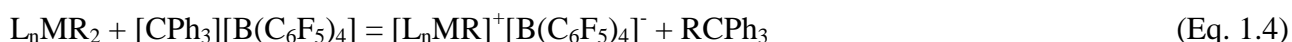
$$v = [\text{Ti}^*] \langle k \rangle [\text{C}_n\text{H}_{2n}]^{\alpha \approx 1} \quad (\text{Eq. 4.1})$$

where $[\text{Ti}^*]$ is the active centre concentration (in general only a small fraction of the analytical concentration of the complex), $\langle k \rangle$ is the average of all the kinetic constant for the reaction and the order of reaction with respect the monomer is practically equal to 1¹⁰. The strategies, generally speaking, to lower the rate of (co)polymerization are three, each based on acting on the three terms of equation 4.1, i.e. :

- Lower the monomer concentration;
- Lower the active centres concentration;
- Lower the rate of all the processes involved in the (co)polymerization.

The first strategy is practically unfeasible, since, as it has been shown in chapter 3, the main chain transfer process is independent on the monomer concentration¹¹ (β -H transfer to the Ti); every lowering of the monomer concentration will affect the v_p/v_t ratio and systematically lower the molecular weight of the polymers; thus the process is not representative with respect all the phenomena that occur during the copolymerization.

The second strategy was pursued using a suitable Lewis base to block the active centres, thus impeding the general reactivity of most of them. The Lewis base of choice must coordinate to the active cations reversibly, so to ensure a temporary deactivation of the polymerization centre^{7,12}. It is well known that the metallocenes active cations undergo reaction of homodinuclear dimerization with the un-activated dimethyl cations (figure 4.11)⁷; this behaviour is easily understood if we look at the common activation reactions of § 1.8, equation 1.4 is reported by way of example:



Since the reaction of equation 1.4 can be regarded as a (hugely right-shifted) Lewis acid-base equilibrium¹², the complex L_nMR_2 is a stronger base than the ‘conjugated’ cation $[\text{L}_n\text{MR}]^+$; homodinuclear adducts are, therefore, possible and have been well documented in the literature.

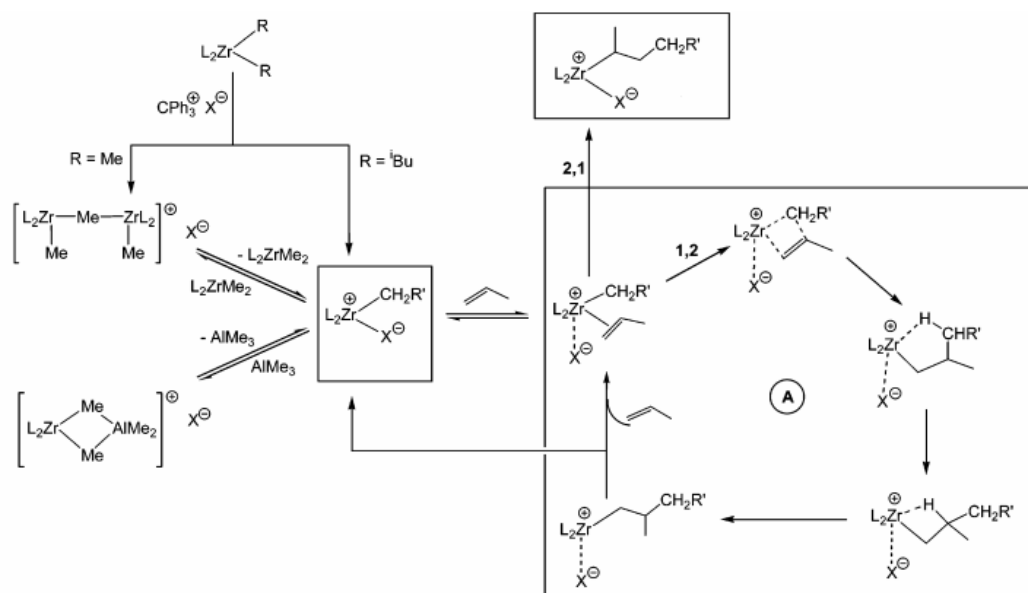


Figure 4.11. Catalytic cycle and side-reaction for a general metallocene catalyst (courtesy from reference 7).

Being the Lewis base of choice the un-activated complex itself, a possible strategy to drive the equilibrium of reaction 1.4 to the left side of the reaction, is to activate the complexes with a sub-stoichiometric amount of boron based salt.

Unfortunately this strategy was unsuccessful for mainly two reasons; i) the activity of the complexes could not be tamed even at very low $[B]/[Ti]$ ratio, ii) as shown with the propene homopolymerization in § 4.2, the activation with B based salt brings to severe catalyst deactivation, leading to severe activity drop-off^{3,7}: catalyst **C0** is not an exception in this respect.

The third strategy was to lower all the processes involved in the copolymerization; this was achieved from the proper kinetic analysis of the EP copolymerizations performed in the fundamental studies of the amidinato-type catalyst **C0** in chapter 3.

From table 3.2, it is possible to see a correlation between the catalyst activity and the copolymer composition; in the limit of propene homopolymerization the activity is very low (due to the catalyst dormancy phenomenon¹³), as far as some ethene is added the release from dormancy is achieved until a plateau is reached, then (after a certain threshold of ethene in the liquid phase and, hence, in the copolymer) the activity takes off (figure 4.12).

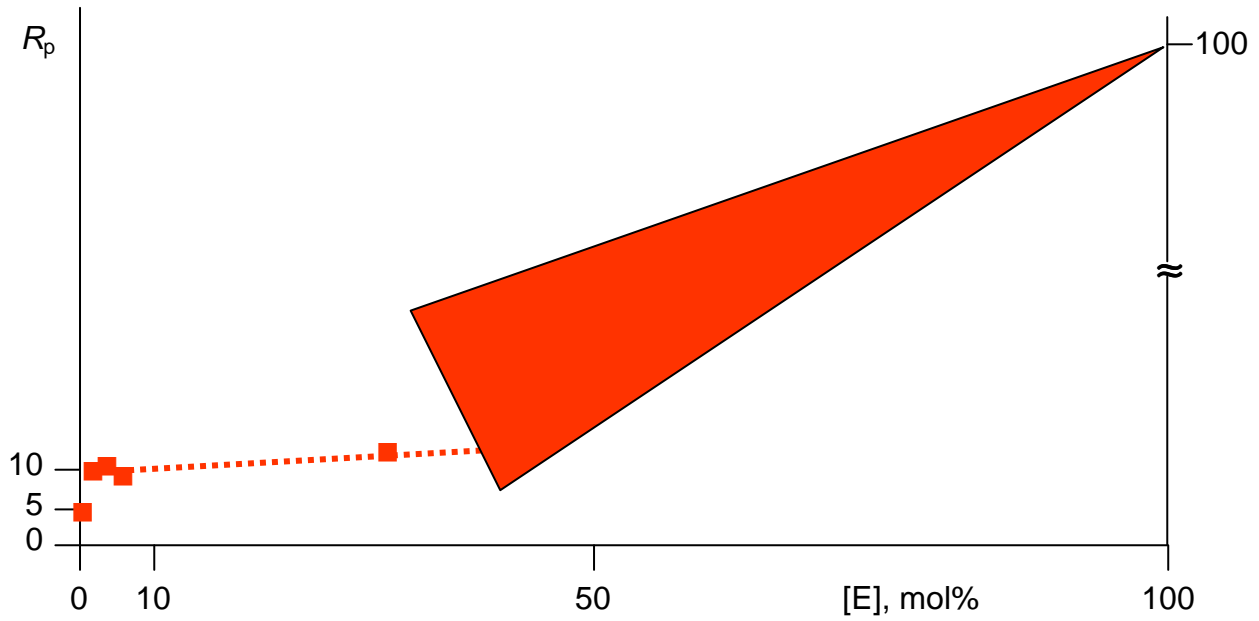


Figure 4.12. Qualitative profile of the amidinato-type catalyst activity with respect to the copolymer based on the EP copolymerization data of table 3.2.

It is possible to perform a qualitative analysis of the EP copolymerization kinetic; the rate of the overall process can be written as in eq. 4.2¹⁴, in which the overall rate of reaction is the summation of the ethene and propene homopolymerization conjugated with the natural cross terms, taking in account for the whole copolymerization process:

$$v = [P](C_P^* \langle k_{PP} \rangle + C_E^* k_{EP}) + [E](C_P^* k_{PE} + C_E^* k_{EE}) \quad (\text{Eq. 4.2})$$

with:

- $[P] - [E]$ is the propene/ethene concentration in the liquid phase;
- $C_{P/E}^*$ is the fraction of chain bearing a last inserted propylene/ethylene unit;
- k_{xy} is the kinetic constant for the insertion of monomer y following the insertion of monomer x, in propene homopolymerization the lower-case 'p' and 's' refer to a last 1,2 and 2,1 inserted propylene unit respectively;
- $\langle k_{PP} \rangle < k_{EP} < k_{PE} < k_{EE}$.

In propene homopolymerization the rate is low and the Eq. 4.2 can be simplified to Eq. 4.3

$$v = [P](C_P^* \langle k_{PP} \rangle) = [P]\{(C_P^* (k_{pp} + k_{ps}) + C_s^* (k_{ss} + k_{sp}))\} \quad (\text{Eq.4.3})$$

with : $0 \sim k_{ss} \ll k_{ps} < k_{ps} < k_{pp}$

In this case the catalyst dormancy has important kinetic effects, hence the propene homopolymerization is not representative of the whole process.

In EP copolymerization at low [E] in the liquid phase (and hence in the copolymer), the rate is moderate, since $C_P^* > C_E^*$; this condition should be feasible for a proper screening in a laboratory scale reactor, since the catalyst dormancy is not an issue any more. Finally at high [E] (till the limit of ethene homopolymerization), the rate boosts since the term $[E]C_E^*k_{EE}$ in equation 4.2 overwhelms all the others; needless to say that the reaction is not controlled, unless homeopathic amounts of catalysts are employed (with a dramatic decrease reproducibility between identical experimental runs, $RSD > 40\%$, figure 4.10).

From the qualitative kinetic analysis, the best way to decrease ‘non-specifically’ the activity of the catalyst is to increase the comonomer content in the liquid phase; moreover it is necessary to assess the effects of regioselectivity of the amidinato-type on the kinetic at these copolymer compositions. As we stated in chapter 3, from the fundamental study of the catalyst **C0** it is possible to calculate the total amount of regiomistakes¹³ that the catalyst does, i.e. Q_{SE} , which is a good approximation of the ratio k_{ps}/k_{pp} ($Q_{SE} = 3.1\%$). The slope of the dormancy regression line fitting equation 3.3 gives the ratio k_{pE}/k_{ps} ($k_{pE}/k_{ps} = 171$ from the regression parameters), by simple substitution it is possible to calculate the ratio k_{pp}/k_{pE} , a ‘pseudo- r_p ’¹³ for EP copolymerization. This ratio is 0.19 and simulates the propylene reactivity ratio in EP copolymerization *in the hypothesis that the enchainment of all the propylene units were totally 1,2-wise*. The proximity of this value with respect the proper r_p for EP copolymerization ($r_p = 0.25$ from table 3.3) is, in our opinion, a good proof that *either the 1,2 enchainment of propylene units dominates in EP copolymerization or the regioselectivity of the catalyst does not affect the kinetic in EP copolymerization, hence the choice of the 1-alkene is immaterial concerning the regioselectivity of the catalyst*. From this important clarification about the kinetics, it is possible to develop a proper protocol to screen different catalysts in a secondary screening platform, provided that the ethene amount in the liquid phase is the best compromise to ensure both that the reaction rate is reasonably low and the dormant catalyst centres are ‘unlocked’; moreover, since *the identity* of the comonomer is rather immaterial, and the amidinato-type catalyst are ‘good incorporators’¹⁵, the comonomer of choice will be 1-hexene¹⁶, due to the easiness to adapt a liquid comonomer in HTE polymerization protocols.

4.4 – A proper protocol for iminato catalyst screening with HTE technologies.

The kinetic assessment of the copolymerization of iminato-type catalysts is based on a qualitative analysis of the polymerization kinetic provided by the experimental data points from the EP copolymerization with the catalyst **C0**. In order to properly demonstrate the reliability and feasibility of the new protocol with iminato-type complexes, a benchmarking phase was arranged with the prototypical **C0** complex and the ketimido complex **C3** (figure 4.13)¹⁵.

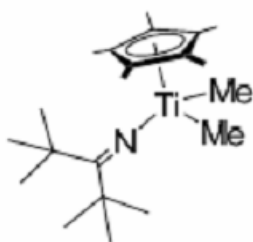


Figure 4.13. **C3** complex employed for the benchmark of the HTE screening protocol development.

For each catalyst a set of experiments have been performed using the Freeslate PPR48[®] Secondary Screening Platform (*vide infra*) in ethene/1-hexene copolymerization with several values of feeding ratios ($[E_0]/[H_0]$)¹⁷. For each copolymer a proper characterization was performed for both the composition and the molecular weight (table 4.2 and 4.3).

Table 4.2. Polymerization activity and polymer properties at different feeding ratios for catalyst **C0** (see experimental section for the reaction conditions).

Library Id	Cell	Ti (nmol)	[E ₀]/[H ₀]	ν H (mL)	H ⁽¹⁾ (mol%)	E ⁽¹⁾ (mol%)	Yield (mg)	Y _p ⁽²⁾	Y _{p,av} ⁽²⁾	RSD, (%)	M _n (KDa)	PDI
117300	2F	2.0	0.404	0.3	5.0	95.0	44.1	377	492	33	636.8	2.4
	2G	1.0	0.404				35.5	607				
116660	1A	2.0	0.177	0.6	13.7	86.3	76.8	392	389	33	209.5	2.2
	1C	2.0	0.168				73.6	378				
	1B	1.0	0.167				38.0	391				
	1D	1.0	0.166				22.6	233				
117300	1F	2.0	0.168				51.2	263				
	1H	2.0	0.192				87.9	442				
	1G	1.0	0.172				60.9	623				
116860	1B	2.0	0.049	1.8	31.5	68.5	144.8	276	247	10	126.6	2.0
	1C	1.0	0.049				61.1	233				
	1D	1.0	0.048				61.1	233				
116860	2A	2.0	0.034	2.4	34.0	66.0	113.8	165	160	4	145.7	1.8
	2B	2.0	0.035				107.4	155				
116860	3A	2.0	0.024	3.0	35.7	64.3	79.5	93	85	14	185.4	1.8
	3B	2.0	0.025				77.5	91				
	3C	2.0	0.025				60.4	71				
	4B	2.0	0.020	3.6	36.5	63.5	59.3	58	47	17	144.4	1.8
	4C	1.0	0.020				20.6	40				
	4D	2.0	0.021				48.6	48				
117021	4B	2.0	0.020				37.6	37				
	4C	4.0	0.020				93.3	46				
	4D	4.0	0.021				105.6	52				

⁽¹⁾ In the copolymer, ¹H NMR; ⁽²⁾ Kg(copolymer) mmol_(Ti)⁻¹ [C_nH_{2n}]⁻¹ h⁻¹

Table 4.3. Polymerization activity and polymer properties at different feeding ratios for catalyst **C3**. (see experimental section for the reaction conditions).

Library Id	Cell	Ti (nmol)	[E ₀]/[H ₀]	ν H (mL)	H ⁽¹⁾ (mol%)	E ⁽¹⁾ (mol%)	Yield (mg)	Y _p ⁽²⁾	Y _{pav} ⁽²⁾	RSD, (%)	M _n (KDa)	PDI
117300	3A	10.0	1.000	0.12	5.2	94.8	66.8	200	210	5	251.1	3.5
	3D	7.0	1.000				51.4	220				
	3B	5.0	1.000				36.5	219				
	3E	5.0	1.000				33.3	200				
	2C	10.0	0.404	0.3	14.9	85.1	55.4	95	97	12	106.7	4.5
	2D	10.0	0.404				67.2	115				
	2B	7.0	0.404				36.8	90				
	2E	7.0	0.404				36.4	89				
	1B	20.0	0.175	0.6	24.2	75.8	135.6	69	57	21	90.6	7.0
	1C	10.0	0.175				57.5	59				
	1E	10.0	0.175				41.6	42				
	1D	15.0	0.178				94.0	64				
117021	1A	10.0	0.173				50.0	51				
	1B	7.0	0.165				24.2	36				
	1C	8.0	0.169				25.6	33				
	1D	8.0	0.168				24.3	31				
	1E	10.0	0.164				24.9	26				
	2A	15.0	0.111				70.6	34				
	2B	15.0	0.106				82.0	39				
	2C	10.0	0.105				25.4	18				
	2D	10.0	0.103				23.8	17				
	2E	10.0	0.107				39.8	29				
	3A	20.0	0.077				131.0	36				
	3D	15.0	0.079				76.3	28				
	3B	10.0	0.080				48.6	27				
	3E	10.0	0.075				37.6	21				
116860	3C	5.0	0.08				17.1	19				
	1F	40	0.048	1.8	41.3	58.7	179.6	17	16	25	33.5	5.0
	1G	30	0.049				166.4	21				
	1E	20	0.049				68.7	13				
	1H	20	0.049				62.0	12				
	2H	30	0.032	2.4	45.5	54.5	107.5	10	10	6	36.3	5.5
	2E	20	0.033				65.0	9				
	2F	20	0.034				72.5	11				
	3G	30	0.025	3.0	53.4	46.6	81.2	6	7	16	28.4	5.6
	3H	30	0.025				109.2	8				
	3E	20	0.024				56.9	7				
	3F	20	0.025				52.9	6				
	4G	30	0.020	3.6	57.7	42.3	76.0	5	5	16	13.9	9.1
	4H	30	0.021				88.1	6				
	4E	20	0.020				38.3	4				
	4F	20	0.020				52.8	5				

⁽¹⁾ In the copolymer, ¹H NMR; ⁽²⁾ Kg(copolymer) mmol_(Ti)⁻¹ [C_nH_{2n}]⁻¹ h⁻¹

As it is possible to see from tables 4.1 and 4.3 the catalyst activity follows the trend qualitatively described in section 4.3, moreover the RSD decreases from 30% to 10-15%; this is due to the fact

that the nominal concentration of the catalyst is high enough to regard as negligible the amount deactivated by impurities. Concerning the molecular weight, it is possible to note an initial shortening of the polymers, until a plateau value, strictly characteristic of the catalyst involved. On an additional note, it is interesting to note that the catalyst **C3** is not a single centre catalyst, since the PDI index of the products is above 2.0, meaning that more than one active center is involved during the polymerization¹⁸ (*vide infra*). In Figures 4.14 and 4.15 the plots of the catalyst activity with respect the polymer composition are reported both for catalyst **C0** and **C3**, while in figure 4.16 a typical MWD is reported after a proper deconvolution of the peaks^{18,19}, thus confirming that the PDI index of the polymer produced by catalyst **C3** is the result of superimposition of, at least, two Schultz-Flory MWD.

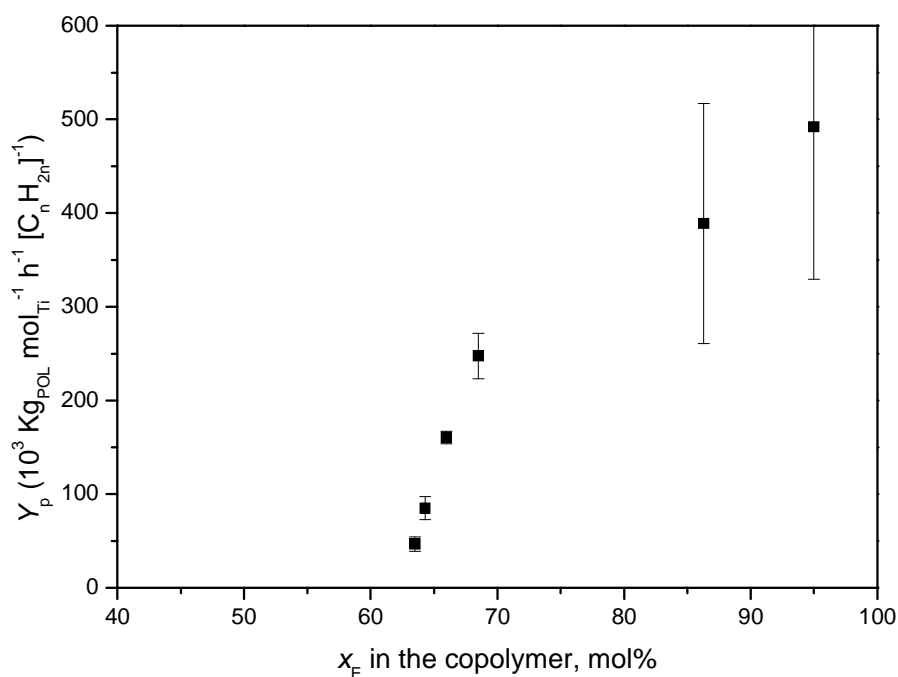


Figure 4.14. Average productivity for catalyst **C0** with respect the ethene content in the copolymer.

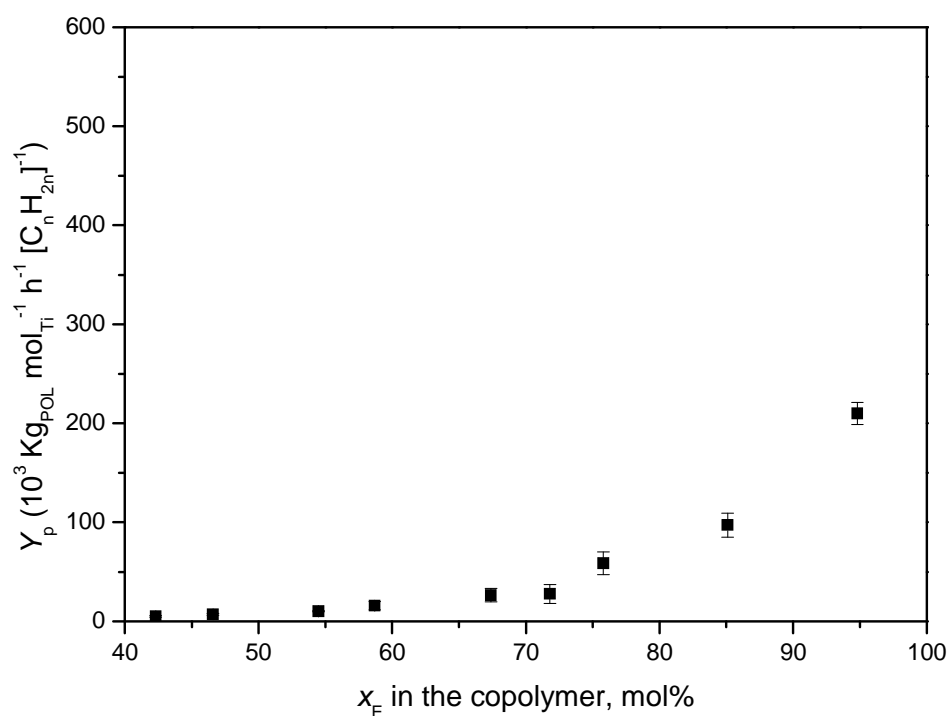


Figure 4.15. Average productivity for catalyst C3 with respect the ethene content in the copolymer.

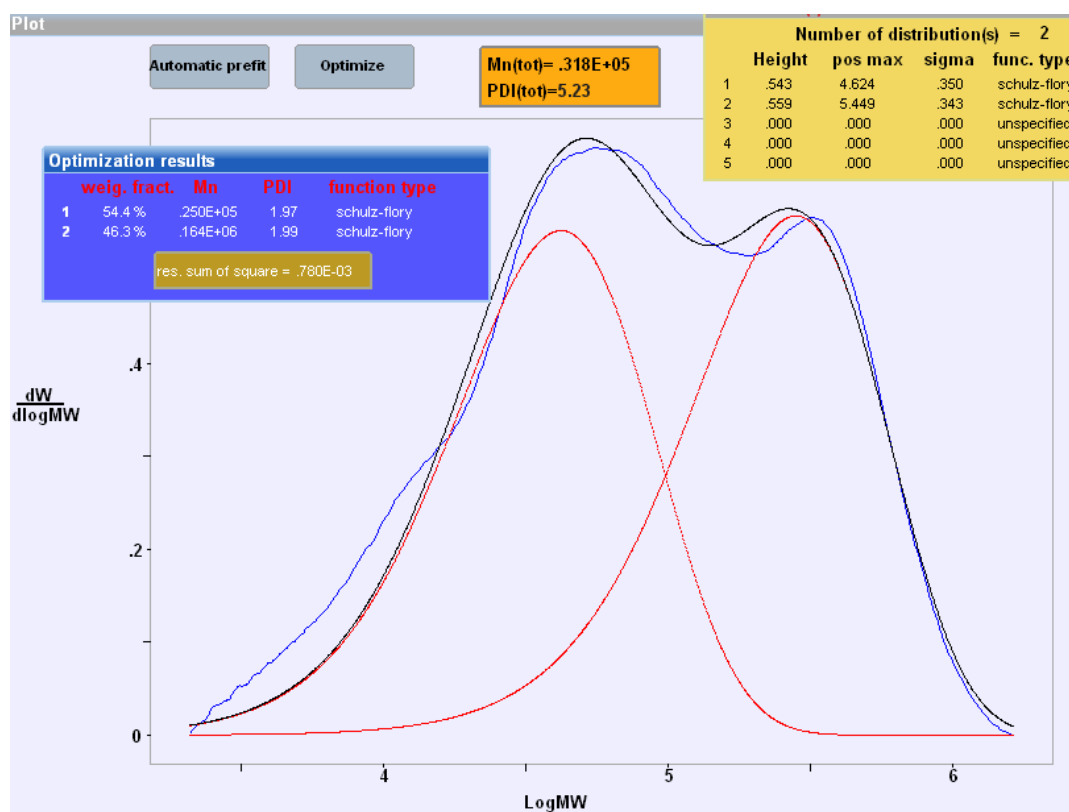


Figure 4.16. MWD distribution of a typical copolymer produced with catalyst C3, $[E_0]/[H_0] \approx 0.050$.

During the activity assessment of the benchmark catalysts, it is worthy to note that the catalyst amount had been changed for different cells, in order to rule out any mass transfer limitation effects. The catalyst activities calculated from the derivative of the regression line are in good agreement with those calculated by the polymer yield evaluation of the single cells (figure 4.17).

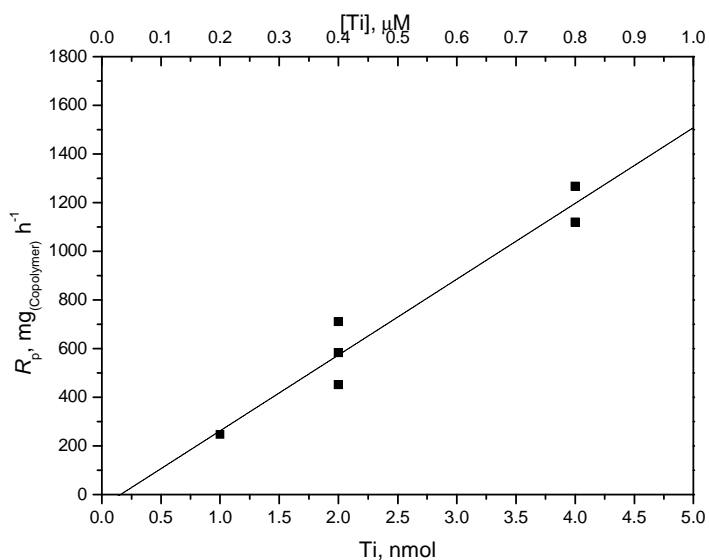


Figure 4.17. Absolute polymerization rate (R_p) vs catalyst amount for the system **C0** at $[\text{E}_0]/[\text{H}_0] = 0.020$, $Y_p = 50 \text{ Kg}_{\text{Copolymer}} \text{mmol}_{\text{Ti}}^{-1} \text{h}^{-1} [\text{C}_n\text{H}_{2n}]^{-1}$.

4.5. - Validation of the copolymerization protocol, from mini-reactors to large scale batch reactors.

In the last part of the present chapter, the last piece of validation of the protocol must be provided, i.e. the comparison of the mini-reactor performances with large scale bench reactors. As was previously demonstrated in the research group where this project was executed, the comparison of small-scale reactors with large scale ones is already well achieved for catalytic polymerization, resulting in an extremely good match¹. Nevertheless, the inherently different protocols used for copolymerizations on molecular catalysts did not rule out *a priori* several issues which can severely affect the reliability of small-scale reactors (viscosity of the liquid phase, stirring effects, etc.), a validation of the protocol with a comparison with a larger scale reactor (>5 mL) is therefore required. The batch scale ethene/1-hexene co-polymerizations were performed in the research centre of Chemelot (Geleen, The Netherlands) with catalyst **C0**. In table 4.4 the experimental results are reported.

Table 4.4. Polymerization results for catalyst **C0** in large scale bench reactors. The experimental condition were chosen as to match as much as possible the conditions of reaction achieved in the PPR[®].

Entry	Ti (nmol)	[E ₀]/[H ₀] ¹⁷	Yield (g)	Y _p ⁽¹⁾
502	200	0,083	18,5	384
517	200	0,034	13,7	139
PPR_Exp_1	2	0,083	0,164	340
PPR_Exp_2	2	0,034	0,085	87

(1) Kg_{Copolymer} mmol_{Ti}⁻¹ h⁻¹ [C_nH_{2n}]⁻¹

From a quick comparison, it is possible to see that the results are in good agreement for both the reaction set-ups, the productivity is slightly higher in a batch reactor at low feeding ratios. This effect could be ascribed to the more efficiency in stirring that a large scale reactor features with respect a mini-scale polymerization set-up. Nevertheless the comparison is a good proof of principle about the total reliability of the mini-scale reactor in catalyst screening for ethene/1-hexene copolymerization at high temperature.

4.6. – Experimental section.

All the catalyst/co-catalyst handling were performed under N₂ or Ar atmosphere, thus using either Schlenk techniques or glove-boxes MBRAUN Lab Master 130, able to keep the O₂ and H₂O value as low as 1ppm_v.

4.6.1. – HTS Freeslate PPR48® homopolymerization self scavenging protocol.

HTS polymerization experiments were carried out with a high throughput parallel reactor setup (PPR48® available from Freeslate), with six reactor modules each containing eight reaction cells (5 mL working volume per cell). The whole system is housed in a triple MBraun LabMaster glovebox maintaining a pure nitrogen atmosphere (oxygen and water levels <1 ppm_v). The monomer gas and quench gas lines are plumbed directly into the reactors and controlled by automatic valves; ethene or propene is fed after purification by passing through columns containing a mixed bed of 4Å molecular sieves (3.2 mm pellets) and an activated copper catalyst (BASF R 3-11G). Liquid reagents are robotically added to individual cells by syringes. Solvents are previously purified in an MBraun SPS unit.

Each cell is fitted with a pre-weighted glass vial insert and a disposable stirring paddle. The reactor modules are closed, then the proper quantity of toluene is injected into each cell through a valve. The reactors are heated at the desired temperature, and stirring is started at a speed of 800 rpm. The reactors are pressurized with the proper amount of bar of monomer (45 psi = 3.1 bar), then the desired amount of pre-catalyst and activator are injected via the robotic sampler without preactivation (pre-catalyst and co-catalyst are kept well separated by a N₂ bubble of 50 µL). The reaction was allowed to proceed at constant pressure for the proper time or until the desired monomer uptake is reached, after that an overpressure of 3.4 bar of dry air was added to quench the reaction. The reactors are cooled, vented and purged with N₂, in order to prevent the glove box pollution with air. After purging with inert gas, the reactors are opened and the glass inserts are unloaded from the cells, transferred to a centrifuge/vacuum drying station (Genevac EZ-2 Plus) for an overnight treatment. The polymer samples are recovered and weighed on a Bohdan BA-100 Balance Automator unit, the polymer yields are automatically stored in a server for further analysis.

4.6.2. – HTS Freeslate PPR48[®] ethene/1-hexene co-polymerization protocol.

HTS polymerization experiments were carried out with a high throughput parallel reactor setup (PPR48[®] available from Freeslate), with six reactor modules each containing eight reaction cells (5 mL working volume per cell). The whole system is housed in a triple MBraun LabMaster glovebox maintaining a pure nitrogen atmosphere (oxygen and water levels <1 ppm_v). The monomer gas and quench gas lines are plumbed directly into the reactors and controlled by automatic valves; ethene or propene is fed after purification by passing through columns containing a mixed bed of 4Å molecular sieves (3.2 mm pellets) and an activated copper catalyst (BASF R 3-11G). Liquid reagents are robotically added to individual cells by syringes. Solvents are previously purified in an MBraun SPS unit.

The cells are fitted with a pre-weighed glass vial insert and a disposable stirring paddle. The reactor is then closed, and 4.0 mL of toluene/1-hexene proper mixture (HPLC grade from Romil, dried and deoxygenated by passing through MBraun SPS mixed bed columns, 1-hexene from Sigma Aldrich, dried and deoxygenated by distillation over Al(C₈H₁₇)₃ at 5% v/v) and 5.0 µmol of MAO/BHT scavenger (MAO from Chemtura, 10%wt toluene solution, 100 µL of a 50mM solution in toluene, [Al]/[BHT] = 1.0) are injected into each cell through a valve. The reactors are thermostated at 90°C, hence the cells are pressurized with ethene (Rivoira, Polymerization Grade, further purified by passing through Grubbs-type columns) at 4,1 bar.

The proper amounts of pre-catalyst and activator (MAO/BHT; [Al]/[BHT] = 1.0, [Al]/[Ti] = 500) are pre-contacted in toluene at RT for 2 min in a 1.2 mL glass vial and then injected in to the cells. The polymerization is run at constant temperature and monomer partial pressure for 5 minutes, then quenched with dry air at 50 psi (3.4 bar) overpressure. The reactors are cooled, vented and purged with N₂, in order to prevent the glove box pollution with air from the quenching. After purging with inert gas, the reactors are opened and the glass inserts are unloaded from the cells, transferred to a centrifuge/vacuum drying station (Genevac EZ-2 Plus) for an overnight treatment. The polymer samples are recovered and weighed on a Bohdan BA-100 Balance Automator unit, the polymer yields are automatically stored for further analysis.

The experiments of copolymerization are summarized in tables 4.2 and 4.3.

Chapter 4 – HTE tools and methods, protocol(s) benchmarking.

4.6.3. Large Scale Batch Reactor copolymerization protocol.

Large scale batch copolymerization were carried out in a 1,5-liter batch autoclave, equipped with a two stage Intermig stirrer and baffles. The reaction temperature was set at 90°C and regulated by a Lauda Thermostat. The feed streams (solvents and monomers) were purified by contacting with various adsorption media to remove catalyst harmful impurities (water, oxygen and any other polar compound). The comonomer used was 1-hexene, further purified via distillation over CaH₂.

In an inert atmosphere of nitrogen, the reactor was filled with the desired amount of pentamethylheptane (PMH), the desired volume of 1-hexene and the MAO/BHT mixture (450mL, MAO-Crompton, 10wt% in toluene; BHT, Aldrich, [Al]/[BHT] = 1.0). The reactor was closed and heated to 90°C, while stirring at 1350 rpm. The reactor was then pressurized to the desired pressure with ethene and conditioned for 15 minutes. The catalyst **C0** was injected via an automated valve and the catalyst vessel was rinsed with 50mL of PMH. After 5 minutes of polymerization, the monomer flow is stopped and the solution is carefully dumped in a 2L Erlenmeyer flask, containing a solution of Irganox-1076 in iso-propanol and dried over night at 100°C under reduced pressure.

4.6.4. – Polymer characterization via HT-GPC and NMR.

The HT-GPC curves were recorded at 135°C with a Waters Alliance GPCV2000 system with dual detection (differential refractometric and differential viscometric), on polymer solutions in 1,2-dichlorobenzene (added with 0.25 mg mL⁻¹ of BHT as a stabilizer). A set of 4 mixed-bed Styragel columns (1 HT-2 and 3HT-6E) was used. Universal calibration was carried out with 12 samples of monodisperse polystyrene (M_n between 1.3 and 3700 KDa). In each carousel of 24 samples, 2 were of a known iPP produced with an *ansa*-zirconocene catalyst used as a standard, to check for consistency. In case the measured M_n and M_w values of the said iPP sample turned out to differ by more than ±20% and ±10% respectively from the “true” values, the calibration procedure was repeated and the whole set of samples re-measured.

The High Throughput SEC profiles were recorded at 145 °C with a Freeslate Rapid GPC system with single detection (Infrared detector IR4 Standalone by Polymer Char), on polymer solutions in 1,2-dichlorobenzene (added with 0,25 mg mL⁻¹ of BHT as a stabilizer). A set of 2 Agilent GPC/SEC columns 10 µm PLGel Mixed bed 300 x 7.5mm was used. Universal calibration was carried out with 10 samples of monodisperse polystyrene (M_n between 1,3 and 3700 KDa). In each of the four racks (48 positions available), 1 was of a known iPP produced with an *ansa*-zirconocene catalyst used as a

Chapter 4 – HTE tools and methods, protocol(s) benchmarking.

standard, to check for consistency. In case the measured M_n and M_w values of the said iPP sample turned out to differ by more than $\pm 20\%$ and $\pm 10\%$ respectively from the “true” values, the calibration procedure was repeated and the whole set of samples re-measured.

The protocol is described as follows: a proper set of unknown polymers was weighted and dissolved with 1,2-dichlorobenzene under stirring at 150°C for two hours (sample concentration $0,5\text{ mg mL}^{-1}$). After 2 h of dissolution each sample was robotically injected into the loop (injection volume $150\text{ }\mu\text{L}$); the system was optimized so to keep the duration of a single analysis down to 20 minutes.

Quantitative NMR spectra of all polypropylene samples were recorded at 120°C , on 35 mg mL^{-1} solutions in tetrachloroethane- $1,2-d_2$, with a Bruker Avance spectrometer (400 Mhz for ^1H) equipped with a 5 mm high temperature cryoprobe. Typical operating parameters were as follows.

- For ^1H NMR: 10.0 ms pulse width (90° pulse); 32K time domain data points, 8.0 kHz spectral width; 2 s acquisition time; 10 s relaxation delay, 200 transients.
- For ^{13}C NMR: 4.5 ms pulse width (45° pulse); 64K time domain data points; 14 kHz spectral width; 2.3 s acquisition time; 5.0 s relaxation delay; 2-10K transient.

Shifted squared sinusoidal weighing functions were used for processing before Fourier transformation.

The spectra were fully simulated with the Shape2004 software package (by Prof. M. Vacatello, University of Naples Federico II; vacatello@chemistry.unina.it).

References.

- [1]. (a) Busico,V.; Pellecchia,R.; Cutillo,F.; Cipullo,R.; *Macromol. Rapid Comm.* **2009**, *30*, 1697-1708; (b) Beighzade, D. *Macromol. React. Eng.* **2007**, *1*, 331-337 ; (c) McWilliams,J.C.; Sidler, R.D.; Sun,Y.; Mathre,D.J.; *Journ. Lab. Autom.* **2005**, *10*, 394-407.
- [2]. Bernardo,R.; Busico,V.; Cipullo,R.; Pellecchia,R.; *Studying olefin polymerization kinetics in High-Throughput mini-reactors*, Poster at Blue Sky Conference 2010.
- [3]. Chen,E.X.; Marks, T.; *Chem Rev.* **2000**, *100*, 1391-1434.
- [4]. (a) Busico,V., Cipullo,R., Cutillo,F., Friederichs,Nic., Ronca,S., Wang,B., *J. Am. Chem. Soc.* **2003**, *125*,12402-12403.; (b) Stapleton,R.A.; Galan,B.R.; Collins,S.; Simons,R.S.; Garrison,J.C.; Youngs,W.J. *J.Am. Chem. Soc.* **2003**, *125*, 9246-9247; (c) Stapleton,R.A.; Al-Humydi,A.; Chai,J.; Galan,B.R.; Collins,S.; *Organometallics* **2006**, *25*(21), 5083,5092.
- [5]. Busico,V., Cipullo,R., Pellecchia,R., Rongo,L., Talarico,G., Macchioni,A., Zuccaccia,C., Froese, R.J.D., Hustad, P.D. *Macromolecules*, **2009**, *42*, 4369-4373.
- [6]. Unpublished data of LSP research group.
- [7]. Piers, W.E.; Zhang,S.; *Organometallics* **2001**, *20*, 2088-2092.
- [8]. Crabtree,R.H.; *The Organometallic Chemistry of the Transition Metals*, Fourth Edition, Wiley-Interscience, 2005.
- [9]. Ciardelli, F.; Crescenzi,V.; Pezzin,G. *Macromolecole, Scienza e tecnologia, vol 1*, **1983**, Pacini editore, chapter IV, 367-399.
- [10]. Kissin,Y.V. *Isospecific Polymerization of Olefins*; Springer-Verlag: New York, 1985; Brintzinger,H.H.; Fischer,D.; Muelhaupt,R.; Rieger,B; Waymouth,R.M. *Angew. Chem., Int. Ed. Engl.* **1995**, *34*, 1143.
- [11]. Kissin,Y.V.; *Isospecific polymerization of olefins*. New York: Springer, 1985.
- [12]. Zhang,S.; Piers, W.E.; Gao,X.; Parvez,M.; *J.Am.Chem.Soc.* **2000**, *122*, 5499-5509.
- [13]. Busico,V.; Cipullo,R.; Talarico,G.; *Macromolecules*, **1998**, *31*, 2387-2390; Busico,V.; Cipullo,R.; Ronca,S.; *Macromolecules*, **2002**, *31*, 1537-1542.
- [14]. Equation 4.2 is an adaptation of the general kinetic equation for the chain propagation as reported by Natta for the propene homopolymerization; Natta,G.; Pasquon,I.; Svab,J.; Zambelli,A.; *La Chimica e L'Industria*, **1962**, *44*, 621-627.
- [15]. E. Ijpeij, P. Windmulle, F. Van Der Burgt, G. Van Doremaele, M. Zuideveld WO2005/090418 A1, 2005 ; Nomura,K.; Liu,J.; *Dalton Trans.***2011**, *40*, 7666.
- [16]. The choice of 1-hexene as the most suitable co-monomer traces its roots in the extremely easiness to handle this chemical (since it is a liquid) and dry/de-oxygenate with $\text{Al}(\text{C}_8\text{H}_{17})_3$. The purification from Al residues is quick and is performed via distillation (see experimental section);

due to the high difference in boiling point between 1-hexene and $\text{Al}(\text{C}_8\text{H}_{17})_3$ (63°C vs $>100^\circ\text{C}$ for $\text{Al}(\text{C}_8\text{H}_{17})_3$), the separation of 1-hexene from any Al residues can be regarded as complete and quantitative.

[17]. Peng, D., Robinson, D.B. *Ind.Eng.Chem., Fundam.*, **1976**, 15, 1.; Dr. Francisco Perez, LANXESS Elastomers B.V., personal communication.

[18]. (a) Bruckner,S.; Allegra,G.; Pegoraro,M.; La Mantia,F.P., *Scienza E Tecnologia dei Materiali Polimerici*, Edises, seconda edizione; (b) Sun,S.F., *Physical Chemistry of Macromolecules: Basic Principles and Issues, Second Edition*; **2004**, John Wiley & Sons, Inc. (c) The existence of more than one active centre in polymerization could be traceable to the ligand modification of the **C3** catalyst due to the presence of residual amounts of Al-C species, e.g. AlMe_3 or $\text{AlMe}_x(\text{O}-2,6\text{-tBu}-4\text{-Me-C}_6\text{H}_2)_{3-x}$. See for instance Nomura, K.; Oya,K.; Imanishi,Y.; *Journ. Of Mol. Catalysis A: Chemical* **2001**, 174, 127-140 and Stelzig,S.H.; Tamm,M.; Waymouth,R.M. *Journ. Of Polymer Science: Part A: Polymer Chemistry*, **2008**, 46, 6064-6070.

[19]. (a) SHAPE© GPC 1.0 – **2008** Rongo,L.; Vacatello,M.; (b) Busico,V.; Cipullo,R.; Pellecchia,R.; Rongo,L.; Talarico,G.; Macchioni,A.; Zuccaccia,C.; Froese,R.J.D.; Hustad,P.D.; *Macromolecules*, **2009**, 42, 4369-4373.

5.1 – Introduction.

After the development and benchmarking of the HTE protocol for the iminato catalysts **C0** and **C3**, the fast database generation can be acquired, using all the potentialities of the HTS platform PPR48[®]. This notwithstanding, the comparison of different catalysts is always inhomogeneous in copolymerization, since the performance depends on a plethora of different variable (both physical and chemicals) and the production of different materials will bias the complexes comparison. In order to overcome this problem, in section 2 the general experimental matrix will be described along with the concept of HTE tools as *trend providers*. The remaining three section of the chapter will describe the database acquisition and the data handling. In section 3 of this chapter, the kinetics of copolymerization will be simulated with a proper function, mostly emphasizing the catalyst deactivation contribution to the kinetic. In section 4, the copolymer characterization will be provided accordingly to the screening protocol and the general matrix of section 2; in section 5 the results will be shown for all the catalysts screened.

5.2 –HTE, the general experimental design matrix.

As stated in chapter 4, the HTE protocol for iminato catalysts screening in EH copolymerization is established, since the proper conditions to tame the huge activity of the catalysts are found. Low feeding ratios will ensure the best kinetic assessment figure 5.1¹.

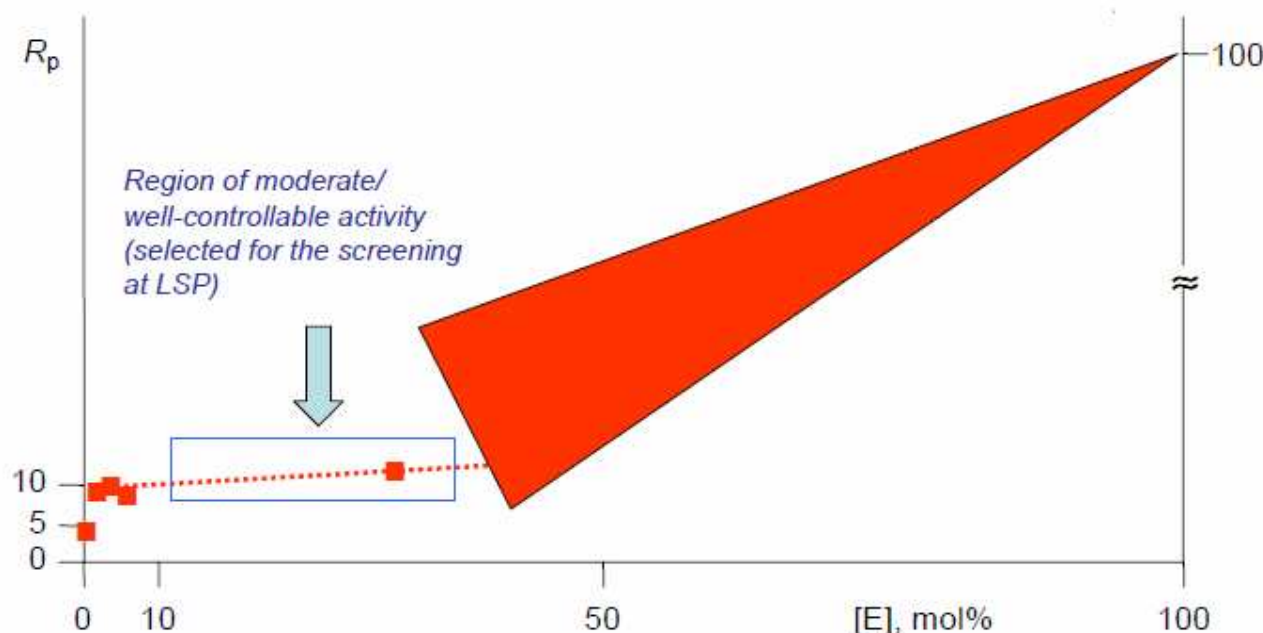


Figure 5.1. Region of moderate and well controllable activity for the iminato catalysts.

It is therefore possible to explore the quoted region in figure 5.1 working at high amount of 1-hexene: for most feeding ratios, the comonomer consisted in more than one half of the liquid phase. The most obvious advantage of HTE technologies in catalyst screening is the possibility to assess thoroughly a large number of structures in a very short time². However, the case copolymerization is tough even for HTE: the iminato catalysts screening raises, as a case history, a conceptual question, i.e. the comparative evaluation of catalysts in copolymerization. In figures 5.2 the performance of four iminato complexes are compared at a discrete feeding ratio. The bar diagram in figure 5.2a shows the average productivity under this given set of conditions; on inspection, catalyst 4 appears to be by far the most active. The bar diagram in figure 5.2b on the other hand, compares the chemical compositions of the four copolymers produced; it is clear that these are appreciably different, which implies that the comparison between complexes is not homogeneous (*vide infra*). This is, in essence, the problem that needs to be overcome: in fact, the performance in copolymerization depends on a plethora of variables (both physical and chemical)³, and each catalyst will respond differently to each of them.

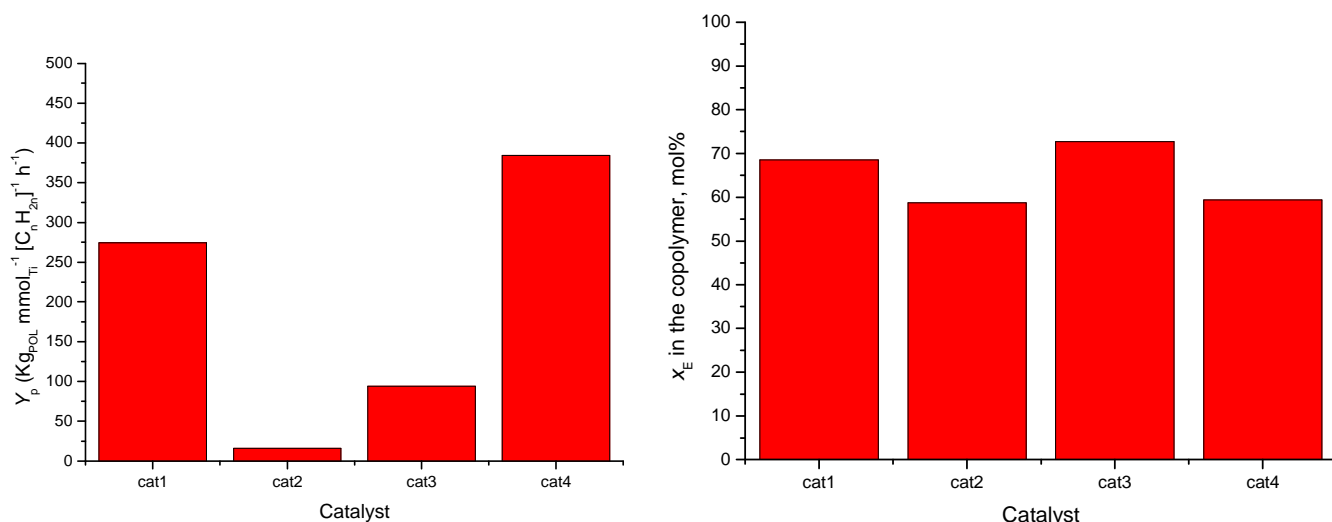


Figure 5.2. a) Catalyst average productivities in EH copolymerization, $[\text{E}_0]/[\text{H}_0] = 0,050$; and b) copolymer compositions at the corresponding feeding ratio.

This concept is well illustrated in figure 5.3, in which the performance of the very same four catalysts is compared on a wide range of E/H feeding ratios (ending up with a correspondingly wide range of copolymer compositions). It is only looking at *trends*, rather than *single data points*, that the true catalyst behavior can be analyzed; in particular for each catalyst, in perfect correspondence to the kinetic qualitative analysis of chapter 4, a threshold x_E value exists, above which the productivity takes off, and any comparisons which ignores this fact is meaningless.

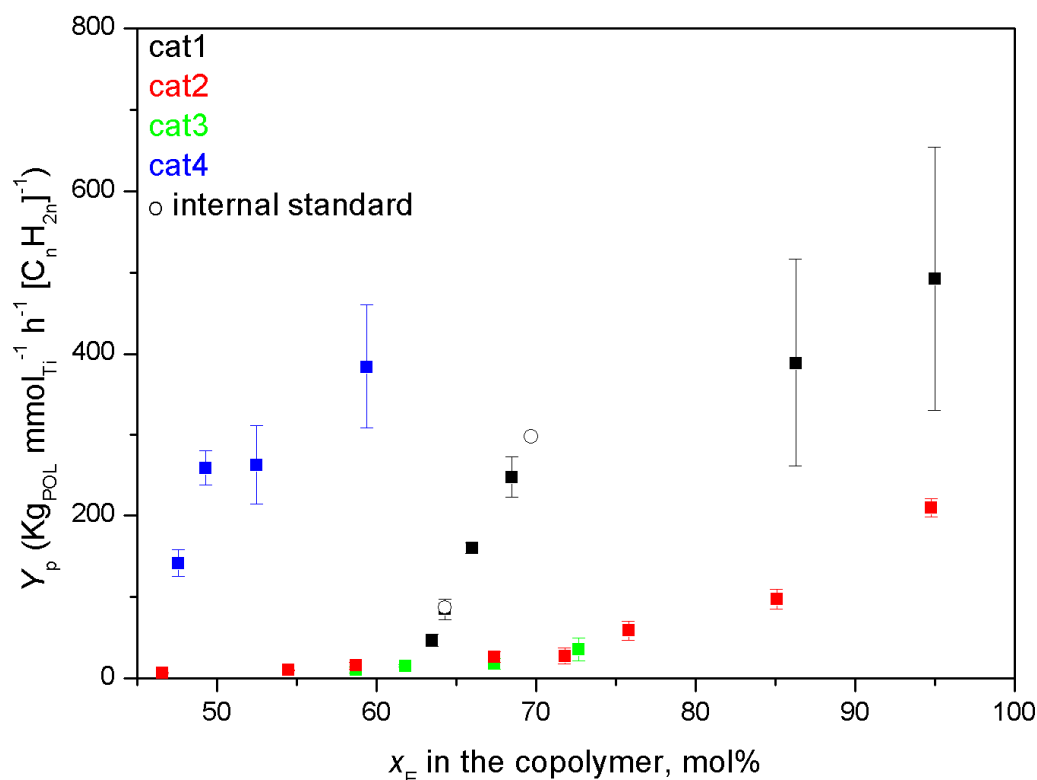


Figure 5.3. Results of E/H copolymerization experiments in the presence of four different catalysts at variable feeding ratios and, therefore, variable copolymer compositions. White dots are experiments with an internal standard for consistency check.

HTE tools and methods can therefore be used as ‘*trend providers*’; several reaction conditions are explored rather than several structures in a very short time. Nevertheless, the huge capability of HTE technologies still makes it possible to maximize both the number of conditions and structures with a proper experimental design. A fair compromise is, in fact, shown in table 5.1: the typical 48-elements PPR[®] matrix of a general experiment is described. As the matrix shows, *four* unknown structures can be screened at *three* different comonomer feeding ratios; for each condition a reference catalyst is tested twice as an internal standard, in order to provide a further check on the reliability and quality of the kinetic data obtained from any experiments. Due to the deep and complete benchmarking of the experimental protocol, the system used as internal standard was the catalyst **C0**. For each structure three matrix elements are dedicated (meaning three experiments); one of which features the catalyst at halved concentration, in order to rule out any mass transfer limitation effects.

Chapter 5 – HTE Copolymerization Screening

Table 5.1. General experimental design matrix for the general screening library.

$[E_0]/[H_0] = x$		$[E_0]/[H_0] = y$		$[E_0]/[H_0] = z$	
Internal Standard C0 (six matrix elements on this row)					
[Cat1]	[Cat3]	[Cat1]	[Cat3]	[Cat1]	[Cat3]
[Cat1]	[Cat3]	[Cat1]	[Cat3]	[Cat1]	[Cat3]
[Cat1]/2	[Cat3]/2	[Cat1]/2	[Cat3]/2	[Cat1]/2	[Cat3]/2
[Cat2]	[Cat4]	[Cat2]	[Cat4]	[Cat2]	[Cat4]
[Cat2]	[Cat4]	[Cat2]	[Cat4]	[Cat2]	[Cat4]
[Cat2]/2	[Cat4]/2	[Cat2]/2	[Cat4]/2	[Cat2]/2	[Cat4]/2
Internal Standard C0 (six matrix elements on this row)					

The quite uncommon usage, to the best of our knowledge, of HTE tools as *trend providers* is the best answer to the conceptual question of catalyst comparison in copolymerization; at this point all the pieces of information are provided, the catalysts comparison can be done both at a definite comonomer feeding ratio and at a definite copolymer composition, usually by interpolation on a suitable data set.

5.3 – Kinetic data simulation and the deactivation constant, k_d .

As already explained in chapter 4, the PPR[®] enables the opportunity to look at the reaction kinetics during the experiment, namely providing a monomer uptake profile during the reaction. As it is stated in the literature⁴, the way the polymerization kinetic profile is generated places its root in a smart and easy way to measure the gaseous monomer consumption: the reaction is allowed to proceed at a certain constant pressure P and, when the monomer is consumed during the reaction, a pressure drop occurs, leading to a new value of reactor pressure $P-\Delta P$. The value of maximum allowable ΔP (pressure deadband) is pre-set in the experimental setup (usually 2 psi – 0,14 bar), whenever this value is exceeded, the reactor valves compensate for the pressure drop, ‘recharging’ the reactor with and additional ΔP of monomer (figure 5.4). The numerical integration of the monomer recharges provides the uptake curve and the uptake/rate curve is calculated as the numerical first derivative of the uptake curve over the polymerization time (figure 5.5).

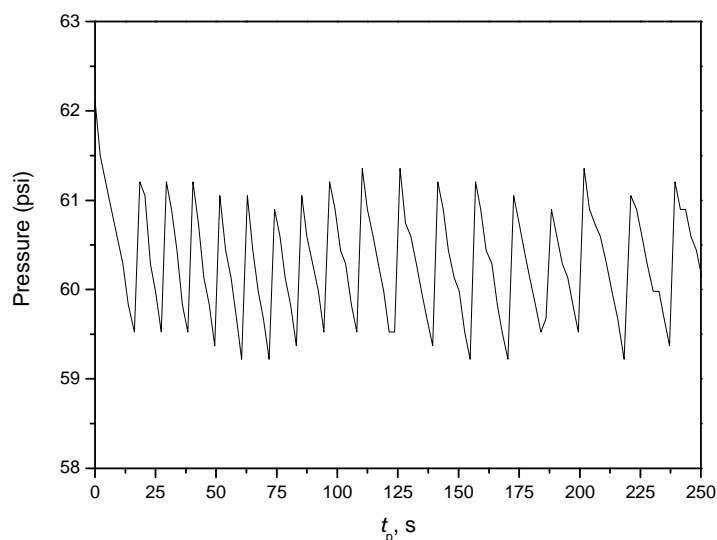


Figure 5.4. Pressure drop during a polymerization in the PPR[®].

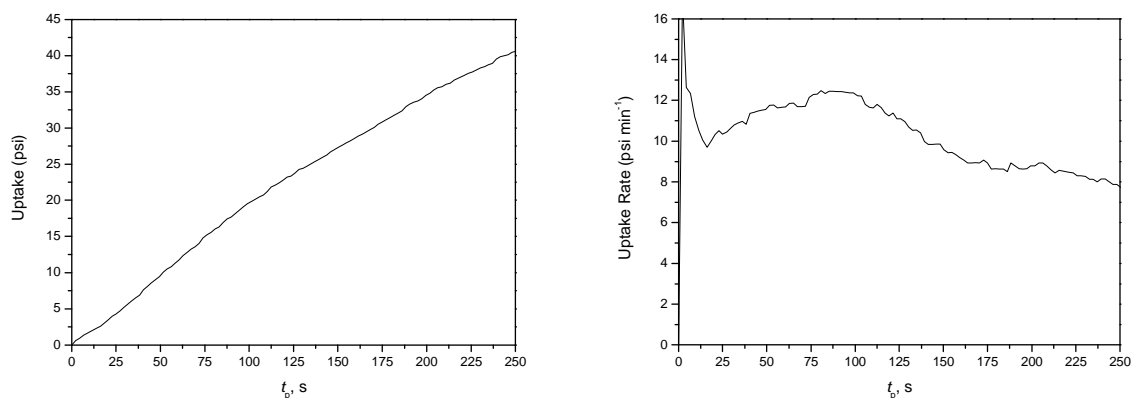


Figure 5.5. Uptake (left) and Uptake Rate (right) profile for a EH copolymerization with C0.

The possibility of access reliably to the reaction kinetic profile allows to state ‘at a glance’ whether a catalyst is prone to deactivation or not in the usual time frame of polymerization⁵. Moreover the possibility to export numerically the kinetic profiles allows the kinetics simulation^{4b} with the calculation of the deactivation constants k_d (figure 5.6). In the experimental section of this chapter the simulating function is described along with the calculation of the deactivation constant.

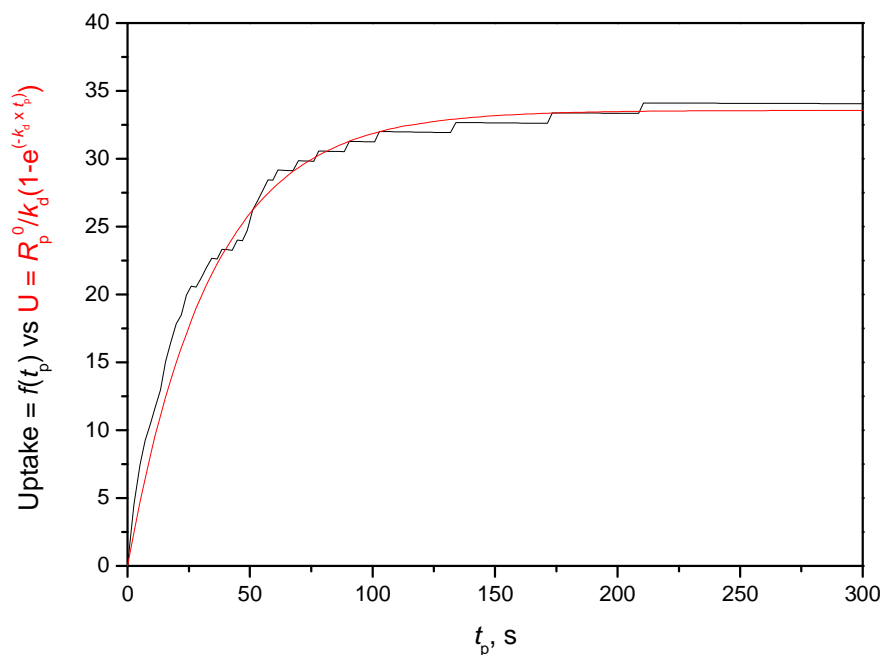


Figure 5.6. Curve simulation and k_d calculation for a deactivating catalyst, **C39** *vide infra* and appendix 5.1.

Besides the numerical value of the deactivation constant; it is possible to discriminate quantitatively whether or not a certain catalysts undergoes deactivation during the polymerization. From the full simulation of all the kinetic profiles of several polymerization, it is possible to state a threshold of k_d , which is internally consistent in this kinetic database, since all the polymerization have a duration of 5 minutes. Accordingly to the simulation reported in figure 5.7, a catalyst does not deactivate in 5 minutes if $k_d \leq 1.0 \times 10^{-4} \text{ s}^{-1}$.

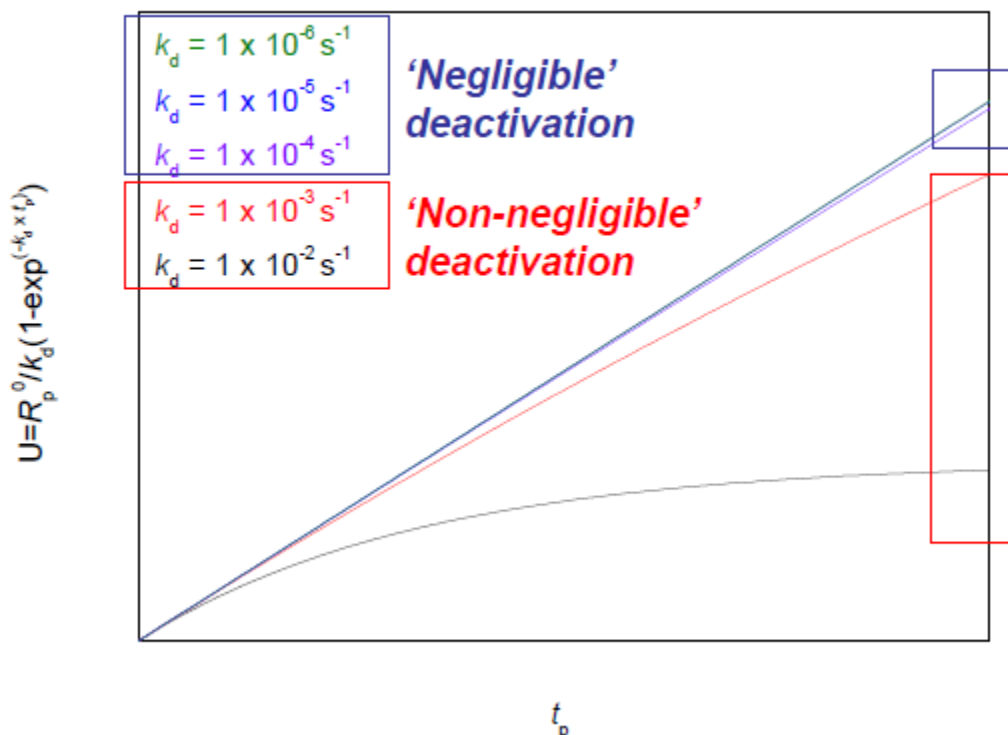


Figure 5.7. Kinetic profile simulation for the deactivation constant threshold.

The deactivation constant can be regarded as an empirical feature related to the screened catalysts, thus it does not provide *per se* any information about the mechanism of catalyst deactivation, on which further and dedicated studies have to be performed, out of the scope of this thesis. Nevertheless it is possible already to rule out that the deactivation process is caused by bimolecular aggregation of active centers: although it is well known that metallocene aggregation occurs during the polymerization⁶, this seems not to be related to the deactivation of amidinato-complexes, since the recorded k_d values do not change with respect to the catalyst concentration (appendix 5.1).

5.4 – Polymer characterization, copolymer composition and reactivity ratios.

The general equation of copolymerization (equation 5.1)⁷ provides the possibility to correlate the copolymers' composition with the comonomer feeding ratios through the reactivity ratios, r_E and r_H (of course, $r_E = k_{EE}/k_{EH}$; $r_H = k_{HH}/k_{HE}$). It will be through these parameters that the quantitative comparison of incorporation capability of the complexes will be implemented.

$$dE/dH = [E_0]/[H_0] (r_E[E_0]/[H_0] + 1)/([E_0]/[H_0] + r_H) \quad \text{Eq. 5.1}$$

The copolymer composition can be, in general, quickly and reliably estimated via NMR spectroscopy and, in order not to have bottlenecks downstream the HTS platform, the fast ^1H NMR spectroscopy seems to be the natural choice (figure 5.8).

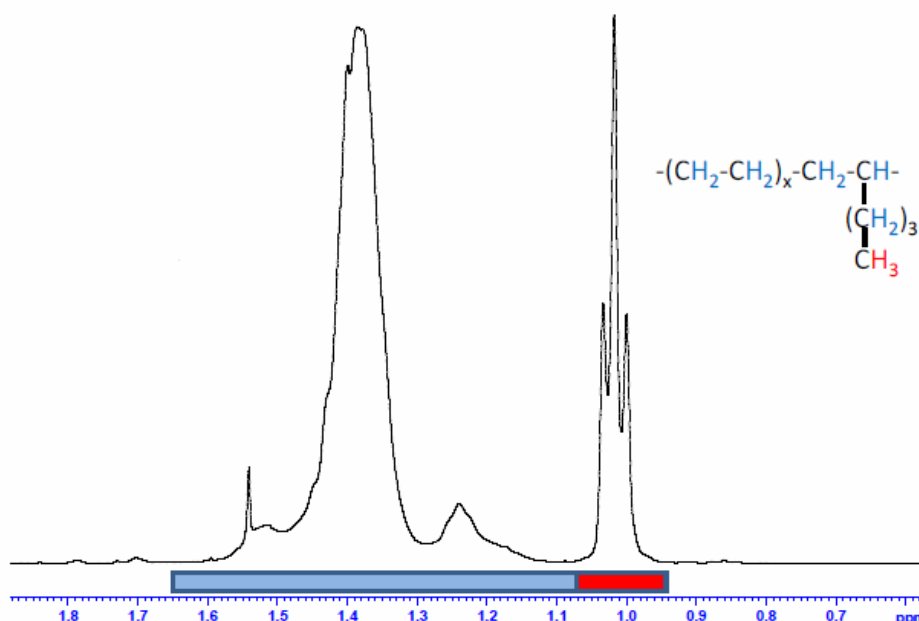


Figure 5.8. Fast acquisition of copolymer composition via ^1H NMR characterization, the color of the peaks refer to the correspondingly protons; the polymer composition is calculated via the Sigma-Aldrich general procedure⁸.

Unfortunately two major drawbacks proved the ^1H NMR characterization insufficient to the proper characterization:

- Low purity of the samples
- Small feeding ratios range stemmed in the PPR[®].

The purity of the sample is not always granted, since the protocol of reaction quenching does not prevent inorganic residues to precipitate along with the polymer (the most common residues are Al-alkoxydes, which arise from the MAO/BHT mixture oxidation by air reaction quenching, experimental section). The region of interest in ^1H NMR spectra is relatively small (2.0 ppm), overlaps between diagnostic and impurities signals always occur, thus jeopardizing the accuracy in polymer composition determination⁸ (figure 5.9).

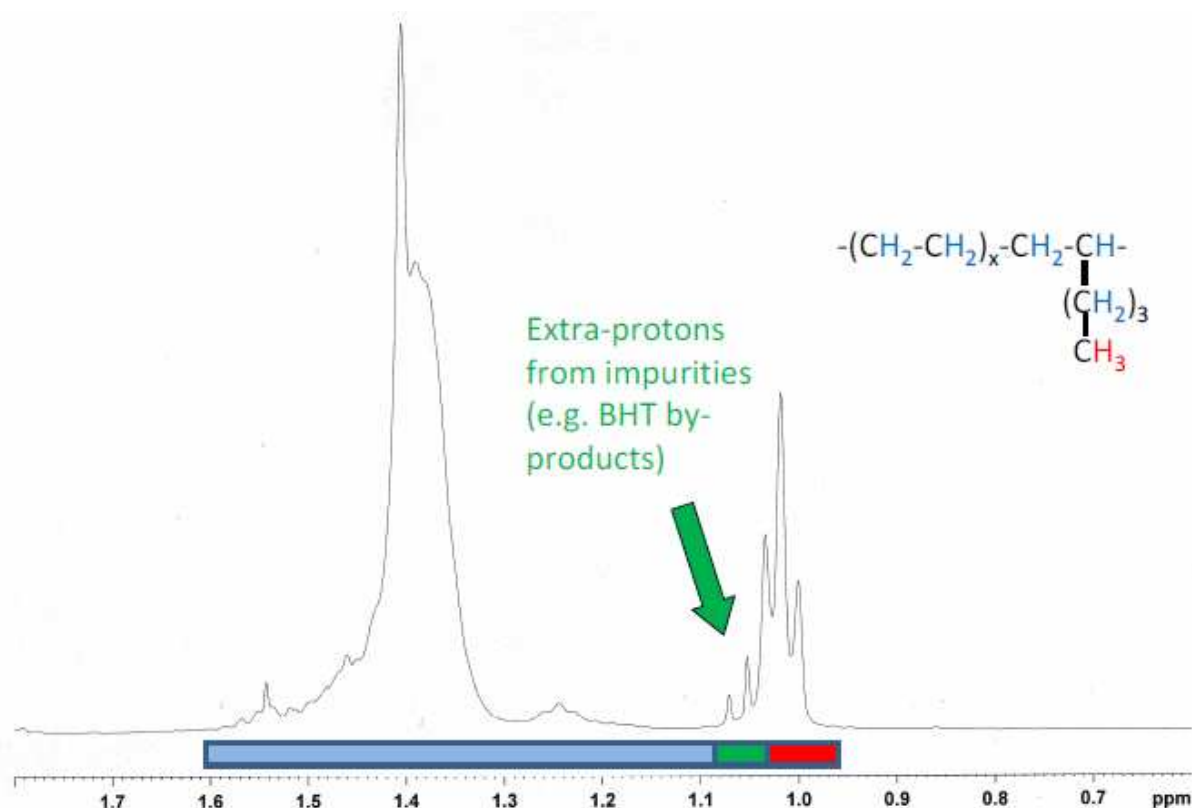


Figure 5.9. Typical ^1H NMR of a EH copolymer from amidinato catalysts (C39) screened in the PPR[®]. As it is possible to see, the overlap of diagnostic signals and impurities peaks is severe.

From the general equation of copolymerization, it is possible to calculate the reactivity ratios of the complexes via the parameterization of equation 5.1 (equation 5.2)⁹.

$$y = (1 + r_E x) / (1 + r_H/x) \quad \text{Eq. 5.2}$$

where $y = dE/dH$ and $x = [E_0]/[H_0]$.

The basic requirement for the highest accuracy of the determination of the reactivity ratios is the wide range of copolymer compositions, which is not allowed by the screening protocol: the region of well controlled activity of the catalyst is inherently limited in the PPR[®] protocol, therefore the use of Eq. 5.2 is ineffective both to determine reliably the reactivity ratios of the catalysts, and to discriminate between different catalysts in a limited, and flat, region of equation 5.2. As an example, in figure 5.10, two regression functions are reported for two different catalysts. Even though the two complexes feature different reactivity ratios, the two functions overlap in the region accessible with the PPR[®], thus leading to an ambiguous determination of the reactivity ratios.

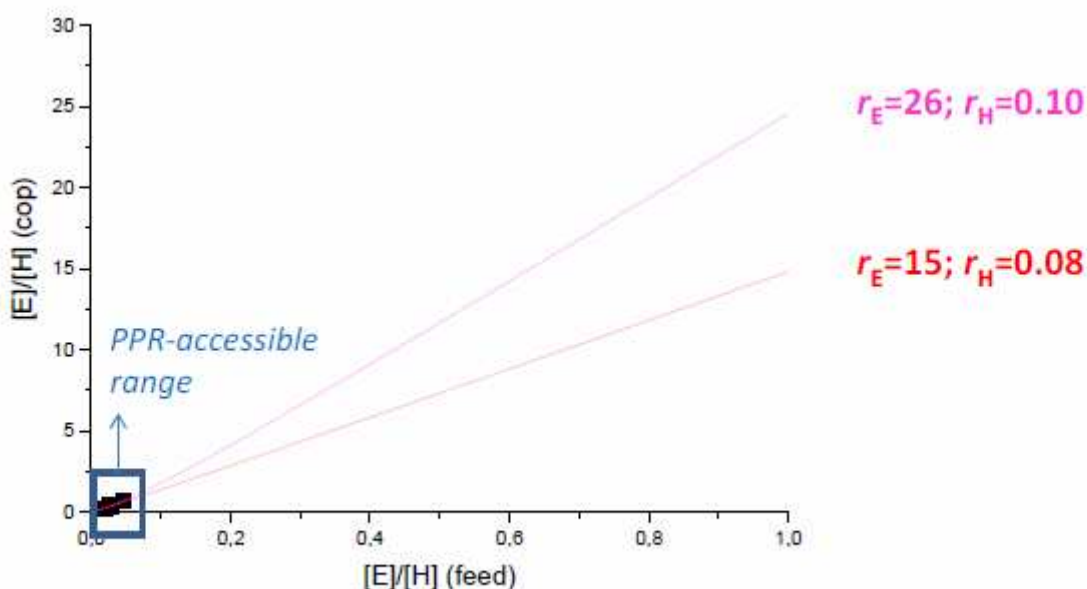


Figure 5.10. Reactivity ratios calculation via the parameterization of the general polymerization equation. In figure two functions are reported, belonging to two different complexes with different reactivity ratios. The method can be applied with reasonable accuracy only at a wide copolymer composition range, thus including relatively high ethene composition; unfortunately this is unfeasible due to the high activity of the amidinato-catalysts at high ethene content in the liquid phase (figure 5.1 and equation 4.2).

The ^{13}C NMR analysis is the perfect answer to the problems that arise during the ^1H NMR characterization of the copolymers; first of all the impurities are not an issue any more, due to the higher region of interest in the spectrum (up to 100 ppm)¹⁰ and the consequent absence of peak overlaps; moreover, from ^{13}C NMR, the sequence distribution becomes accessible, thus ruling out any ambiguities regarding the reactivity ratios ¹¹(table 5.2).

Table 5.2. Triad sequence distribution for two copolymers produced at $[\text{E}_0]/[\text{H}_0] = 0.020$, with the two complexes featuring the reactivity ratios of figure 5.10.

Copolymer triad distribution	$r_{\text{E}} = 26$ $r_{\text{H}} = 0.10$	$r_{\text{E}} = 15$ $r_{\text{H}} = 0.08$
$[\text{EEE}]^*$	0.0237	0.0109
$[\text{EEH}]^*$	0.0919	0.0730
$[\text{HEH}]^*$	0.0892	0.1222
$[\text{EHE}]^*$	0.0230	0.0318
$[\text{EHH}]^*$	0.2244	0.2540
$[\text{HHH}]^*$	0.5478	0.5080
$[\text{E}]^*$	0.2048	0.2062

* Normalized integral.

Chapter 5 – HTE Copolymerization Screening

The possibility to access to the sequence distribution allows the calculation of the reactivity ratios directly, moreover, as it appears clear from table 5.2, the differences between the two quoted copolymers become evident, even though the average composition is quiet the same (the [E] value for both of them is almost coincident).

5.5 – Catalyst Screening Results, the experimental database.

The fast experimental database generation for amidinato-complexes had been executed for several structures, with respect the catalyst activity, the copolymer compositions (and hence the reactivity ratios), the molecular weight of the copolymers at three/four feeding ratios. The catalyst structures span several structural amplification motives¹², both on the Cp ring and on the donor ligand. The experimental results are summarized in table 5.3.

Table 5.3. Data collection for all the amidinato-complexes screened.

Library Id	Cell	Catalyst	$[E_0]/[H_0]$	$[H]^{(1)}$ (mol%)	r_E	r_H	$Y_p^{(2)}$	M_n , KDa
116860	1F (1G-1E-1H)	C3	0.049	50.7	19	0.044	15.8	33.5*
	2H (2E-2F)	C3	0.033	n.d.	n.d.	n.d.	10.1	36.3*
	3G (3H-3E-3F)	C3	0.025	67.5	15	0.033	6.9	28.4*
	4G (4H-4E-4F)	C3	0.020	71.6	15	0.033	4.9	13.9*
119180	1C (1E)	C26	0.050	37.0	30	0.019	92	103
	2C (2E)	C26	0.035	44.0	33	0.020	62	74
	4C (4D-4E)	C26	0.025	46.1	38	0.019	28	93
	1F (1H)	C27	0.050	36.4	32	0.021	112	88
	2F (2H)	C27	0.035	42.8	33	0.020	78	68
	4F (4H)	C27	0.025	47.2	40	0.018	44	101
119240	1D	C24	0.050	30.3	48	0.021	117	255
	2E (2D)	C24	0.035	37.0	52	0.019	94	n.d.
	4C (4E)	C24	0.025	45.9	52	0.021	57	n.d.
	5D (5E)	C24	0.020	51.2	54	0.021	48	364
	1F (1B)	C28	0.050	38.2	30	0.024	87	150
	2B (2G)	C28	0.035	46.2	30	0.024	55	n.d.
	4F (4H)	C28	0.025	52.6	33	0.023	35	n.d.
	5G (5F-5H)	C28	0.020	57.7	33	0.023	24	127
119280	1C (1E-1D)	C31	0.050	42.8	29	0.036	190	191
	2C (2E-2D)	C31	0.035	47.1	34	0.034	134	n.d.
	3C (3E-3D)	C31	0.025	57.2	34	0.034	105	n.d.
	4D (4E-4C)	C31	0.020	61.1	35	0.031	88	294
	1F (1G-1H)	C34	0.050	47.3	26	0.046	105	311
	2F (2G-2H)	C34	0.035	57.4	23	0.046	67	n.d.
	3F (3G-3H)	C34	0.025	66.1	22	0.044	54	n.d.
119300	1E (1D)	C38	0.050	38.0	29	0.021	264	163
	2C (2D-2E)	C38	0.035	48.9	27	0.027	169	n.d.
	3C (3D-3E)	C38	0.025	54.3	32	0.026	117	n.d.
	4B (4D-4C)	C38	0.020	55.9	37	0.022	81	108
	2F (2G-2H)	C39	0.035	44.0	36	0.027	2	n.d.
	3F (3G-3H)	C39	0.025	51.0	45	0.028	1.5	n.d.
	4F (4G-4H)	C39	0.020	55.2	47	0.026	1.3	29
117600	2C (2D-2E)	C17	0.035	42.9	36	0.021	19	482
	3E (3F)	C17	0.025	52.1	36	0.024	17	n.d.

Chapter 5 – HTE Copolymerization Screening

	4E (4F)	C17	0.020	56.3	37	0.023	13	551
	1F (1G)	C18	0.050	30.5	33	0.0073	65	170
	2F (2G-2H)	C18	0.035	37.8	32	0.0077	32	143
	3G (3H)	C18	0.025	43.2	33	0.0079	20	137
	4G (4H)	C18	0.020	48.2	32	0.0083	12	154
117720	1C (1D-1E)	C19	0.050	34.5	37	0.021	94	54
	2C (2D-2E)	C19	0.035	41.3	39	0.020	46	42
	3B (3D-3E)	C19	0.025	46.0	43	0.017	40	44
	4D (4E)	C19	0.020	48.8	49	0.016	27	47
	1F (1G-1H)	C20	0.050	49.7	33	0.071	384	482
	2F (2G-2H)	C20	0.035	59.3	37	0.075	262	448
	3F (3G-3H)	C20	0.025	69.0	28	0.062	258	409
	4F (4G-4H)	C20	0.020	71.8	29	0.052	142	n.d.
117740	1C (1D-1E)	C21	0.050	26.9	54	0.015	62	41
	2C (2D-2F)	C21	0.035	37.1	50	0.018	32	41
	3B (3D-3E)	C21	0.025	42.3	59	0.018	24	53
	4B (4C-4D)	C21	0.020	47.3	59	0.017	32	50
	1F (1G-1H)	C22	0.050	22.2	70	0.013	214	99
	2G (2H)	C22	0.035	28.1	73	0.012	140	90
	3F (3G-3H)	C22	0.025	33.9	79	0.011	81	88
	4F (4G-4H)	C22	0.020	39.3	78	0.012	51	65
122600	1C (1E)	C23	0.050	26.5	78	0.034	76	n.d.
	2B (2D)	C23	0.029	39.2	91	0.035	37	329
	3E (3C)	C23	0.020	51.7	100	0.032	23	371
	1G (1H)	C25	0.050	29.9	45	0.011	101	230
	2H (2G)	C25	0.029	41.8	47	0.017	51	124
	3F (3H)	C25	0.020	50.3	46	0.016	29	203
	4E (4B)	C30	0.050	27.5	53	0.016	141	n.d.
	5C (5D)	C30	0.029	39.3	55	0.017	71	300
	6C (6E)	C30	0.020	46.3	62	0.017	52	231
	4G (4F)	C32	0.050	31.3	50	0.028	20	216
	5F (5B)	C32	0.029	51.8	42	0.034	10	72
122640	1D (1E)	C33	0.049	25.5	79	0.029	20	164
	2B (2D)	C33	0.030	35.2	86	0.026	8	138
	3C (3D-3E)	C33	0.021	44.4	89	0.024	4	124
	1F (1G)	C35	0.048	58.6	16	0.065	40	165
	2F (2H)	C35	0.028	73.9	13	0.062	23	286
	3H (3G)	C35	0.020	81.1	17	0.080	13	269
	4C	C36	0.047	52.9	34	0.084	133	n.d.
	5B	C36	0.029	57.1	41	0.054	94	582
	6B (6E)	C36	0.020	70.1	36	0.054	75	574
	4H (4F)	C37	0.049	35.3	52	0.041	70	183
	5H (5F)	C37	0.029	47.7	54	0.037	32	333
	6F (6H)	C37	0.019	59.6	55	0.036	21	321
122760	1C (1E)	C40	0.050	48.1	24	0.047	70	283
	2C (2E)	C40	0.028	62.3	24	0.044	38	301
	3C (3E)	C40	0.020	71.2	20	0.043	24	352
	1H	C41	0.047	64.7	12	0.074	76	162
	2G	C41	0.028	75.3	11	0.065	62	159
	3F	C41	0.019	83.8	9	0.064	52	346
	4C	C42	0.046	36.6	34	0.020	228	178
	5E	C42	0.029	43.4	44	0.020	116	286
	6C (6E)	C42	0.020	52.1	43	0.019	59	175

(1) In the copolymer, evaluated via ^{13}C NMR;

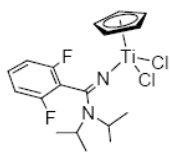
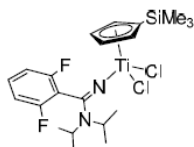
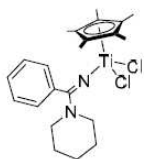
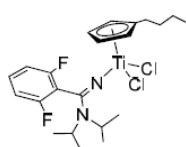
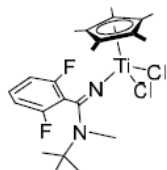
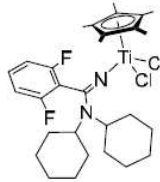
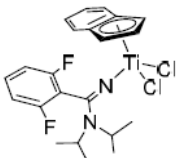
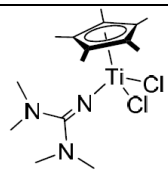
(2) $\text{Kg}_{\text{Copolymer}} \text{ mmol}_{\text{Ti}}^{-1} \text{ h}^{-1} [\text{C}_n\text{H}_{2n}]^{-1}$;

(3) $\text{PDI} = 2.0$

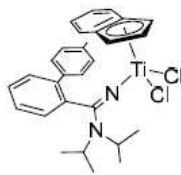
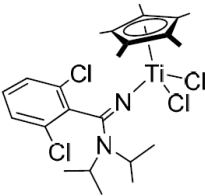
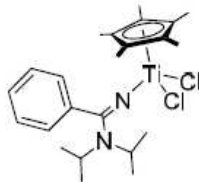
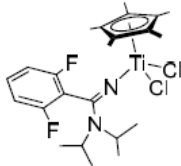
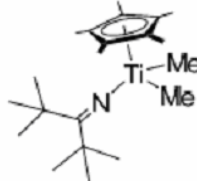
* $\text{PDI} > 2.0$

Chapter 5 – HTE Copolymerization Screening

Legenda

Complex Codename	Structure
C26	
C27	
C24	
C28	
C31	
C34	Not Allowed to disclose
C38	
C39	
C17	
C18	Not Allowed to disclose
C19	Not Allowed to disclose
C20	Not Allowed to disclose

Chapter 5 – HTE Copolymerization Screening

C21	
C22	
C23	Not Allowed to disclose
C25	
C30	Not Allowed to disclose
C32	Not Allowed to disclose
C33	Not Allowed to disclose
C35	Not Allowed to disclose
C36	Not Allowed to disclose
C37	Not Allowed to disclose
C40	Not Allowed to disclose
C41	Not Allowed to disclose
C42	
C3	

As it is possible to see from table 5.3, the amount of data that can be gained is enormous, nevertheless it is possible to compare each complex to the others, even though the behavior is inherently different at each feeding ratio. The comparison, at this stage, is empirical *per se*, but the amount of data can be used for the developing of a QSAR model, in order to start the approach of rationally-wise catalyst design.

5.6 – Fast database generation, the *in-situ* complexation approach.

As it was stated several times during the thesis, the amidinato catalysts are perfectly suited to HTE tools and method due to their general synthetic approach. At odds to the typical metallocenes (e.g. the structures introduced by Spaleck, featuring synthesis of more than 5 steps)¹³, the amidinato complexes are much easier to be synthesized, moreover several pathways are available (figure 1.6); notwithstanding the complexation reaction is one of the most delicate steps, being relatively time consuming. As it is possible to see from figure 1.6, unless an alkylated metal precursor is employed, the complexation reaction needs a Lewis base to be performed (Et_3N is the most widely used)¹², thus bringing an additional step for the purification. The use of an alkylated metal precursor in general saves synthetic steps, but the complex is inherently more vulnerable to impurities and polar compounds due to the higher reactivity of Ti–R bonds with respect Ti–Cl bonds³.

In order to quicken as much as possible the secondary screening workflow, we have studied the possibility to carry out the ligand/metal complexation with the HTE protocols, thus using a $\text{Cp}'\text{Ti}(\text{CH}_2\text{C}_6\text{H}_5)_3$ as a metal precursor ($\text{Cp}' = \text{R}_n\text{H}_{5-n}\text{Cp}$) in combination with the usual protonated ligand (e.g. scheme 1, *vide infra*).

For this reason we tried the complexation synthesis with an *in situ* approach in a fully automated organometallic synthesis platform, i.e. the Freeslate™ eXtended Core Module™ (XCM™, figure 5.11), completely housed in a triple glove box, so to ensure high purity of the environment during the chemicals manipulation.



Figure 5.11. Freeslate™ eXtended Core Module™ (XCM™) primary screening/organic and organometallic synthesis. The fully automated platform enables the primary screening and the synthesis of organic and organometallic intermediates; both the housing in a triple glove box and the off-line integration with solvent and chemical purification facilities enable the highest reproducibility and reliability in organometallic synthesis.

The potentialities of this approach are dramatic in a secondary screening workflow: as it is possible to see in the present chapter, the catalyst evaluation and polymer characterization methods enable the evaluation of 4 structures *per die* thus moving the rate limiting step of the entire workflow to the catalyst synthesis. The automation of the synthesis would move the rate limiting step within the catalyst preparation loop and, in particular, on the ligand synthesis (figure 1.6).

In order to verify the relevance of the *in situ* complexation we investigated the co-polymerization performances of catalyst **C0** compared to its complexation mixtures, previously reacted at two different temperature over two hours ($T_c = 50^\circ\text{C} - 80^\circ\text{C}$) and at a reagent concentration similar to the usual polymerization stocks ($[\text{Ti}] = [\text{Ligand}] = 1 \div 2 \text{ mM}$). The results are summarized in table 5.4.

Table 5.4. Copolymerization experiments for the complex **C0** and the *in situ* complexes counterparts; entry # 4 is the ‘blank’ polymerization, in which the metal precursor $\text{Cp}^*\text{Ti}(\text{CH}_2\text{C}_6\text{H}_5)_3$ is tested in copolymerization (further details are provided in the experimental section).

Entry	Catalyst	$[\text{E}_0]/[\text{H}_0]$	$Y_p^{(1)}$ (RSD ²)	x_E (mol %)	M_n (KDa)	PDI
1	C0	0,050	250 (10)	68	126	2.0
2	C0-Bz₂ @ 50°C		101 (44)	n.d.	129	3.0
3	C0-Bz₂ @ 80°C		163 (9)	68	126	2.5
4	Cp[*]Ti-Bz₃		21 (n.d.)	49	35	2.3

(1) $\text{Kg}_{\text{Copolymer}} \text{ mmol}_{\text{Ti}}^{-1} \text{ h}^{-1} [\text{C}_n\text{H}_{2n}]^{-1}$.

(2) Evaluated on a polymerization experiment set ≥ 4 .

As it is possible to see from table 5.4, the comparison is in favour of the isolated complex **C0**, at least concerning the activity. Besides the fact that the complexation could not be quantitative in the explored conditions, the results are promising. The activity is lower (and, in general, catalyst productivity could still be roughly estimated in a secondary screening phase), but the polymer is practically similar to the one obtained with the isolated complex **C0**, with the exception of entry # 2. The possible explanation to this broadening of the PDI could rise in the un-efficient complexation of the metal precursor (the metal precursor residues could be active in polymerization).

Given that the *in situ* approach is extremely appealing, due to the fact that it is completely in the spirit of the secondary screening (identification of *leads* to be further refined in a larger scale screening), the experiments of table 5.4 signal that the complexation is still not complete. Even though the optimization is out of scope of the present work, but the feasibility study is not, we focused on a simpler complex **C27** (Scheme 1), thus enhancing both the temperature and the concentration of complexation ($T_c = 90^\circ\text{C}$ and $[\text{Ti}] = 80 \text{ mM}$), in order to verify whether or not substantial hindrances were present for the approach in general. In figure 5.12 the ^1H NMR spectra of the ligand, metal precursor and reaction mixture are reported.

Scheme 1. Complexation reaction for complex **C27**.

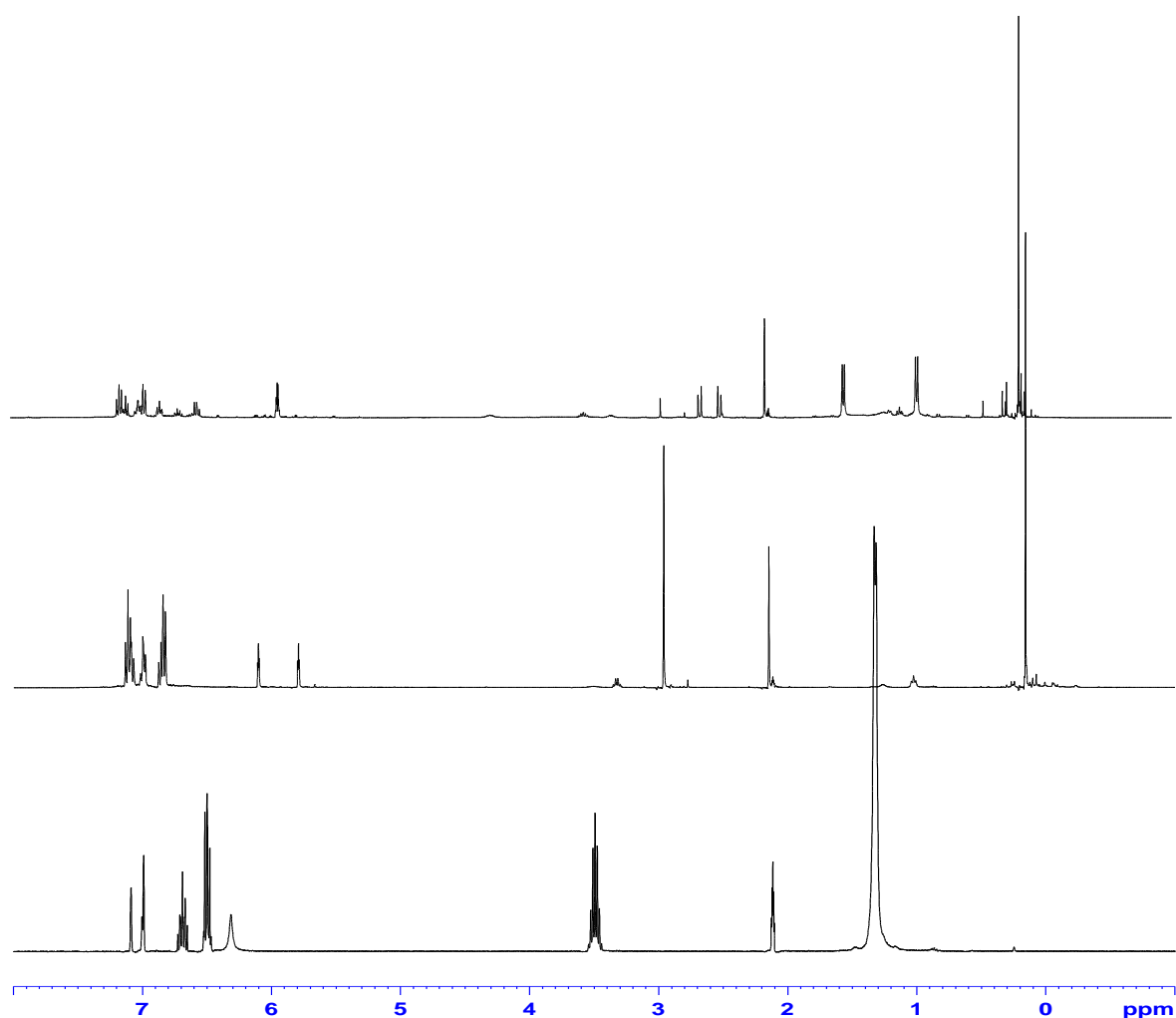
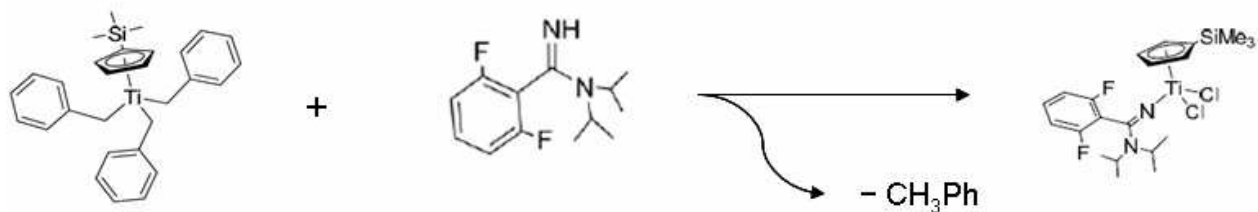


Figure 5.12. ^1H NMR spectrum of reaction complexation for the complex **C27**; ligand (bottom), metal precursor (middle), complexation mixture (top) after 1h of reaction at 90°C .

From figure 5.12 it is possible to follow the complexation within the single spectrum. Starting from the metal precursor, it is possible to appreciate the reorganization of the benzyl moieties from three equivalent groups in two different groups (the singlet at 2.96 ppm becomes a dd at 2.50 and 2.65); this phenomenon occurs also for the ligand (the iso-propyl protons in a broad singlet at 1.25 ppm are split in two doublets at 0.98 and 1.55 ppm). On addition it is clear that the electronic features

of the complex change, as it is possible to see from the shift of the -SiMe₃ signal to lower fields (the variation is of 0.20 ppm).

From the comparative analysis of the metal precursor and complex peaks (Cp region), it is possible to estimate the composition of the mixture and devise the kinetic of complex synthesis at 90°C (figure 5.13).

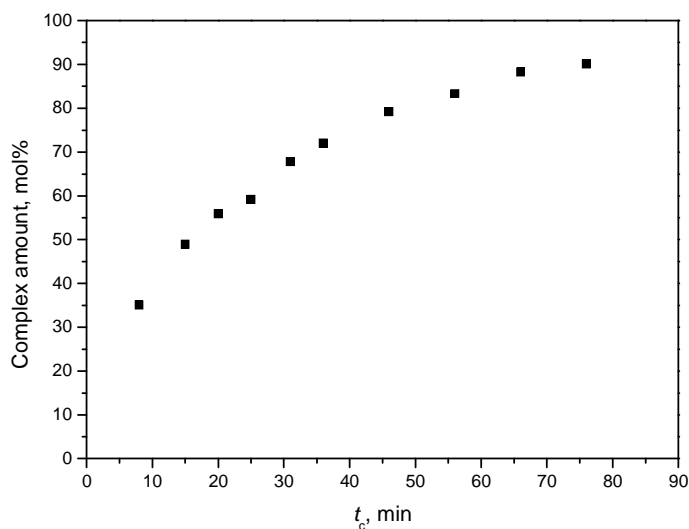


Figure 5.13. Preliminary complexation kinetics for the reaction as depicted in scheme 1, complex **C27** $T_c = 90^\circ\text{C}$, $[\text{Ti}] = [\text{Ligand}] = 80\text{mM}$.

From figure 5.13 it is possible to see that the complexation reaction is almost complete at the quoted conditions, which are, by the way, harder and relatively more severe than the ones previously employed.

The feasibility of the quick *in situ* approach is, at this stage, granted for catalyst **C27**, although the accuracy of the approach is still to be demonstrated (several complexes should be tested, **C0** *in primis*, in order to state that the complexation is facile for most of the metal/ligand combinations). Nevertheless further studies, which are out of scope of the present thesis, are needed from these point and should be aimed to shed light on the kinetic of complexation, the Eyring parameters ($\Delta_c H^\ddagger$ and $\Delta_c S^\ddagger$) and the optimal complexation conditions within the secondary screening workflow.

5.7 – Experimental section

All the catalyst/co-catalyst handling were performed under N₂ or Ar atmosphere, thus using either Schlenk techniques or glove-boxes MBRAUN Lab Master 130, able to keep the O₂ and H₂O value as low as 1ppm_v.

5.7.1 – HTS Freeslate PPR48[®] ethene/1-hexene co-polymerization protocol.

HTS polymerization experiments were carried out with a high throughput parallel reactor setup (PPR48[®] available from Freeslate), with six reactor modules each containing eight reaction cells (5 mL working volume per cell). The whole system is housed in a triple MBraun LabMaster glovebox maintaining a pure nitrogen atmosphere (oxygen and water levels <1 ppm_v). The monomer gas and quench gas lines are plumbed directly into the reactors and controlled by automatic valves; ethene or propene is fed after purification by passing through columns containing a mixed bed of 4Å molecular sieves (3.2 mm pellets) and an activated copper catalyst (BASF R 3-11G). Liquid reagents are robotically added to individual cells by syringes. Solvents are previously purified in an MBraun SPS unit.

The cells are fitted with a pre-weighed glass vial insert and a disposable stirring paddle. The reactor is then closed, and 4.0 mL of toluene/1-hexene proper mixture (HPLC grade from Romil, dried and deoxygenated by passing through MBraun SPS mixed bed columns, 1-hexene from Sigma Aldrich, dried and deoxygenated by distillation over Al(C₈H₁₇)₃ at 5% v/v) and 5.0 µmol of MAO/BHT scavenger (MAO from Chemtura, 10%wt toluene solution, 100 µL of a 50mM solution in toluene, [Al]/[BHT] = 1.0) are injected into each cell through a valve. The reactors are thermostated at 90°C, hence the cells are pressurized with ethene (Rivoira, Polymerization Grade, further purified by passing through Grubbs-type columns) at 4.1 bar.

The proper amounts of pre-catalyst and activator (MAO/BHT; [Al]/[BHT] = 1.0, [Al]/[Ti] = 500) are pre-contacted in toluene at RT for 2 min in a 1.2 mL glass vial and then injected in to the cells. The polymerization is run at constant temperature and monomer partial pressure for 5 minutes, then quenched with dry air at 50 psi (3.4 bar) overpressure. The reactors are cooled, vented and purged with N₂, in order to prevent the glove box pollution with air. After purging with inert gas, the reactors are opened and the glass inserts are unloaded from the cells, transferred to a centrifuge/vacuum drying station (Genevac EZ-2 Plus) for an overnight treatment. The polymer samples are recovered and weighed on a Bohdan BA-100 Balance Automator unit, the polymer yields are automatically stored in a server for further analysis.

5.7.2 – Kinetic profile simulation.

The kinetic profile simulation was performed via fitting of the Gas Uptake Curve provided by the PPR[®] after the experiment.

All the profiles were recorded and exported as numerical table via the software Symyx Polyview[®]; for each deactivating profile, a the amount of monomer saturation uptake was calculated according to the pre-injection gas uptake of the liquid phase. The reaction and saturation monomer uptake were fitted respectively with the following functions (eq. 5.3 and 5.4)^{4b}:

$$U = R_p^0/k_d (1-\exp^{(-k_d \times t_p)}) \quad \text{Eq. 5.3}$$

$$S = a (1-\exp^{(-b \times t_s)}) \quad \text{Eq. 5.4}$$

with a and b as adjustable parameters in equation 5.4. In case the deactivation constant k_d turned out to be higher than $1.0 \times 10^{-3} \text{ s}^{-1}$, the catalyst deactivation process was considered ‘non-negligible’, and the productivity at $t_p = 0$ was calculated as an additional piece of information.

The fitting process was carried out minimizing the squared root of the deviation of equation 5.3 with the experimental uptake curve, and the possibility of local minima and not convergent fitting had been ruled out via setting, as a starting point, for the parameter R_p^0/k_d the polymer yield of the quoted reaction.

5.7.3 – EXtended Core ModuleTM Complexation protocol.

The complexation was performed with the Freeslate platform EXtended Core ModuleTM, figure 5.11. The metal precursor (36,8 mg) and the ligand (18,9 mg) were dissolved in anhydrous toluene (purified through a MBraun SPS unit) and the solvent amount was adjusted to obtain at a concentration as low as 10mM.

10 μ mol of both the metal precursor and the ligand were robotically mixed and dissolved in a 8 mL vial and the final volume was adjusted to 5 mL ($[\text{Ti}] = [\text{Ligand}] = 2.0 \text{ mM}$). The vials were closed and put in an aluminium rack located in an heated bay: the temperatures were set at the desired set point (50/80 °C) and the complexation allowed to proceed for two hours. After the quoted time, the reaction was stopped removing the vials from the heated rack and subsequently transferred to the Freeslate PPR48[®] for polymerization testing.

5.7.4 - Polymer characterization via HT-GPC and NMR.

The HT-GPC curves were recorded at 135°C with a Waters Alliance GPCV2000 system with dual detection (differential refractometric and differential viscometric), on polymer solutions in 1,2-

dichlorobenzene (added with 0.25 mg mL⁻¹ of BHT as a stabilizer). A set of 4 mixed-bed Styragel columns (1 HT-2 and 3HT-6E) was used. Universal calibration was carried out with 12 samples of monodisperse polystyrene (M_n between 1.3 and 3700 KDa). In each carousel of 24 samples, 2 were of a known iPP produced with an *ansa*-zirconocene catalyst used as a standard, to check for consistency. In case the measured M_n and M_w values of the said iPP sample turned out to differ by more than $\pm 20\%$ and $\pm 10\%$ respectively from the “true” values, the calibration procedure was repeated and the whole set of samples re-measured.

Quantitative NMR spectra of all polypropylene samples were recorded at 120°C, on 35 mg mL⁻¹ solutions in tetrachloroethane-1,2-*d*₂, with a Bruker Avance spectrometer (400 Mhz for ¹H) equipped with a 5 mm high temperature cryoprobe. Typical operating parameters were as follows.

- For ¹H NMR: 10.0 ms pulse width (90° pulse); 32K time domain data points, 8.0 kHz spectral width; 2 s acquisition time; 10 s relaxation delay, 200 transients.

- For ¹³C NMR: 4.5 ms pulse width (45° pulse); 64K time domain data points; 14 kHz spectral width; 2.3 s acquisition time; 5.0 s relaxation delay; 2-10K transient.

Shifted squared sinusoidal weighing functions were used for processing before Fourier transformation.

The spectra were fully simulated with the Shape2004 software package (by Prof. M. Vacatello, University of Naples Federico II; vacatello@chemistry.unina.it).

5.7.5 – Complexation kinetics, ¹H NMR kinetic assessment.

The preparation of the model complex **C27** was done in a NMR Jung tube; all the operation at this stage were done in a glove box Mbraun LabMaster 130, under N₂. The proper amounts of ligand and complexes (40 μmol) were dissolved in 500 μL of anhydrous deuterated toluene and the NMR tube was placed in the spectrometer probe at 90°C.

The spectra were recorded with a Bruker AVANCE 400 Mhz NMR spectrometer at different complexation times, 90° pulse, 1.0 s as acquisition time,; relaxation delay, 2.0 s; 32 transients.

All the values of chemical shift are reported as downfield the TMS, the measurement was done referring to the residual protons of the deuterated toluene (methyl signal $\delta = 2.35$ ppm).

Tribenzyl-trimethyl-silyl-cyclopentadienyltitanium.

¹H NMR (400 MHz, tol., 363K): 0.16 (s, 9H, Si(CH₃)₃), 2.96 (s, 6H, CH₂Ph), 5.79 (s, 2H, CpTMS), 6.10 (s, 2H, CpTMS), 6.83 (d, 6H, Ph), 6.86 (t, 3H, Ph), 7.10 (t, 6H, Ph) ppm.

N,N-diisopropyl-2,6-difluoro-benzamidine.

¹H NMR (400 MHz, tol., 363K): 1.33 (s, 6H, CH(CH₃)₂), 1.33 (s, 6H,

CH(CH₃)₂), 3.48 (s, 1H, CH(CH₃)₂), 3.48 (s, 1H, CH(CH₃)₂), 6.31 (s, 1H, NH), 6.49 (d, 2H, Ph), 6.68 (t, 1H, Ph) ppm.

Dibenzyl-trimethyl-silyl-cyclopentadienyltitanium-N,N-diisopropyl-2,6-difluoro-benzamidato.

¹H NMR (400 MHz, tol., 363K): 0.18 (s, 9H, Si(CH₃)₃), 0.91 (s, 6H, CH(CH₃)₂), 1.53 (s, 6H, CH(CH₃)₂), 2.46 (s, 2H, CH₂Ph), 2.65 (s, 2H, CH₂Ph), 3.57 (s, 1H, CH(CH₃)₂), 4.33 (s, 1H, CH(CH₃)₂), 5.93 (s, 4H, CpTMS), 6.55 (d, 2H, CH), 6.71 (t, 1H, CH), 6.95 (d, 6H, CH), 6.83 (t, 3H, CH), 7.1 (t, 6H, CH) ppm.

References.

- [1]. (a) <http://www.azom.com/article.aspx?ArticleID=1822>; (b) Noordermeer, Ethylene-propylene Polymers from Kirk-Othmer Encyclopedia of Chemical Technology, Vol. 10, 704-719, John Wiley and Sons; *World Rubber Statistics 2000*, International Institute of Synthetic Rubber Producers, Inc., Houston, Tex.
- [2]. Hagemeyer,A.; Strasser,P.; Volpe,A.F., Jr. (Eds) *High Throughput Screening in Catalysis*; Wiley-VCH: Weinheim, **2004**.
- [3]. Friederichs, N.; Wang,B.; Budzelaar, P.H.M.; Coussens,B.B. *Journ. Of Molecular Catalysis A: Chemical* **2005**, 242, 91-104.
- [4]. (a) Busico,V.; Pellecchia,R.; Cutillo,F.; Cipullo,R. *Macromol. Rapid. Comm.* **2009**,30, 1697-1708.; (b) Beighzade, D. *Macromol. React. Eng.* **2007**, 1, 331-337.
- [5]. Bernardo,R.; Busico,V.; Cipullo,R.; Pellecchia,R.; *Studying olefin polymerization kinetics in High-Throughput mini-reactors*, Poster at Blue Sky Conference 2010.
- [6]. (a) Endeward,B.; Brant,P.; Nielsen,R.D.; Bernardo,M.; Zick,K.; Thomann,H.; *J. Phys. Chem. C* **2008**, 112, 7818-7828; (b) Chen,E.Y.X.; Marks, T.J. *Chem.Rev.* **2000**, 100, 1391-1434; (c) Macchioni,A. *Chem. Rev.* **2005**, 105, 2039-2073; (d) Beck,S.; Geyer,A.; Brinztinger,H.H.; *Chem.Comm.* **1999**, 2477-2478; (e) Babushkin,D.E.; Brintzinger,H.H.; *J.Am.Chem.Soc.*, **2002**,124, 12869-12873.
- [7]. (a) Ciardelli, F.; Crescenzi,V.; Pezzin,G. *Macromolecole, Scienza e tecnologia, vol 1*, **1983**, Pacini editore, chapter IV, 367-399; (b) Bruckner,S.; Allegra,G.; Pegoraro,M.; La Mantia,F.P., *Scienza e Tecnologia dei Materiali Polimerici*, Edises Seconda Edizione.
- [8]. <http://www.sigmaaldrich.com/materials-science/polymer-science/polymer-analysis.html>
- [9]. Finemann, M.; Ross,S.D. *Journ. Pol. Science.* **1950**, 5, 259-262.
- [10]. (a) Sun,S.F., *Physical Chemistry of Macromolecules: Basic Principles and Issues, Second Edition*; **2004**, John Wiley & Sons, Inc.; (b) Busico,V.; Cipullo,R. *Prog. Polym. Sci.*, **2001**, 26, 443-533; (c) Lambert, J.B.; Mazzola,E.P.; *Nuclear Magnetic Resonance Spectroscopy*, **2003**; Pearson Education Inc.
- [11]. Randall,J.C.; *J.Macromol.Sci., Rev., Macromol.Chem.Phys.* **1989**, C29, 201.
- [12]. (a) E. G. Ijpeij, M. A. Zuideveld, H. J. Arts, F. van der Burgt and G.H. J. van Doremaele, WO, 2007031295, 2007; (b) E. G. Ijpeij, P. J. H. Windmuller, H. J. Arts, F. von der Burgt, G. H. J. van Doremaele and M. A. Zuideveld, WO, 2005090418, 2005.
- [13]. Spaleck,W.; Kuber,F.; Winter,A.; Rohrmann,J.; Bachmann,B.; Antberg,M.; Dolle,V.; Paulus,E.F. *Organometallics* **1994**, 13, 954-963.

[14]. Crabtree, R.H.; *The Organometallic Chemistry of the Transition Metals*, Fourth Edition, Wiley-Interscience, 2005.

APPENDIX 5.1. DEACTIVATION CONSTANTS FOR DEACTIVATING CATALYSTS.

Catalyst Codename	[Ti], $\mu\text{M}^{(1)}$	k_d , 10^{-3} s^{-1} .
C19	2.0	8.5
	2.0	8.9
	1.2	8.5
C21	12.0	14
	8.0	15
	4.0	17
C26	0.8	5.2
	0.4	5.5
	0.8	6.4
C27	0.8	4.1
	0.4	3.0
	0.8	4.5
C24	0.8	4.0
	0.8	4.3
	0.4	3.2
C28	0.8	4.8
	0.8	5.1
	0.4	3.8
C39	12.0	19
	12.0	21
	8.0	25

(1) Nominal concentration of the injected catalyst in the PPR[®] cell.

6.1 – Introduction.

Computational methods are used more and more for molecular modeling among all the fields of chemistry: polymerization catalysis is not an exception in this respect. The technology, nowadays, is powerful enough to handle complicated chemical processes and the possibility of saving synthetic and/or laboratory efforts is indeed an appreciated corollary, along with the confirmation of mechanistic pathways for several chemical reactions. In addition to the mechanistic purposes, also the statistical QSAR modeling is extremely valuable in polymerization catalysis, especially if aimed to the reduction of synthetic efforts of new complexes and to the rational design of new molecular precursors; in view of all this, the present chapter will be related to the computational approach towards the iminato catalysts. In the first section, the main computational methods will be applied to the iminato catalysts in order to confirm the chain termination pathway and acquire more and more pieces of information on these complexes, in the second part the QSAR approach will be elucidated, along with the main principles and applications on catalysis. In the last two sections (6.4 and 6.5), the molecular descriptors of the complexes will be introduced along with the preliminary results of the statistical modeling for the iminato-type complexes.

6.2 – Computational methods applied to the iminato-complexes.

One of the main reasons for the application of modern computational methods to olefin polymerization catalysts, especially for the molecular species, is that the approach is extremely simplified due to the inherent simplicity of the monomers and the relatively small molecules that are the catalyst centers involved in polymerization¹.

The first application of computational methods on iminato catalysts involved the study on the chain transfer mechanism, in order to get and confirm the self consistent picture of the mechanism already unravelled in chapter 2 via the kinetic analysis on polymerization. The limit of chain growth is the principal factor to study, as it is well represented by the polymerization degree of the polymers²:

$$P_n = (\text{Propagation Rate})/(\Sigma \text{ Chain transfer Rate}).$$

The evaluation was done, in collaboration with Prof. Talarico (U-Naples), via the computation of the energy difference between the corresponding transition states (TS – figure 6.1).

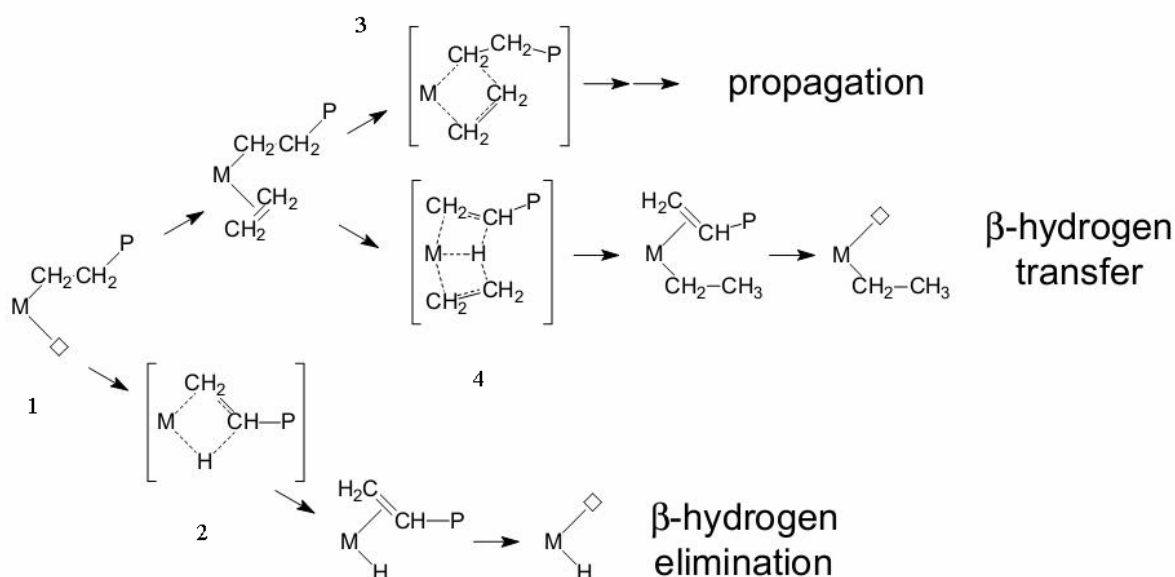


Figure 6.1. The typical pathway for olefin polymerization chain growth.

The story is unfortunately not so simple, since the iminato active species are ion couples, therefore both the counterion and the solvent should be present in the treatment³. Last, but not least, the process is a copolymerization of ethene/1-hexene: unlikely to what found for the common 1-alkene, for ethene it is not possible to state univocally which is the rate limiting step in polymerization⁴. At odds to what was stated in chapter 3 for the experimental approach, propene homopolymerization can indeed simulate *in silico* the copolymerization process: the catalyst dormancy is not a phenomenon involved (it is possible to limit the study only to non-dormant active centres, the ones

of interest) and, like any other 1-alkene^{4a-b}, the rate limiting step in polymerization is well known to be the insertion in the M-C σ bond^{4a-b}.

The catalyst investigated in this study was a reduced version of the complex **C3** of chapter 4 (**C3-red**), as in figure 6.2; the choice of which was done to lower the computational efforts, due to its simpler structure and higher symmetry compared to **C3**^{4c}.

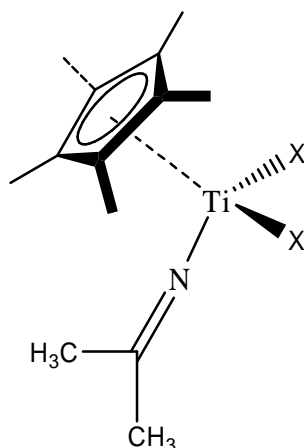


Figure 6.2. Reduced **C3** catalyst (**C3-red**) for the computational study of this section (X = Me, Cl).

Concerning the chain transfer processes, two competing paths can be followed, i.e. intramolecular β -H elimination (BHE) and β -H transfer to the monomer (BHT). Concerning the energy of BHT for the **C3-red** catalysts, the only possibility is to calculate the energy difference between the transition state (*TS*) for the structure 4 and 3 in figure 6.1; for the BHE energy, on the other hand, the best way is to calculate the energy difference between *TS* of 2 and the structure 1 of figure 6.1 (although structure 1 is *not* a *TS*). Using the complex **C3-red**, the energy difference between transition states are calculated and the values are reported in table 6.1.

Table 6.1. Energy difference between transition states for the BHT and BHE processes of chain transfer for the catalyst **C3-red**; refer to figure 6.1 for the transition states.

	BHT (kcal mol ⁻¹) $\Delta E^\ddagger = E(4) - E(3)$	BHE (kcal mol ⁻¹) $\Delta E^\ddagger = E(2) - E(1)$
ΔE^\ddagger	13,2	11,7

The comparison between the two values of ΔE^\ddagger is daring, since the molecularity of the two processes is inherently different (BHE is an intramolecular process, therefore an entropy gain could be expected^{5,7}). On an additional note the experimental trend of the P_n vs the monomer concentration is a good proof for the preference of the chain transfer processes to follow the BHE pathway⁶.

As a second piece of work on chain transfer processes, the metal identity was studied both for BHE and BHT, thus varying the metal over the periodic table group. For both the processes, the calculations enlightened that Ti is the only metal suited to the scope to achieve the best molecular weights of the polymer. This can be easily ascribed, besides electronic effects deriving from the metal, also on the steric properties of the complex featuring Ti: the lower ionic radius ensures, in fact, less space and more congested transition states, thus raising the energy for chain transfer (table 6.2).

Table 6.2. Energy comparison for BHE and BHT processes for the **C3-red** complex with three different metals, i.e. Ti, Zr and Hf.

ΔE^\ddagger	Ti (kcal mol ⁻¹)	Zr (kcal mol ⁻¹)	Hf (kcal mol ⁻¹)
BHE	13,2	11,7	10,8
BHT	11,2	2,0	5,0

The ligand framework substitution surely plays a role in the molecular weight of the final polymerization products, as it can be estimated via the calculation of BHT processes for the system **C3-red** and the complete **C3** catalyst, figure 6.3.

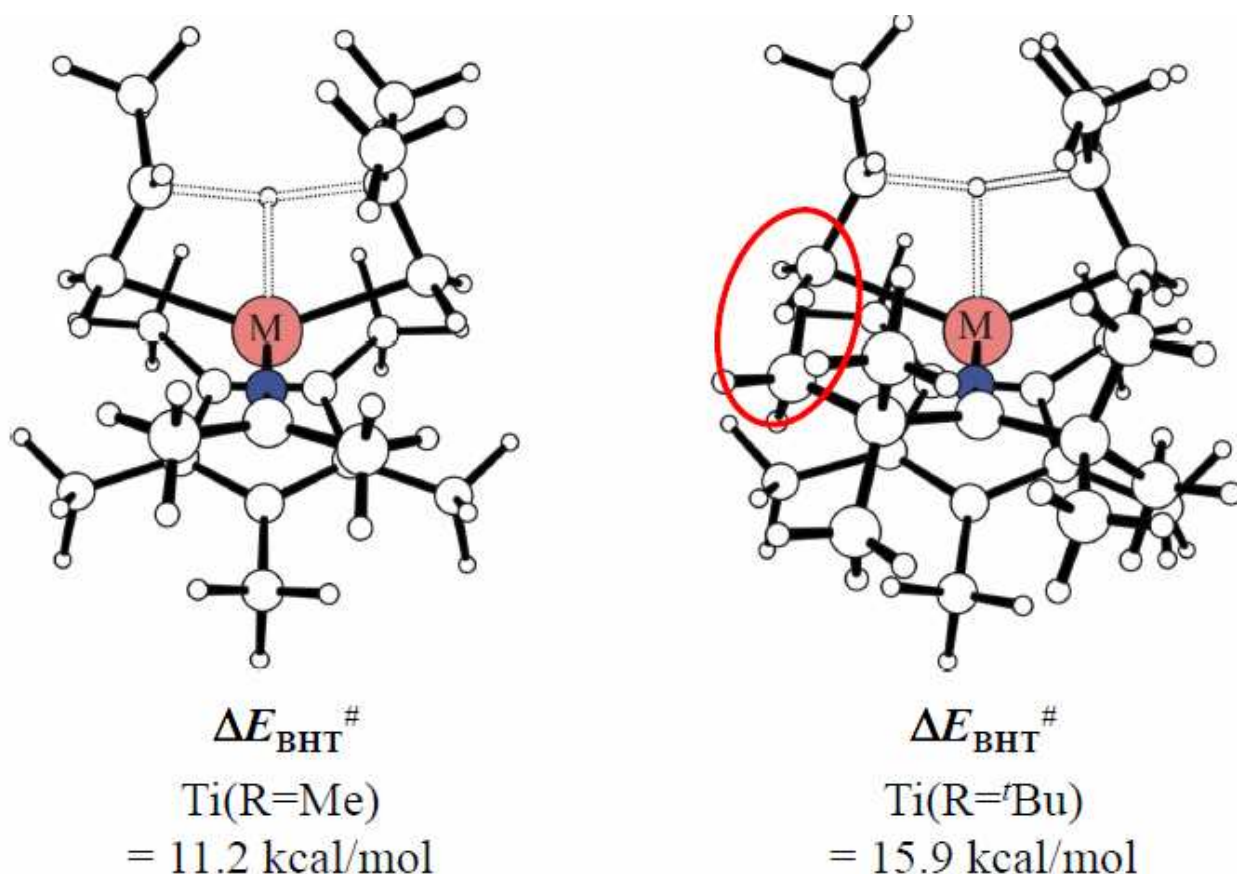


Figure 6.3. Substituent effect on BHT process. The steric expansion of the ligand framework raises the energy of the transition state, meaning that the ligand substitution, not necessarily close to the transition metal atom, plays an active role in determining the molecular weight. Even though the BHT is not the chain transfer process involved with the iminato catalysts, an educated guess is that the general trend for BHT is also respected for BHE.

The application of computational chemistry to iminato catalysts enables the possibility to estimate the steric hindrance the ligand framework provides to the metal coordination sphere, according to the method developed by Prof. Talarico and Prof. Budzelaar⁷. The existence of two possible competing transition states for BHT (BHT_A and BHT_B)⁷ with different steric requirements provides the measurement, through the energy difference between the two different transition states, of the steric hindrance provided by the ligand framework. The comparison of different systems gives a scent on the steric requirement of the **C3-red** ligand framework (figure 6.4). In figure 6.4 a comparison of the steric requirement of the complex **C3-red** with respect the Cp*/acetamidinate systems discovered by Sita⁸ is provided.

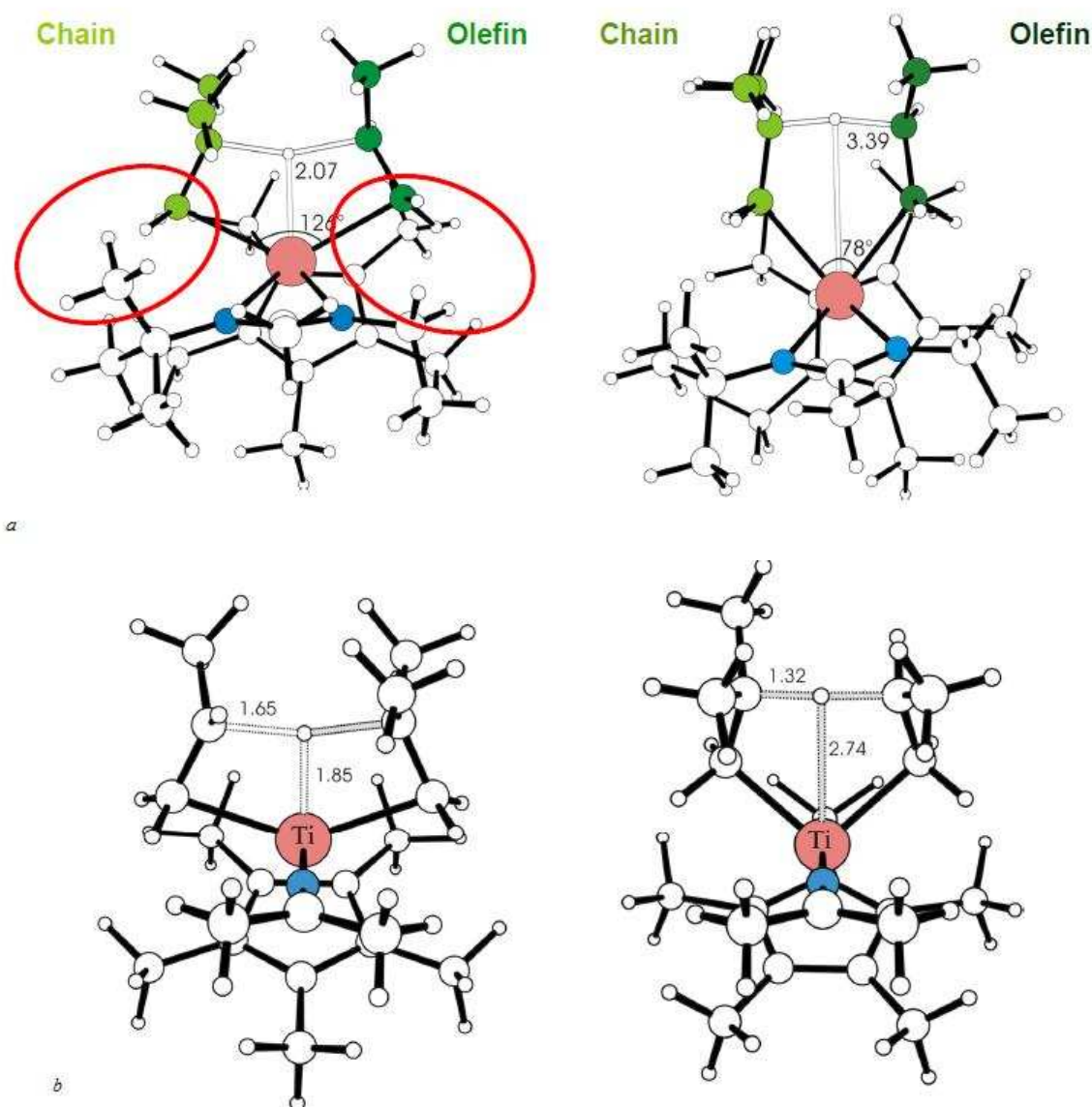


Figure 6.4. a) Ligand steric requirement measurement for the Cp*/acetamidinate system discovered by Sita (BHT_A on the left and BHT_B on the right; $\Delta E^\ddagger = \Delta E_{\text{BHTA}}^\ddagger - \Delta E_{\text{BHTB}}^\ddagger = 9.0 \text{ kcal mol}^{-1}$)⁸ and b) ligand steric requirement measurement for the **C3-red** system ($\Delta E^\ddagger = \Delta E_{\text{BHTA}}^\ddagger - \Delta E_{\text{BHTB}}^\ddagger = -2.0 \text{ kcal mol}^{-1}$). As it is possible to see the steric congestion is less severe for the complex **C3-red** than for Cp*/acetamidinate system; the result can be easily transferred also for amidinato complexes (e.g. **C0** catalyst).

The comparison of different systems can be instructive also with respect the ease of monomer insertion in the M-C bond: on inspection it is possible to compare the **C3-red** catalysts with a highly representative CGC⁹ system and the Cp*/acetamidinate system previously reported⁸. Since the behaviour of each system can be different, especially in relationship with a counterion in a non-polar solvent, a new parameter was calculated for the comparison, i.e. the $\Delta E_{\text{INS}}^\ddagger$. As a matter of definition, $\Delta E_{\text{INS}}^\ddagger$ can be regarded as the estimation of the insertion barrier of a propene molecule in a Ti-C bond, being the polymer chain well simulated by an iso-butyl fragment on the Ti atom. The calculated value of $\Delta E_{\text{INS}}^\ddagger$ is not a prediction of the catalyst activity, but gives a scent on a possible

ranking of the complexes with respect the ease of insertion of monomer in the M-C bond; it is possible, according to figure 6.1, to translate the definition from theoretical to operational¹⁰ (equation 6.1):

$$\Delta E_{\text{INS}}^{\ddagger} = E(1) + E(\text{propene}, \infty) - E^{\ddagger}(3) \quad (\text{Eq.6.1})$$

The calculation is performed scaling the energy of the insertion transition state of figure 6.1 (structure 1 in the quoted figure) to the cationic system with a monomer molecule at infinite distance, thus assuming that the monomer coordination energy for the three classes is similar¹⁰ (all the systems are cationic, featuring high electrophilic metal centers) and disregarding of the energy of the ion pairs (naked cation approach¹¹). The results of calculation are reported in table 6.3 and reveal that the iminato catalysts can be regarded as catalysts which are ‘in between’ the CGC and the Cp*/acetamidinate systems.

Table 6.3. Calculation of the $\Delta E_{\text{INS}}^{\ddagger}$ estimative parameter for the energy barrier for the insertion of a propene molecule in a M-C bond. Even though the value can be used for comparison among different systems, it is not able to predict the catalyst activity.

System of interest	$\Delta E_{\text{INS}}^{\ddagger} = E(1) + E(\text{propene}, \infty) - E^{\ddagger}(3)$ (kcal mol ⁻¹)
CGC	- 3
C3-red	0.1
Cp*/acetamidinate	20

6.3 - Molecular modelling and QSAR approach, principles and applications.

The continuous search for better performing molecules, in all the field of chemistry, brought to the need to develop some methods to correlate the molecular structure of a certain compound and/or compound class with respect their chemical activity¹² (eq. 6.2):

$$\text{Property} = f(\text{Structure}) \quad (\text{Eq. 6.2})$$

Unfortunately, it is not possible to use equation 6.2 directly, instead a different version of it must be employed, i.e. the inclusion of a reference (eq. 6.3),

$$\Delta\text{Property} = \Delta f(\text{Structure}) \quad (\text{Eq. 6.3})$$

since only changes in the activity can be in general recorded for a chemical system.

The modelling of structure/activity relationships was born from this specific need; moreover a appreciated corollary is that, if a strict correlation is found within a self-consistent model, new structures could be predicted, with undeniable benefits for what concerns synthetic efforts and laboratory time.

The quantitative modelling of structure activity relationship bases its roots in a century. Being the first correlations based on empirics (toxicity of a certain class of compound vs solubility), the very first quantitative approach was developed by the Hammett's approach on the benzoic acid systems¹³, using the couple of equations 6.4 and 6.5:

$$\log K_{R-X} - \log K_{R-H} = \rho\sigma \quad (\text{Eq. 6.4})$$

$$\log k_{R-X} - \log k_{R-H} = \rho\sigma \quad (\text{Eq. 6.5})$$

where capital K refers to the equilibrium constant ionization of the benzoic substituted acid, and the lower case *k* refers to the kinetic constant for the same process. The two parameters ρ and σ refer respectively to the sensitivity of the substitution on the benzoic acid frame structure and to the electronic properties (both in the sense of withdrawal and releasing electrical charge density) of the substituent itself.

The major development of QSAR went 30 years later, with Hansch and Fujita with their publication on ρ - σ - π analysis¹⁴; more sophisticated mathematical approaches were applied to the structure

activity studies, thus developing a model able to describe different kinds of biological activities (the approach worked well especially *in vitro*).

Nowadays, with the ongoing progress in combinatorial chemistry and high throughput techniques, several compounds can be produced in a relatively short time¹⁷. Besides the high capability of the technology, still screening and/or synthesizing an inactive compound is a waste of time, QSAR modelling is, especially for time and labour expensive molecules, necessary¹⁵. Nowadays the statistical models developed in QSAR are far more sophisticated than the ones produced years ago, since a higher computational power is available, moreover the parameters to replicate (and hopefully predict) the experimental data have increased both in number and in complexity (such as the usage of molecular descriptors^{16,17}).

6.4 – QSAR modelling on iminato complexes, molecular descriptors.

The application of QSAR modelling on olefin polymerization catalysts is mandatory, since, especially when coupled to HTE, it opens the way to study correlations in a virtually unlimited hyperspace, which can be beneficial especially in the rational improvement design of a certain class of catalysts^{12,16}. The most immediate approach that is devisable is to use a QSAR white-box approach, in which the catalyst performance is related to a certain molecular property within a definite model. Nevertheless this is not doable with the iminato catalysts due to a series of drawbacks, inherently present in the topic. First of all the catalyst productivities fall in a comparatively narrow range which, comparing the energies, is on the order of 1~2 kcal mol⁻¹ (comparable to the DFT error bar in this case). On a second note, a copolymerization is not an elementary process and, lastly, the catalyst structures do not have a unique framework leitmotiv. To the best of our knowledge, this reasons are sufficient to prevent the use of a white box approach QSAR to the topic; nevertheless a completely ‘black box’ approach could totally impede the rational approach to the catalyst design. The choice to proceed was, thanks to the fruitful collaboration with Prof. Budzelaar (U-Manitoba) and Dr. Betty Coussens (DSM Resolve), to choose the best compromise: devising a hybrid QSAR approach, entailing the bests from both the white and the black box approaches, namely the use of proper molecular descriptors and the ‘unguessing’ and unbiased attitude on the copolymerization mechanistic features.

The first step is to develop a large and meaningful database of experimental data (calculated and replicated within a statistical model) which puts its bases on certain variables (molecular descriptors). From the comparison of the experimental data and calculated ones, the validation of the model is performed and, therefore, the prediction capability is assessed. Needless to say that the

higher is the capability of the model to replicate experimental data, the better is the simulation and, hopefully, the capability to predict valuable structures.

During this study the selection of the molecular descriptor fell among structural and electronic descriptors, some of which are listed in table 6.4.

Table 6.4. Molecular descriptors chosen for the QSAR modelling of the iminato type catalysts.

Structural molecular descriptor	Electronic molecular descriptor
Ti-N distance	Total energy
Ti-N-C angle	HOMO
Ti-Cp centre of gravity	LUMO
N-Ti-Cp angle centre of gravity	Partial charge on Ti
Solid-angle(N)	
Cone-angle(N)	
Buried-Volume(N)	
Cone-asimmetry(N)	

In the last part of the present section, the less trivial molecular descriptors chosen so far (solid-angle, the cone-angle, the cone-asimmetry and the buried volume) will be illustrated.

The solid-angle is defined as in figure 6.5, i.e. the angle which is spanned by the ligand, taking as a reference a sphere of radius r . According to figure 6.5 the solid angle can be calculated with the following equation:

$$\text{Solid-angle (N)} = 720 \times A/4\pi r^2 \quad (\text{Eq.6.6})$$

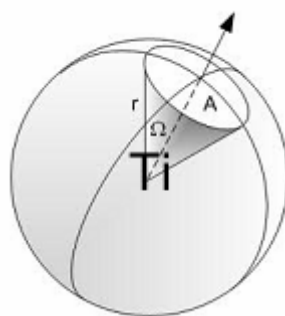


Figure 6.5. Definition of solid angle as a molecular descriptor.

The cone angle molecular descriptor follows the original definition of Tolman for the phosphine ligands¹⁸ (figure 6.6), i.e. the solid angle formed with the metal at the vertex and the perimeter of the cone, ideally described by the ligand.

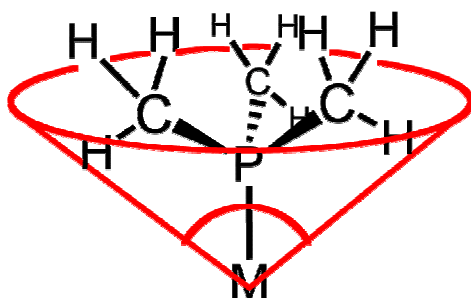


Figure 6.6. Figurative description of the Tolman's solid angle as defined for phosphine ligands. In the case of amidinato, the metal is Ti and the phosphine is the amidinato ligand (figure from reference 18b).

The buried volume is defined, on the other hand, as the fraction of the volume of the sphere with radius of 3.5Å around Ti, which is occupied by the amidinato ligand.

The 'cone asymmetry' is the last descriptor which will be illustrated, and is a quantification of the shape of the projection of the amidinato ligand on the sphere: it is worthwhile to refer to the area *A* already used in figure 6.5 for the calculation of the solid angle. From figure 6.5, the surface *A* is embedded in another coordinate system perpendicular to the main axe of the cone, and any atoms of the ligand is defined by a couple of coordinate x_i and y_i , figure 6.7.

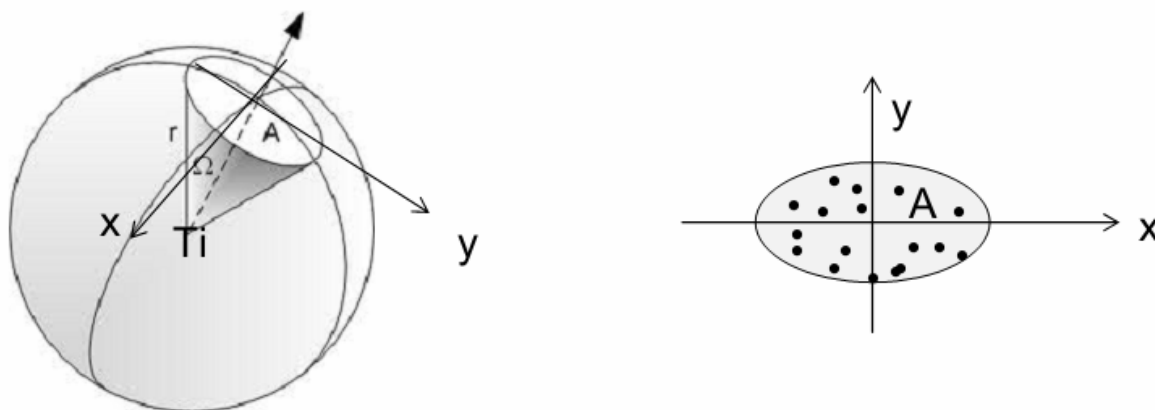


Figure 6.7. Definition of cone asymmetry; on the left the surface *A* and the new coordinate system are depicted with an angle of 90° correlating each other, on the right the projection of surface *A* in the new coordinate system. Each black dot is the projection of the ligand atoms on the surface *A*.

The quantitative evaluation of the shape of surface *A* can be done by the evaluation of the moment of inertia of the ellipsoid *A*, i.e. $M_{xx} = \sum y_i^2$, $M_{yy} = \sum x_i^2$ and $M_{xy} = \sum -x_i y_i$, it is possible, grouping the inertia moments in a matrix to be diagonalized, to reduce in two principal moments of inertia M_1 and M_2 . The two diagonal components are, in fact, the components of the resulting moment of inertia on the two axes, *x* and *y*. The linear combination of equation 6.7 is a quantification of the shape of the area *A* (and of the ligand therefore):

$$(M_2-M_1)/M_1 \quad (\text{Eq. 6.7})$$

The moment of inertia is thus a number comprised between two limits, i.e. 0 (A is a circle) and 1 (A is a line).

6.5 – QSAR modelling, application and results.

As already explained in the introductory chapter, the general aim of this work is the development of a general workflow method to enhance molecular catalyst development with state of the art technologies and tools. The amidinato class investigation is a nice and useful example of a though and ambitious purpose: developing new and better catalysts in a copolymerization process, for which the rate-determining step is generally unknown¹⁹.

Since the aim of the present work is mostly methodological the presentation of the results will consist only of some preliminary calculation on a structure database for which we do not want to be explicit on.

With a QSAR modelling, several catalyst properties can be predicted or calculated within a certain choice of descriptors; by way of example the correlation between the experimental reactivity ratio r_E versus the calculated ones will be illustrated within a reduced database (each catalyst will be treated as a single point within a code-based nomenclature).

The best way to compute the correlation is to look whether or not the values of the experimental values are in a linear correlation (diagonal distribution) with the calculated values within a model: for instance a first model for r_E was of the kind of equation 6.8:

$$r_{E_calculated} = A + B(\text{Partial charge on Ti}) + C(\text{Ti-N-C angle}) + D(\text{ConeAsymmetry}). \quad (\text{Eq.6.8})$$

Within a relatively poor model, already a fair correlation between the experimental values and the calculated value for a limited database was found, as it is possible to evaluate from the R^2 higher than 0.725 (figure 6.8).

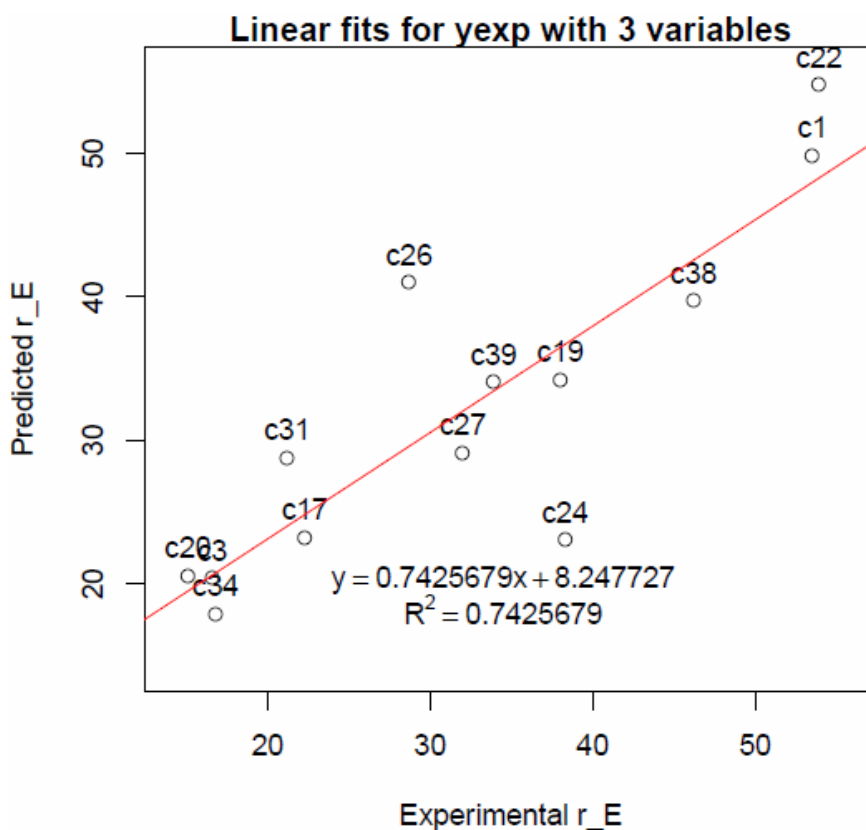


Figure 6.8. Linear correlation between the experimental and calculated values of r_E with a three descriptors model.

The increasing in complexity of the model(s) allows the usage of more and more descriptors, thus evaluating several models in a comparative way: the accordance of course increases and the coefficient of each descriptor will describe its importance within the model itself. By way of example in figure 6.9 two more correlations (four and five descriptors models) are presented, according to equations 6.9 and 6.10 (the coefficients are not related to equation 6.8 and between each others):

$$r_{E_calculated} = A + B(\text{HOMO}) + C(\text{Partial charge on Ti}) + D(\text{Ti-N-C angle}) + E(\text{ConeAsymmetry}) \quad (\text{Eq. 6.9})$$

$$r_{E_calculated} = A + B(\text{Ti-N distance}) + C(\text{N-Ti-Cp angle centre of gravity}) + D(\text{Solid-angle}) + E(\text{Cone-angle}) + F(\text{Burried-Volume}) \quad (\text{Eq. 6.10}).$$

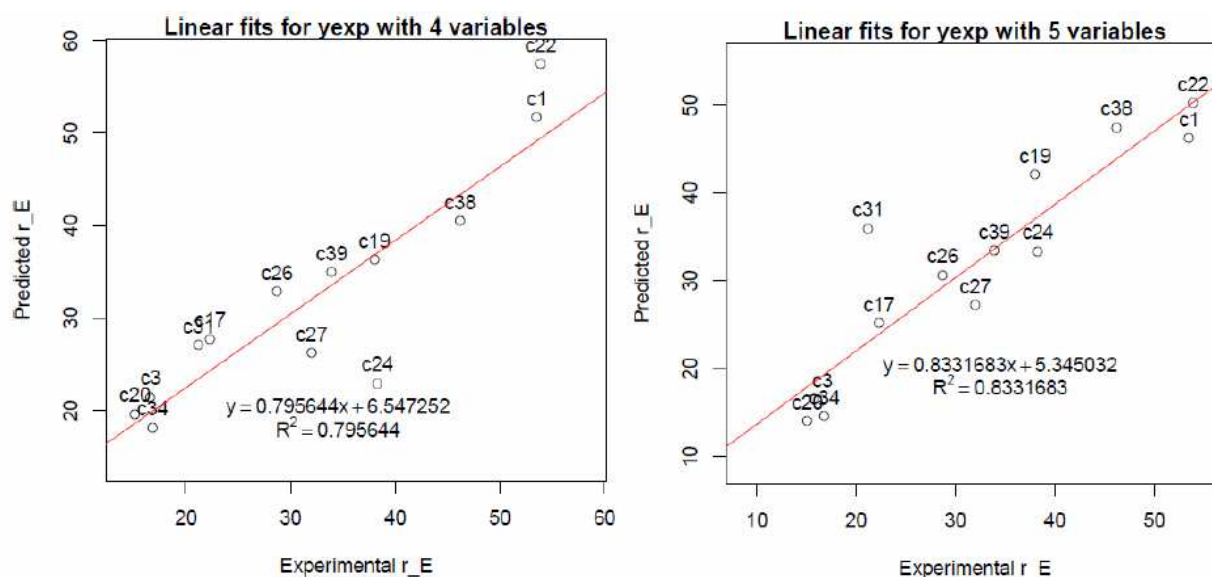


Figure 6.9. Linear correlation between the experimental and calculated values of r_E with a four (left) and a five (right) descriptors model.

As a matter of fact, the correlation increases (the values of R^2 are higher than 0.75), moreover it is instructive to realize that, after the choice of a certain model with respect the others, the identity of the off-diagonal structures changes.

These first and preliminary results, although on an extremely limited database of structure, are very promising, nevertheless, both the low correlation coefficients and the change in the identity of the off-diagonal structures signal that the picture is still far from being reached and an increase in model/database complexity is needed.

6.6 – Computational section.

6.6.1 –Molecular modelling.

All structures were fully optimized, without any constraints. All stationary points were characterized by a vibrational analysis, and thermal corrections (ZPE, enthalpy, entropy; 273K, 1 bar) were calculated from these using standard formulae of statistical thermodynamics (imaginary frequencies were excluded).

These calculations (Tables 6.1 ÷ 6.3) were performed with Gaussian03,²⁰ using the optimizer contained in that program. They all used the B3LYP functional²¹ and the SVP basis set on the light atoms,²² LANL2DZ basis and ECP on the metal atoms.²³

6.6.2 – QSAR modelling.

The QSAR modelling was done using the structures fully optimized with the functionals of paragraph 6.6.1 and, for each complex, only the dimethyl form in the lowest energy conformation was considered. Statistical regression were performed using the freeware package R²⁴.

References.

- [1]. (a) Busico,V., *Dalton Trans.* **2009**,41, 8794-8802; (b) Corradini,P.;Guerra,G.; Cavallo,L. *Acc. Chem. Rev.* **2004**, 37,231-241.
- [2]. (a) Natta,G., Pasquon,I., *Adv. Catal.* **11**, 1 (**1959**); (b) Keii,T.; Terano,M.; Kimura,K.; Ishii,K.; *Makromol. Chem. Rapid. Comm.* **1987**, 8(11), 583-587.
- [3]. (a) Ziegler,T.; Vanka,K.; Xu,Z.; C.R. *Chimie* 8 (**2005**) 1552-1565; (b) Correa,A.; Cavallo,L. *J. Am. Chem. Soc.* **2006**, 128, 10952-10959; (c) Lanza,G.; Fragalà,I.L.; Marks,T.J. *Organometallics* **2002**, 21, 5594-5612.
- [4]. (a) Boor, J., Jr. *Ziegler-Natta Catalysts and Polymerizations*; Academic Press: NewYork, NY, 1979.; (b) a good example of this topic for ethene polymerization is provided by Yang,S.Y., Ziegler,T. *Organometallics* **2006**, 25, 887-900; (c) the symmetry of the complex **C3-red** is higher due to the existence of a σ plane passing through the centre of the Cp ligand and the Ti atom, whereas in **C0** this element of symmetry is not present. This has influences on the calculation of the two reaction sites according to the Cossee mechanism.
- [5]. Atkins, P.; De Paula,J. *Physical Chemistry*, 8th ed., Oxford University Press, 2006.
- [6]. Busico,V; Cipullo,R. *Prog.Pol.Science*, **2001**, 26, 443-533 and reference therein.
- [7]. Talarico,G.; Budzelaar,P.H.M. *Organometallics*, **2008**, 27, 4098-4107.
- [8]. (a) Sita, L. R.; Jayaratne, K. C. *J. Am. Chem. Soc.* **2000**, 122, 958. (b) Jayaratne, K. C.; Keaton, R. J.; Henningsen, D. A.; Sita, L. R. *J. Am.Chem. Soc.* **2000**, 122, 10490. (c) Sita, L. R.; Keaton, R. J.; Jayaratne, K. C.; Fettingner, J. C. *J. Am. Chem. Soc.* **2000**, 122, 12909.
- [9]. (a) McKnight,A.L.; Masood,Md.A.; Waymouth,R.; *Organometallics*, **1997**, 16, 2879-2885; (b) Britovsek, G.P.J.; Gibson,V.C.; Wass,D.F. *Angew. Chem. Int. Ed.* **1999**, 38, 428-447; (c) McKnight,A.L.; Waymouth,R.; *Chem. Rev.* **1998**, 98, 2587-2598.
- [10]. The parameter of $\Delta E_{\text{INS}}^{\ddagger}$ can be regarded as a tentative QM descriptor in view of a QSAR approach. Beside its precise definition, using this parameter for a QSAR approach means that energetic approximations must be done in depicting the mechanism of the amidinato catalyst copolymerization. First of all, neglecting the ion pair energy in equation 6.1 must imply that the cation-anion interactions are similar for all the complexes belonging to the investigated catalyst class (which is an educated, although not granted, guess) and they do not concur to the activation energy of the process; secondly using $E(1)$ as one term of the reference ground energy state implies that for *all the structures* the lowest energy state is the one reported as 1 in figure 6.1. This parameter, can in general be used as a descriptors of *trends* rather than punctual energy differences, therefore, it will be used only for comparing the amidinato complexes (namely the **C3-red** catalyst) with respect two well literature-known and documented systems to study the ease of insertion due

to steric repulsion of the incoming monomer and the polymer chain in propene homopolymerization.

[11]. (a) H. Kawamura-Kuribayashi, N. Koga, K. Morokuma, *J. Am. Chem. Soc.* **1992**, *114*, 8687. (b) C.A. Jolly, D.S. Marynick, *J. Am. Chem. Soc.* **1989** *111*, 7968. (c) L.A. Castonguay, A.K. Rappé, *J. Am. Chem. Soc.* **1992** *114* 5832. (d) A.A. Rappé, W.A. Skiff, C.J. Casewit, *Chem. Rev.* **2000** *100* 1391. (e) P. Margl, L. Deng, T. Ziegler, *J. Am. Chem. Soc.* **1999** *121* 154–162. (f) P. Margl, L. Deng, T. Ziegler, *Organometallics*, **1998**, *17*, 933. (g) T.K. Woo, L. Fan, T. Ziegler, *Organometallics* **1994**, *13*, 432. (h) G. Talarico, A. Blok, T.K. Woo, L. Cavallo, *Organometallics*, **2002**, *21*, 4939.

[12]. Kubinyi, H. *Quant. Struct.-Act. Relation.* **2002**, *21*, 348-356.

[13]. (a) Hammett, L.P. *J. Am. Chem. Soc.* **1937**, *59*, 96; (b) *Advanced Organic Chemistry Part A* Second Edition F.A. Carey, R.J. Sundberg Plenum Press [ISBN 0-306-41198-9](#); (c) Hansch, C.; Leo, A.; Taft, R. W. *Chem. Rev.* **1991**, *91*, 165–195.

[14]. (a) Hansch, C.; Fujita, T.; *J. Am. Chem. Soc.*, **1964**, *86*, 1616-1626; (b) Hansch, C.; Fujita, T.; *Classical and Three dimensional QSAR in Agrochemistry*, Chapter 1, **1995**, American Chemical Society.

[15]. In this case the approach is similar to what is already known as *virtual screening* (VS) for drug discovery. For an interesting perspective article, see Schneider, G. *Nature Review Drug Discovery* **2010**, *9*, 273-276 and references therein.

[16]. Jensen Frank, *Introduction to Computational Chemistry Second edition*, Wiley, Chapter 17; for a nice and instructive for olefin polymerization half metallocenes, see (a) Manz, T.; Caruthers, J.M.; Sharma, S.; Phomphrai, K.; Thomson, K.T.; Delgass, W.N., Abu-Omar, M.M. *Organometallics* **2012**, *31*, 602-618; (b) Manz, T.A.; Phomphrai, K.; Medvedev, G.; Krishnamurthy, B.B.; Sharma, S.; Haq, Jesmin, Novstrup, K.A.; Thomson, K.T.; Delgass, W.N.; Caruthers, J.M.; Abu-Omar, M.M. *J. Am. Chem. Soc.* **2007**, *129*, 3776-3777. (c) Ciancaleoni, G.; Fraldi, N.; Cipullo, R.; Busico, V.; Macchioni, A.; Budzelaar, P.H.M. *Macromolecules* **2012**, *45*, 4046-4053.

[17]. Burello, E.; Rothenbergh, G.; *Int. J. Mol. Sci.* **2006**, *7*, 375-404.

[18]. (a) Tolman, C.A. *Chem. Rev.* **1977**, *77*(3), 313-348 and references therein; (b) http://en.wikipedia.org/wiki/Ligand_cone_angle

[19]. A nice example for this topic is found in Friederichs, N.; Wang, B.; Budzelaar, P.H.M., Coussens, B. *Journ. Of Mol. Catalysis A: Chemicals* **2005**, *242*, 91-104, and references therein.

[20]. Gaussian 03, Revision C.02, Frisch, M.J.; Trucks, G.W.; Schlegel, H.B.; Scuseria, G.E.; Robb, M.A.; Cheeseman, J.R.; Montgomery, Jr., J.A.; Vreven, T.; Kudin, K.N.; Burant, J.C.; Millam, J.M.; Iyengar, S.S.; Tomasi, J.; Barone, V.; Mennucci, B.; Cossi, M.; Scalmani, G.; Rega, N.;

Petersson, G.A.; Nakatsuji, H.; Hada, M.; Ehara, M.; Toyota, K.; Fukuda, R.; Hasegawa, J.; Ishida, M.; Nakajima, T.; Honda, Y.; Kitao, O.; Nakai, H.; Klene, M.; Li, X.; Knox, J.E.; Hratchian, H.P.; Cross, J. B.; Bakken, V.; Adamo, C.; Jaramillo, J.; Gomperts, R.; Stratmann, R.E.; Yazyev, O.; Austin, A.J.; Cammi, R.; Pomelli, C.; Ochterski, J.W.; Ayala, P.Y.; Morokuma, K.; Voth, G.A.; Salvador, P.; Dannenberg, J.J.; Zakrzewski, V.G.; Dapprich, S.; Daniels, A.D.; Strain, M.C.; Farkas, O.; Malick, D.K.; Rabuck, A.D.; Raghavachari, K.; Foresman, J.B.; Ortiz, J.V.; Cui, Q.; Baboul, A.G.; Clifford, S.; Cioslowski, J.; Stefanov, B.B.; Liu, G.; Liashenko, A.; Piskorz, P.; Komaromi, I.; Martin, R.L.; Fox, D.J.; Keith, T.; Al-Laham, M.A.; Peng, C.Y.; Nanayakkara, A.; Challacombe, M.; Gill, P.M.W.; Johnson, B.; Chen, W.; Wong, M.W.; Gonzalez, C.; and Pople, J.A.; Gaussian, Inc., Wallingford CT, **2004**.

[21]. (a) Lee, C.; Yang, W.; Parr, R.G. *Phys. Rev. B* **1988**, 37, 785; (b) Becke, A.D. *J. Chem. Phys.* **1993**, 98, 1372; (c) Becke, A.D. *J. Chem. Phys.* **1993**, 98, 5648.

[22]. Schäfer, A.; Horn, H.; Ahlrichs, R. *J. Chem. Phys.* **1992**, 97, 2571.

[23]. (a) Dunning Jr., T.H.; Hay, P.J. in "Modern Theoretical Chemistry", Schaefer III, H.F., Ed., Vol. 3 (Plenum, New York, **1976**) 1-28; (b) Hay, P.J.; Wadt, W.R. *J. Chem. Phys.* **1985**, 82, 270; (c) Wadt, W.R.; Hay, P.J. *J. Chem. Phys.* **1985**, 82, 284; (d) Hay, P.J.; Wadt, W.R. *J. Chem. Phys.* **1985**, 82, 299.

[24]. <http://www.r-project.org/index.html>.

In this work of thesis we have developed new methods for the HTE investigation of molecular catalysts for solution copolymerization processes, aimed for the production of elastomers. Serendipity and ‘trial and error’ approach are still major driving forces in discovery, and, at a first evaluation, HTE is a tool to enhance the luck occurrence¹. This is true until a certain point, and the iminato catalysts are the perfect example in this respect. Beside the fact that these catalysts are extremely suitable for the HTE investigation due to the existence of general synthetic pathways, their extreme activity in ethene polymerization prevents any laboratory scale investigations: the ‘homeopathic’ amount of active complex in the reactor is not enough to guarantee a decent RSD (>40%) between identical experiments, due to catalyst deactivation by impurities. HTS tools and equipments, therefore, are useless without the precise knowledge of the catalyst behaviour in polymerization.

In general, for solution polymerization processes, the general research must be aimed to increase the operational temperature, in order to enhance the polymer production per loop² in the industrial plant. In Chapter 3, therefore, the basis of this work lie, in which the chain transfer processes are investigated (and confirmed in Chapter 6 via computational approach) as a starting point, thus revealing that the preferred pathway is intramolecular β -H elimination (BHE). From the systematic mechanistic investigation, a previously unrecorded behaviour (on which further studies must be dedicated) of the amidinato complexes is found, namely the C–H toluene activation (at the benzyl position) and the consequent enchainment of benzyl fragments into the polymer. From the polymer microstructure and the balance of the chain ends detected via both ¹H and ¹³C NMR, it is clear that the toluene activation is related to the 2,1 units (section 3.2). So far, the experimental and computational data are, unfortunately, not enough to unravel properly the mechanism; moreover the possible existence of Ti–H bond in the reaction media adds more and more complications due to the utmost reactivity of the latter³.

Chapter 7 – Conclusions.

The mechanistic of chain transfer revealed that the phenomenon of dormancy ‘pesters’ also the amidinato catalysts⁴ in propene homopolymerization; thus revealing that 70% of the catalyst is dormant. In Chapter 4, starting from the catalyst dormancy, a qualitative analysis of the polymerization rate was performed, leading to the development of an ‘on purpose’ HTS protocol. Moreover, since the catalyst regioselectivity is not a specific issue and a good comonomer incorporation is expressed by the amidinato complexes, the ethene/propene copolymerization can be well simulated by ethene/1-hexene copolymerization, according to the modern HTE screening protocols. As it already happened in Chapter 3, another unexpected behaviour was revealed during the systematic work on the protocol benchmark, i.e. the plausible catalyst **C3** *in-situ* modification⁵ as it was suggested by the broadening of the PDI indexes of the copolymers produced (section 4.5), thus signalling a non ‘single-centre’ nature of the catalyst (a plausible culprit could be the residual amounts of nucleophiles arising from the co-catalyst⁶).

In Chapter 5 the HTE screening is undertaken and, along all the usual things that HTE can provide such as polymerization kinetic analysis, high automation and reliability, the concept of using HTE tools and methods as *trend providers* is introduced⁷. The approach of unravelling kinetic trends rather acquiring single data points on several molecular structures is of utmost importance in copolymerization: the proper comparison of different catalysts can be effectively made either at the same feeding ratio (with an inherently different response) or at the same copolymer composition. Looking at trends, rather single data point is beneficial in this respect: the comparison can be done easier by extrapolation of suitable data sets, in order to compare the catalytic complexes ‘homogeneously’. The protocol screening developed so far, and the capability of a modern state of the art HTE secondary screening platform, enabled both the access to the deactivation kinetic constant of the catalysts and the reactivity ratios of all the complexes via polymer sequence distribution analysis via ¹³C NMR microstructural analysis.

In Chapter 6 the modern computational approaches are applied to the iminato complexes, in order to confirm and give support to the mechanistic pieces of information gained in Chapter 3 on the chain transfer processes⁸. Given the huge kinetic database, which had been generated in Chapter 5 (but not fully reported due to secrecy reasons), the modern statistical approach was applied to the amidinato complexes, i.e. the QSAR approach (Quantitative Structure Activity/Relationships)⁹. The QSAR is useful to shed light on mechanism, since it can provide correlations between catalyst properties and generic combinations of molecular descriptors; moreover it enables the possibility to write a structure on paper and predict a certain property: if the model is well built on the kinetic database, this will certainly represent another step toward the rational design of a polymerization catalyst. The first results, although on a limited kinetic database, are very promising, and ‘fair’

(although still unsatisfactory) correlations have already been found in relatively simple models ($0.70 < R^2 < 0.90$, between three and five molecular descriptors).

Olefin catalytic polymerization is, nowadays, considered a mature field: this notwithstanding, the research is still extremely active on this topic, thus affording new products and new processes in a society in continuous change. The developing of new countries (China, Brazil, India, etc.)¹⁰ means, by strict terms, the birth of new markets among the newborn developed societies. The worldwide polyolefin demand is still far from being satisfied: research is therefore still needed in this field to increase production and product grades availability. As a matter of fact, research means also *technological breakthroughs*, which, for olefin based polymers, haven't depleted for over fifty years¹¹.

As it was stated in Chapter 1, the ethylene-propylene based elastomers (both EPM and EPDM) are mostly produced with the old V-based technology^{2a}, featuring low productivity. The need of higher sustainability of chemical processes makes imperative the research to gain better catalysts, processes and product grades: HTE technologies are of utmost importance to speed up the research. The present work, a fruitful collaboration between our research group and LANXESS Elastomers B.V., is mainly methodological, i.e. how apply HTE tools and method to a delicate branch of research of olefin polymerization catalysis; nevertheless this represent the clear symptom of HTE technologies spreading all over the applied science, according to a 'vulgarization' process already occurred for informatics (e.g. we *all* use mobile phones nowadays, don't we?). Like informatics brought changes in our life, so HTE will revisit the research methods, thus requiring more skilled researchers but, at a same time, affording more results per research-time unit and less chemical wastes; needless to say, however, that the general approach to research (i.e. the scientific method) should never change. The work of this thesis is another demonstration of HTE potentialities: what would have been considered a tremendous work with conventional methods (both in labour and pollution terms) has been done in a three year time-frame.

References.

- [1]. Hagemeyer,A.; Strasser,P.; Volpe,A.F., Jr. (Eds) *High Throughput Screening in Catalysis*; Wiley-VCH: Weinheim, **2004**.
- [2]. (a) Noordermeer, Ethylene-propylene Polymers from Kirk-Othmer Encyclopedia of Chemical Technology, Vol. 10, 704-719, John Wiley and Sons ;(b) E. G. Ijpeij, M. A. Zuideveld, H. J. Arts, F. van der Burgt and G.H. J. van Doremaele, WO, 2007031295, 2007; (c) E. G. Ijpeij, P. J. H.Windmuller, H. J. Arts, F. von der Burgt, G. H. J. van Doremaele and M. A. Zuideveld, WO, 2005090418, 2005.
- [3]. Ma,K.; Piers,W.; Parvez,M. *J. Am. Chem. Soc.* **2006**, *128*,3303-3312.
- [4]. Busico,V.; Cipullo,R.; Talarico,G.; *Macromolecules*, **1998**, *31*, 2387-2390; Busico,V.; Cipullo,R.; Ronca,S.; *Macromolecules*, **2002**, *31*, 1537-1542.
- [5]. Nomura, K.; Oya,K.; Imanishi,Y.; *Journ. Of Mol. Catalysis A: Chemical* **2001**, *174*, 127-140; Stelzig,S.H.; Tamm,M.; Waymouth,R.M. *Journ. Of Polymer Science: Part A: Polymer Chemistry*, **2008**, *46*, 6064-6070.
- [6]. The co-catalyst of election for this work was MAO in mixture with an hindered phenol (2,6-^tBu-4-Me-C₆H₂) in order to lower the reactivity of the free AlMe₃; (a) Stapleton,A.R.; Galan,B.R.; Collins,S.; Simon,R.S.; Garrison,J.C.; Youngs,W.J. *J. Am. Chem. Soc.* **2003**, *125*, 9246-9247. (b) Busico,V.; Cipullo,R.; Cutillo,F.; Friederichs,N.; Ronca,S.; Wang,B. *J. Am. Chem. Soc.* **2003**, *125*, 12402-12403.
- [7]. Bernardo,R.; Busico,V.; Cipullo,R.; Pellicchia,R.; *Studying olefin polymerization kinetics in High-Throughput mini-reactors*, Poster at Blue Sky Conference 2010.
- [8]. Talarico,G.; Budzelaar,P.H.M. *Organometallics*, **2008**, *27*, 4098-4107 and references therein.
- [9]. Kubinyi,H. *Quant. Struct.-Act. Relation.* **2002**, *21*, 348-356.
- [10]. Despite the fact that the review presented here is quite old, it is instructive since represent the point of view in polyolefin research of the DOW Chemical Company with respect the investment on polyolefin research and product/market benefits, Chum, P.S.; Swogger,K.W. *Prog. Pol. Sci.* **2008**, *33*, 797-819.
- [11]. Busico,V.; *Dalton Trans.* **2009**, 8794-8802.